

**Corrosion Resistant CMZP and Mg-Al₂TiO₅ Coatings
for SiC Ceramics**

by

Shaokai Yang

Thesis submitted to the Faculty of the

Virginia Polytechnic Institute and State University

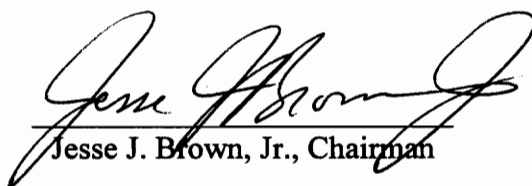
in partial fulfillment of the requirements for the degree of

Master of Science

in

Materials Science and Engineering

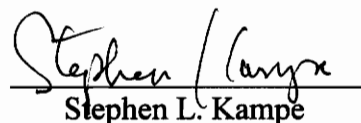
APPROVED:



Jesse J. Brown, Jr., Chairman



Deidre A. Hirschfeld



Stephen L. Kampe

May 1996

Blacksburg, Virginia

Keywords: CMZP, Mg-Al₂TiO₅, SiC, Coating, Corrosion

C.2

LD

5655

V855

1996

Y364

C.2

CORROSION RESISTANT CMZP AND Mg-Al₂TiO₅ COATINGS FOR SiC CERAMICS

By

Shaokai Yang

J. J. Brown, Jr., Chairman

Department of Materials Science and Engineering

(ABSTRACT)

Thin film coatings of (Ca_{0.6}Mg_{0.4})Zr₄(PO₄)₆ (CMZP) and Mg stabilized Al₂TiO₅ (Mg-Al₂TiO₅) on dense SiC substrates were investigated using sol-gel coating techniques. The thickness and quality of both CMZP and Mg-Al₂TiO₅ coatings were found to depend on the solution concentration and lift rate. Double coatings were applied to obtain homogeneous and crack-free coatings. The quality of double coatings was influenced by different first and second coating thickness. The CMZP coated samples were fired in controlled atmospheres to have the pure CMZP phase. Unhydrolyzed solution of Mg-Al₂TiO₅ was utilized instead of hydrolyzed solution to improve the quality of Mg-Al₂TiO₅ coatings. Aging process was found to improve the quality of CMZP and Mg-Al₂TiO₅ coatings. SiC samples coated with CMZP and Mg-Al₂TiO₅ exhibited good thermal shock resistance and greatly improved the high temperature alkali corrosion resistance.

ACKNOWLEDGMENT

I would like to express my gratitude to my advisor Dr. Jesse J. Brown, Jr. for the opportunity to work under his guidance and for his valuable advice and encouragement.

I also wish to thank the members of my committee Dr. Deidre A. Hirschfeld and Dr. Stephen L. Kampe for their help. Thanks are also extended to Dr. Ran Datta for his help and suggestion.

I would also like to thank LeeAnn Ellis, George Knobl, Jr., Amy Hill, Jan Doran, G. Chen, Jud Marte, James Clarke and Y. Lu for their help.

Finally, I would like to thank My family, my wife Yunbo and two sons Fan and Yili, for their love and support.

TABLE OF CONTENTS

	PAGE
ABSTRACT	ii
ACKNOWLEDGMENTS	iii
LIST OF TABLES	vi
LIST OF FIGURES	viii
SECTION	
1. INTRODUCTION	1
2. REVIEW OF LITERATURE	3
2.1 Silicon Carbide	3
2.2 CMZP	5
2.3 Al₂TiO₅	6
2.4 Sol-Gel Techniques	7
3. EXPERIMENTAL PROCEDURE	9
3.1 Substrate Pre-Treatment	9
3.2 Preparation of CMZP Solution	10
3.3 Preparation of Al₂TiO₅ Solution	10
3.4 Coating Techniques	11
3.5 Thermal Shock Resistance Test	15

SECTION	PAGE
3.6 Alkali Corrosion Resistance Test	15
3.7 100-Hour Slagging Combustion Test	17
3.8 Aging Process	22
4. RESULTS AND DISCUSSION	24
4.1 Characterization of Coatings on SiC	24
4.2 Obtaining Pure CMZP Phase	47
4.3 Improving Al ₂ TiO ₅ Coating Procedure	54
4.4 Thermal Shock Resistance	57
4.5 Alkali Corrosion Resistance	63
4.6 100-Hour Slagging Combustion Test	73
4.7 Aging Process	81
5. CONCLUSION	97
REFERENCES	98
VITA	103

LIST OF TABLES

TABLE	PAGE
1. The Properties of the Illinois No. 6 Coal	23
2. Comparison of Different CMZP Coatings under Different Solution Concentrations and Lift Rates	25
3. Comparison of Single and Double CMZP Coatings	26
4. Comparison of Different Mg-Al ₂ TiO ₅ Coatings under Different Solution Concentrations and Lift Rates	37
5. Comparison of Single and Different Double Mg-Al ₂ TiO ₅ Coatings	38
6. Comparison of Different CMZP Coatings under Different Firing Atmospheres	48
7. Thermal Shock Resistance of CMZP Coated SiC Samples	57
8. Thermal Shock Resistance of Mg-Al ₂ TiO ₅ Coated SiC Samples	60
9. Weight Loss of CMZP Coated and Uncoated Samples after Sodium Corrosion	63
10. Flexural Strength of CMZP Coated and Uncoated SiC Samples before and after Sodium Corrosion	63
11. Weight Loss of Mg-Al ₂ TiO ₅ Coated and Uncoated Samples after Sodium Corrosion	68
12. Flexural Strength of Mg-Al ₂ TiO ₅ Coated and Uncoated SiC Samples before and after Sodium Corrosion	68

LIST OF TABLES (Continued)

TABEL	PAGE
13. Thermal Shock Resistance of Aged and Unaged CMZP Coated SiC Sample	81
14. Thermal Shock Resistance of Aged and Unaged Mg-Al ₂ TiO ₅ Coated SiC Samples	84
15. Weight Loss of Aged and Unaged CMZP Coated SiC Samples after Sodium Corrosion	87
16. Flexural Strength of Aged and Unaged CMZP Coated SiC Samples before and after Sodium Corrosion	89
17. Distribution of Ca, Mg, Zr, P and Si on the Sample Surfaces after the Sodium Corrosion at 1000°C	89
18. Weight Loss of Aged and Unaged Mg-Al ₂ TiO ₅ Coated SiC Samples after Sodium Corrosion	92
19. Flexural Strength of Aged and Unaged Mg-Al ₂ TiO ₅ Coated SiC Samples before and after Sodium Corrosion	92
20. Distribution of Mg, Al, Ti and Si on the Sample Surfaces after the Sodium Corrosion at 1000°C	94

LIST OF FIGURES

FIGURE	PAGE
1. The Heat Treatment Schedule for CMZP Coating Dense SiC	13
2. The Heat Treatment Schedule for Mg-Al ₂ TiO ₅ Coating Dense SiC	14
3. Isometric Drawing of the Combustion Test System	21
4. SEM Micographs of the As-received SiC Samples	27
5. SEM Micrographs of CMZP Coatings under the High Solution Concentration of 0.2 mol/L and Lift Rate of 6.5 cm/min	28
6. SEM Micrographs of CMZP Coatings under the Low Solution Concentration of 0.05 mol/L and Lift Rate of 6.5 cm/min	30
7. SEM Micrographs of CMZP Coatings under the Medium Solution Concentration of 0.1 mol/L and Lift Rate of 6.5 cm/min	32
8. SEM Micrographs of Double CMZP Coatings of Different First and Second Coatings	34
9. SEM Micrographs of Mg-Al ₂ TiO ₅ Coatings under the High Solution Concentration of 2.5 mol/L and Lift Rate of 6.5 cm/min	39
10. SEM Micrographs of Mg-Al ₂ TiO ₅ Coatings under the Low Solution Concentration of 0.3 mol/L and Lift Rate of 6.5 cm/min	41
11. SEM Micrographs of Mg-Al ₂ TiO ₅ Coatings under the Medium Solution Concentration of 1.2 mol/L and Lift Rate of 6.5 cm/min	43
12. SEM Micrographs of Double Mg-Al ₂ TiO ₅ Coatings of Different First and Second Coatings	45

LIST OF FIGURES (Continued)

FIGURE	PAGE
13. X-Ray Diffraction Patterns of CMZP Coating Fired in Air (a) and CMZP Powder (b)	49
14. X-Ray Diffraction Patterns of CMZP Coating Fired Isolated from Air (a) and CMZP Powder (b)	50
15. X-Ray Diffraction Patterns of CMZP Coating Fired in the Atmosphere of Poor Oxygen (a) and CMZP Powder (b)	51
16. X-Ray Diffraction Patterns of CMZP Coating Fired in the Atmosphere of Rich CO ₂ (a) and CMZP Powder (b)	52
17. X-Ray Diffraction Patterns of CMZP Coating Fired in the Atmosphere of Partial Oxygen (a) and CMZP Powder (b)	53
18. X-Ray Diffraction Patterns of Mg-Al ₂ TiO ₅ Coating Utilizing Hydrolyzed Solution (a) and Mg-Al ₂ TiO ₅ Powder (b)	55
19. X-Ray Diffraction Patterns of Mg-Al ₂ TiO ₅ Coating Utilizing Unhydrolyzed Solution (a) and Mg-Al ₂ TiO ₅ Powder (b)	56
20. Surface Microstructure of CMZP Coated Samples Exhibited Cracks and Small Spalling after a Thermal Shock of 1000°C	58
21. Surface Microstructure of CMZP Coated Samples Exhibited Cracks after a Thermal Shock of 750°C	58
22. Surface Microstructure of CMZP Coated Samples Exhibited no Cracks after a Thermal Shock of 500°C	59
23. Surface Microstructure of Mg-Al ₂ TiO ₅ Coated Samples Exhibited Cracks and Small Spalling after a Thermal Shock of 1000°C	61

LIST OF FIGURES (Continued)

FIGURE	PAGE
24. Surface Microstructure of Mg-Al ₂ TiO ₅ Coated Samples Exhibited Cracks after a Thermal Shock of 750°C	61
25. Surface Microstructure of Mg-Al ₂ TiO ₅ Coated Samples Exhibited Cracks after a Thermal Shock of 500°C	62
26. Weight Loss of CMZP Coated and Uncoated SiC Samples after Sodium Corrosion	65
27. Flexural Strength of CMZP Coated and Uncoated SiC Samples before and after Sodium Corrosion	65
28. Corrosion of Uncoated SiC Samples by Sodium Carbonate	66
29. Dense Protective Layer on Surface of CMZP Coated SiC Samples Formed after Sodium Corrosion	66
30. Distribution of Ca, Mg, Zr, P, and Si on Sample Surfaces, Obtained by EDX, Proves that the Protective Layer Came from CMZP Coating	67
31. Weight Loss of Mg-Al ₂ TiO ₅ Coated and Uncoated SiC Samples after Sodium Corrosion	70
32. Flexural Strength of Mg-Al ₂ TiO ₅ Coated and Uncoated SiC Samples before and after Sodium Corrosion	70
33. Dense Protective Layer on Surface of Mg-Al ₂ TiO ₅ Coated SiC Samples Formed after Sodium Corrosion	71
34. Distribution of Mg, Al, Ti and Si on Sample Surfaces, Obtained by EDX, Proves that the Protective Layer Came from Mg-Al ₂ TiO ₅ Coating	72

LIST OF FIGURES (Continued)

FIGURE	PAGE
35. SEM Micrographs of Uncorroded Areas (a) and Corroded Areas (b) of the CMZP Coated Samples	74
36. X-Ray Diffraction Patterns of the Uncorroded Areas of the CMZP Coating (a) and the Sample before the Corrosion Test (b)	75
37. EDX Spectrum on a Cross-Section of the Uncorroded Areas of the CMZP Coating	76
38. EDX Spectrum on a Cross-Section of the Corroded Areas of the CMZP Coating	76
39. SEM Micrographs of Uncorroded Areas (a) and Corroded Areas (b) of the Mg-Al ₂ TiO ₅ Coated Samples	78
40. X-Ray Diffraction Patterns of the Uncorroded Areas of the Mg-Al ₂ TiO ₅ Coating (a) and the Sample before the Corrosion Test (b)	79
41. EDX Spectrum on a Cross-Section of the Uncorroded Areas of the Mg-Al ₂ TiO ₅ Coating	80
42. EDX Spectrum on a Cross-Section of the Corroded Areas of the Mg-Al ₂ TiO ₅ Coating	80
43. Surface Microstructure of Aged CMZP Coated Samples after a Thermal Shock of 1000°C	82
44. Surface Microstructure of Unaged CMZP Coated Samples after a Thermal Shock of 1000°C	82
45. Surface Microstructure of Aged CMZP Coated Samples after a Thermal Shock of 750°C	83

LIST OF FIGURES (Continued)

FIGURE	PAGE
46. Surface Microstructure of Unaged CMZP Coated Samples after a Thermal Shock of 750°C	83
47. Surface Microstructure of Aged Mg-Al ₂ TiO ₅ Coated Samples after a Thermal Shock of 1000°C	85
48. Surface Microstructure of Unaged Mg-Al ₂ TiO ₅ Coated Samples after a Thermal Shock of 1000°C	85
49. Surface Microstructure of Aged Mg-Al ₂ TiO ₅ Coated Samples after a Thermal Shock of 750°C	86
50. Surface Microstructure of Unaged Mg-Al ₂ TiO ₅ Coated Samples after a Thermal Shock of 750°C	86
51. Weight Loss of Aged and Unaged CMZP Coated SiC Samples after Sodium Corrosion	88
52. Flexural Strength of Aged and Unaged CMZP Coated SiC Samples before and after Sodium Corrosion	88
53. Distribution of Ca, Mg, Zr, P and Si on Aged CMZP Coated Sample Surfaces, Obtained by EDX	90
54. Distribution of Ca, Mg, Zr, P and Si on Unaged CMZP Coated Sample Surfaces, Obtained by EDX	91
55. Weight Loss of Aged and Unaged Mg-Al ₂ TiO ₅ Coated SiC Samples after Sodium Corrosion	93
56. Flexural Strength of Aged and Unaged Mg-Al ₂ TiO ₅ Coated SiC Samples before and after Sodium Corrosion	93

LIST OF FIGURES (Continued)

FIGURE	PAGE
57. Distribution of Mg, Al, Ti and Si on Aged Mg-Al ₂ TiO ₅ Coated Sample Surfaces, Obtained by EDX	95
58. Distribution of Mg, Al, Ti and Si on Unaged Mg-Al ₂ TiO ₅ Coated Sample Surfaces, Obtained by EDX	96

Section 1

Introduction

Silicon carbide is a promising candidate for a variety of high temperature structural applications because of its high thermal shock resistance, high thermal conductivity, low thermal expansion, high fracture toughness, creep resistance and corrosive resistance in air. The shortcoming of this material is its instability in the presence of oxygen at high temperature.

High temperature alkali corrosion has been known to cause premature failure of ceramic components used in advanced high temperature coal combustion systems such as coal gasification and clean-up, coal fire gas turbines, and high efficiency heat engines. The non-oxide ceramics, such as SiC, are applied in these systems for their well-known and desirable high temperature thermal and mechanical properties. However, these materials are prone to rapid corrosion under high temperature coal combustion conditions.

In the past several years, new high temperature-low thermal expansion materials such as $(\text{Ca}_{0.6}\text{Mg}_{0.4})\text{Zr}_4(\text{PO}_4)_6$ (CMZP) and Mg stabilized Al_2TiO_5 (Mg- Al_2TiO_5) have been developed[1-6]. These materials have been produced with near zero bulk thermal expansion and low crystal anisotropy, very low thermal conductivity, thermal stability up to 1500°C , excellent thermal shock resistance, and good corrosion resistance to alkali attack.

Li et al [7] coated CMZP on SiC and Si₃N₄ substrates using sol-gel techniques. The coatings exhibited good thermal shock resistance and greatly improved the alkali corrosion resistance of SiC and Si₃N₄ substrates. Brown et al [8] have developed a method of sol-gel coating of a magnesia stabilized Al₂TiO₅ material that is stable at low temperatures. Kang [9] coated Mg-Al₂TiO₅ and CMZP to porous SiC filters resulting in a significant improvement of the alkali corrosion resistance of the SiC samples.

The objective of this research is to apply CMZP and Mg-Al₂TiO₅ as coatings to SiC in an attempt to improve its alkali corrosion resistance under coal combustion atmospheres as well as improve high temperature mechanical properties. The research will not only develop and characterize CMZP and Mg-Al₂TiO₅ coatings but will also strive to expand the existing knowledge of the mechanism of coal combustion corrosion of SiC in the temperature range of 1000-1400°C.

Section 2

Literature Review

2.1 Silicon Carbide

Silicon carbide is one of the promising candidates for a variety of high temperature structural applications because of the high temperature shock resistance, high thermal conductivity, low thermal expansion, high fracture toughness, creep resistance and corrosion resistance in air[10-12]. This material is unstable in the presence of oxygen at high temperature and exhibit either active or passive oxidation depending on the partial pressure of oxygen.

In the presence of low oxygen partial pressure, the active oxidation of silicon carbide occurs resulting in formation of SiO gas[13-17]. While in the presence of higher oxygen partial pressure, the passive oxidation occurs resulting in a thin, self-healing, passive SiO₂ scale on all exposed surface of silicon carbide[18-29].

The oxidation of silicon carbide is governed by oxygen transport through the silica layer. The oxidation is greatly accelerated when the protective scale, silica layer, reacts with the alkali. The alkali corrosion in this case can be envisioned as a continuous dissolution-oxidation process in which the oxide layer is readily dissolved in the alkali to form an alkali silicate melt, while oxygen diffuses through the liquid to oxidize the underlying carbide[30,31].

Some authors have studied the oxidation of silicon carbide in wet O_2 or H_2O and pointed out that the oxidation rate is much higher than in the atmosphere without water vapor[32-38]. Water vapor is an oxidizing agent for SiC. The rate of oxidation is accelerated when water vapor was added to oxygen, and possibly water vapor is accelerating the diffusion of oxygen, carbon monoxide, or carbon dioxide through the layer of SiO_2 or that water vapor promoting the transition of amorphous silica to cristobalite might account for the accelerated rate.

Many authors have investigated the alkali corrosion behavior of SiC. Horn[39] reported dislocation etch pitting at $1000^\circ C$ and Amelincks et al[40] and Buchner et al[41] pointed out complete dissolution at temperatures less than $900^\circ C$. McKee et al[42] studied both salt immersion and thin film deposition of sodium sulfate and sodium carbonate on β -SiC and reported active corrosion by deep basic melts with carbon added. When SiC specimens coated with sodium sulfate were exposed to air at $1000^\circ C$, the sodium sulfate decomposed and the SiC became corroded. Buchner et al[41] also pointed out bubble formation and devitrification of protective silica scales were observed upon examination of the morphology of corrosion products deposited on the SiC substrate. Jacobson et al[43] deposited thin film of molten sodium sulfate and sodium carbonate to corrode sintered SiC at $1000^\circ C$. They found that these films lead to glassy products on the SiC surface after 48 hours at $1000^\circ C$. These products contained small amounts of sodium silicate and 10 to 20 times the amount of silica. The attack produced pitting due

to gas evolution and grain boundary etching. It was found that the corrosive attack led to 32% decrease in strength of SiC. Kim et al[44] pointed out that the room temperature flexural strength of sintered SiC was reduced significantly by sulfate defects that formed during active oxidation. The strength of the material was reduced by up to 50% when exposed for 10 hours at 1400°C to H₂-H₂O atmosphere, and up to 40% when similarly exposed to O₂-Ar atmosphere.

2.2 (Ca_{0.6}Mg_{0.4})Zr₄(PO₄)₆ (CMZP)

CMZP is one of the sodium zirconium phosphate (NaZr₂(PO₄)₃ or (NZP) type materials) characterized with an open structure and ability to allow other ions to replace Na⁺ and /or P⁺⁵ cations forming new compounds[45]. Hong[46] and Goodenough et al [47] reported Na_{1+x}Zr₂Si_xP_{3-x}O₁₂ (NASICON) and proposed the substitution of β-Al₂O₃ used in high temperature batteries for industrial solid-state electrolyte applications. Some other authors[48-50] studied the ion conductivity of some NZP type materials and the structure.

Since it was found that some NASICON compounds exhibited low thermal expansion, the studies were focused on the development of new NZP type materials with a low thermal expansion. The driving force for developing low expansion ceramics was a desire to find potential high temperature structural materials with a high thermal shock resistance.

Brown et al[51] studied $(\text{Ca}_{1-x}\text{Mg}_x)\text{Zr}_4(\text{PO}_4)_6$ compounds with x less than or equal to 0.4 and pointed out that at $x=0.4$, the compound $(\text{Ca}_{0.6}\text{Mg}_{0.4})\text{Zr}_4(\text{PO}_4)_6$ (CMZP) exhibited the lowest thermal expansion, low bulk coefficient of thermal expansion, low thermal conductivity, excellent thermal shock resistance, good corrosion resistance to alkali attack, and stability up to 1500°C .

Li et al[7] investigated the thin film coatings of CMZP on SiC and Si_3N_4 substrates utilizing sol-gel coating techniques. The CMZP coatings exhibited good thermal shock resistance and greatly improved alkali corrosion resistance of SiC and Si_3N_4 .

Kang [9] studied alkali/steam corrosion resistance of commercial SiC products coated with sol-gel deposited CMZP. It was pointed out that in high temperature high pressure (HTHP) environments, CMZP coatings improved the thermal shock resistance, corrosion resistance and mechanical properties of SiC substrates.

2.3 Aluminum Titanate

Aluminum titanate is being considered for use in many high temperature structural applications because of the well known high temperature-low thermal expansion properties, and therefore it exhibits good thermal shock resistance.

Aluminum titanate was selected for vehicle engine components testing for its thermal insulation and higher exhaust temperature and the testing was completed without

engine failure[52,53]. Several researchers developed aluminum titanate composites to increase the strength[54] or improve the microcracking[55].

Brown et al[8] have developed the sol-gel coating techniques for a magnesia stabilized aluminum titanate material. Kang [9] investigated the effects of high temperature, high pressure, steam/alkali environments on the corrosion resistance of silicon carbide coated with aluminum titanate. It was pointed out that the aluminum titanate coatings significantly improved the alkali corrosion resistance of the silicon carbide as compared to the uncoated material.

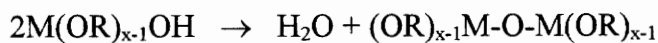
2.4 Sol-Gel Techniques

In recent years, sol-gel processing has been the important techniques for coating a variety of metallic or ceramic substrates to improve the corrosion resistance, wear resistance, electrical and optical properties. The advantages of sol-gel coating techniques are attractive, especially for the purity and homogeneity on the molecular level; although they involve high costs and long processing time[56].

The sol-gel techniques involve two key steps, that is hydrolysis and condensation,

hydrolysis:
$$M(OH)_x + H_2O \rightarrow M(OR)_{x-1}OH + ROH$$

condensation-polymerization:



where M is a metal species (Si, Al, Ti, Zr etc.) and R is an organic group (methyl, ethyl, isopropyl etc.)[57].

Acid and base catalysts can influence both the hydrolysis and condensation rates and the structure of the condensed products. Acids produced good leaving groups and increased the reaction rate, while alkalis produced strong nucleophiles[56]. The condensation rate was enhanced under basic condition.

Section 3

Experimental Procedure

3.1 Substrate Pre-Treatment

The SiC substrates used in the study were prepared by cutting commercial grade SiC plate into 8×10×50 mm pieces. The substrates used for 100-hour slagging combustion test were cut into 8×25×155 mm shapes. In order to prepare crack-free coatings and enhance the adhesion of the coating to substrate, the substrates were treated to form an oxide layer or groups.

The samples to be coated with CMZP were first washed with deionized water for 30 minutes in a solid state/ultrasonic cleaner, then soaked in acetone for 1 hour, and dried at 110°C for 2 hours. Next, the samples were washed with 10% HF solution, rinsed with deionized water, dried at 110°C for 2 hours, and calcined at 1200°C for 6 hours. Finally, the calcined samples were washed with 10% HCl solution, rinsed with deionized water, and dried at 110°C for 2 hours.

The samples to be coated with Mg-Al₂TiO₅ were first washed with deionized water for 30 minutes in a solid state/ultrasonic cleaner, then soaked in 1 : 1 HNO₃ solution for 6 hours, washed with deionized water, dried at 110°C for 2 hours, and calcined at 1200°C for 6 hours. Finally, the calcined samples were washed with 10% HCl solution, rinsed with deionized water, and dried at 110°C for 2 hours.

3.2 Preparation of CMZP Solution

The precursors for CMZP solution are calcium chloride (CaCl_2), magnesium perchlorate hexahydrate ($\text{Mg}(\text{ClO}_4)_2 \cdot 6\text{H}_2\text{O}$), zirconium propoxide ($\text{Zr}(\text{C}_3\text{H}_7\text{O})_4$), triethyl phosphate ($(\text{C}_2\text{H}_5\text{O})_3\text{P}(\text{O})$) and hydrochloric acid (HCl). The stoichiometric amounts of calcium chloride and magnesium perchlorate hexahydrate were mixed in ethyl alcohol. The mixture was constantly stirred while hydrochloric acid was added drop by drop until a pH of between 2.2 and 4.0 was reached, then zirconium propoxide and triethyl phosphate were added drop by drop. The concentration of the CMZP solution was 0.1 mol/L and the solution was clear with a slight yellow color.

3.3 Preparation of Mg- Al_2TiO_5 Solution

The precursors for Mg- Al_2TiO_5 solution are magnesium nitrate hexahydrate ($\text{Mg}(\text{NO}_3)_2 \cdot 6\text{H}_2\text{O}$), aluminum tri-sec butoxide ($\text{Al}[\text{C}_2\text{H}_5\text{CH}(\text{CH}_3\text{CH})\text{O}]_3$), titanium butoxide ($\text{Ti}[\text{CH}_3(\text{CH}_2)_3\text{O}]_4$) and nitric acid (HNO_3). The stoichiometric amounts of magnesium nitrate hexahydrate, aluminum tri-sec butoxide and titanium butoxide were first weighed and homogenized by stirring. A solution of ethyl alcohol and nitric acid with a resultant pH between 1.0 and 4.5 was added drop by drop to the mixture of the magnesium, aluminum and titanium precursors under constant stirring conditions. The concentration of the $\text{Mg}_{0.1}\text{Al}_{1.8}\text{Ti}_{1.1}\text{O}_5$ solution was 1.2 mol/L. The solution was clear with a slight green color.

3.4 Coating Techniques

1). CMZP Coating

The pre-treated samples were soaked in the boiling CMZP solution for 30 minutes and remained in the solution while being cooled slowly to room temperature. The samples were withdrawn at a rate of 4-8 cm/min at room temperature. The coated samples were cured at room temperature for 72 hours at a relative humidity of 40-80%, then air-dried at room temperature for an additional 72 hours and dried at 40-60°C for 48 hours, then, finally heat treated at 400°C in air for 6 hours. The rates of increasing and decreasing the temperature were 1°C/min and 5°C/min, respectively.

The second coating was applied following the same procedure used for the first coating. In order to obtain the pure CMZP phase, the samples were fired in covered crucibles fully filled with CMZP powder at 1200°C for 24 hours. The rates of increasing temperature were 1°C/min and 5°C/min, respectively, before and after 400°C, while the rate of decreasing temperature from 1200°C to room temperature was 5°C/min. Figure 1 shows the heat treatment schedule for CMZP coatings on dense SiC.

2). Mg-Al₂TiO₅ Coating

The pre-treated samples were immersed in the Mg-Al₂TiO₅ solution and vibrated for 30 minutes. The samples were withdrawn at a rate of 4-8 cm/min. The coated samples were put in a container with saturated humidity for 72 hours. Next, the samples

were dried at room temperature in air for 24 hours, then dried at 65°C for 24 hours.

Finally, the samples were fired at 400°C in air for 6 hours. The rates of increasing and decreasing temperature were 1°C/min and 5°C/min, respectively.

The second coating was applied following the same procedure used for the first coating. The coated samples were fired at 1300°C in air for 10 hours. The rates of increasing temperature were 1°C/min and 5°C/min, respectively, before and after 400°C, while the rate of decreasing temperature from 1300°C to room temperature was 5°C/min.

Figure 2 shows the heat treatment schedule for Mg-Al₂TiO₅ coatings on dense SiC.

first coating: room temperature
↓ 1°C/min
400°C, for 6 hours
↓ 5°C/min
room temperature
second coating: room temperature
↓ 1°C/min
400°C, for 6 hours
↓ 5°C/min
1200°C, for 24 hours
↓ 5°C/min
room temperature

Figure 1. The Heat Treatment Schedule for CMZP Coating Dense SiC

first coating: room temperature
↓ 1°C/min
400°C, for 6 hours
↓ 5°C/min
room temperature
second coating: room temperature
↓ 1°C/min
400°C, for 6 hours
↓ 5°C/min
1300°C, for 10 hours
↓ 2°C/min
room temperature

Figure 2. The Heat Treatment Schedule for Mg-Al₂TiO₅ Coating Dense SiC

3.5 Thermal Shock Resistance Test

The thermal shock resistance of CMZP coated samples was investigated. Four groups of samples were heated to 300, 500, 750 and 1000°C, respectively, and then quenched in water at room temperature (25°C). The surface microstructure of coatings and adhesion between the coatings and substrates were examined by SEM and EDX. A Environmental Scanning Electron Microscope E-3 was used.

Four groups of samples coated with Mg-Al₂TiO₅ were heated to 300, 500, 750 and 1000°C, respectively, and then quenched in water at room temperature (25°C). The surface microstructure of coatings and adhesion between the coatings and substrates were examined by SEM and EDX.

3.6 Alkali Corrosion Resistance Test

The alkali corrosion resistance of both CMZP coated and uncoated SiC samples was examined by determining the weight loss and flexural strength degradation of samples exposed to molten Na₂CO₃ and atmosphere containing sodium. Weighed samples were heated to 200°C, then dipped into a saturated solution of Na₂CO₃ to have a thin layer of Na₂CO₃ on the surface. The sodium-coated samples were heated in sodium atmosphere at 900, 1000 and 1100°C, respectively, for 48 hours.

The crucible containing Na_2CO_3 was weighed before and after each run to determine the amount of weight loss of the Na_2CO_3 during the corrosion time interval. Assuming the vapors behave like ideal gasses and using the data from the weight loss and volume of the furnace tube, the alkali vapor concentration was calculated to be approximately 5 vol %. To determine the weight loss after the exposure, the samples were rinsed in acetone and washed in distilled water at 100°C to remove any physically absorbed salt and sodium silicates. Any glass which formed on the surface of the samples was then dissolved in dilute hydrofluoric acid. The etching was repeated until no noticeable difference in weight change was detected.

The room temperature flexural strength of both as-received and corroded SiC samples was determined by 4-point bending using an ATS Test System. To decrease the effect of random errors, the average strength of every group is reported.

The microstructure and fracture surfaces of the samples before and after corrosion were examined by EDX and the phases of sample surfaces before and after corrosion were identified using XRD.

The alkali corrosion testing of $\text{Mg-Al}_2\text{TiO}_5$ coatings follows the same procedure for CMZP coatings as described previously.

3.7 100-Hour Slagging Combustion Test

The SiC samples coated with CMZP and Mg-Al₂TiO₅, respectively, and uncoated samples were tested in a 100-hour slagging combustion test at the Energy and Environmental Research Center at the University of North Dakota, in June 1995 as part of the combustion 2000 project. The objective of this test is to examine CMZP and Mg-Al₂TiO₅ coated SiC samples for improvement in corrosion resistance under coal combustion atmospheres at 1350-1400°C for 100 hours.

1). Coating Procedure

(a). Substrate Pre-Treatment. The SiC samples (8 × 25 × 155 mm) to be coated with CMZP were first washed with deionized water for 30 minutes in a solid state/ultrasonic cleaner, then soaked in acetone for 1 hour, and dried at 100°C for 2 hours. Next, the samples were washed with 10% HF solution, rinsed with deionized water, dried at 100°C for 2 hours, and calcined at 1200°C for 6 hours. Finally the calcined samples were washed in 10% HCl solution, rinsed with deionized water, and dried at 100°C for 2 hours.

The samples to be coated with Mg-Al₂TiO₅ were first washed with deionized water for 30 minutes in a solid state/ultrasonic cleaner, then soaked in 1 : 1 HNO₃ solution for 6 hours, washed with deionized water, dried at 100°C for 2 hours, and calcined at 1200°C for 6 hours. Finally, the calcined samples were washed in 10 % HCl solution, rinsed with deionized water, and dried at 100°C for 2 hours.

(b). Preparation of Solution. The precursor for CMZP solution are CaCl_2 , $\text{Mg}(\text{ClO}_4)_2 \cdot 6\text{H}_2\text{O}$, $\text{Zr}(\text{C}_3\text{H}_7\text{O})_4$ and $(\text{C}_2\text{H}_5\text{O})_5\text{P}(\text{O})$. The stoichiometric amounts of CaCl_2 and $\text{Mg}(\text{ClO}_4)_2 \cdot 6\text{H}_2\text{O}$ were mixed in ethyl alcohol. The mixture was constantly stirred while HCl was added until a pH of between 2.0 and 4.0 was reached. Then $\text{Zr}(\text{C}_3\text{H}_7\text{O})_4$ and $(\text{C}_2\text{H}_5\text{O})_5\text{P}(\text{O})$ were added drop by drop. The concentration of CMZP solution was 0.1 mol/L, while the corresponding lift rate of the samples was 6.5 cm/min.

The precursors for $\text{Mg-Al}_2\text{TiO}_5$ solution are $\text{Mg}(\text{NO}_3)_2 \cdot 6\text{H}_2\text{O}$, $\text{Al}[\text{C}_2\text{H}_5\text{CH}(\text{CH}_3\text{CH})\text{O}]_3$ and $\text{Ti}[\text{CH}_3(\text{CH}_2)_3\text{O}]_4$. The stoichiometric amounts of $\text{Mg}(\text{NO}_3)_2 \cdot 6\text{H}_2\text{O}$, $\text{Al}[\text{C}_2\text{H}_5\text{CH}(\text{CH}_3\text{CH})\text{O}]_3$ and $\text{Ti}[\text{CH}_3(\text{CH}_2)_3\text{O}]_4$ were first weighed and homogenized by stirring. A solution of ethyl alcohol and HNO_3 solution with resultant pH between 1.0 and 4.5 was added drop by drop to the mixture. The concentration was 1.2 mol/L, while the corresponding lift rate of the samples was 6.5 cm/min.

(c). Coating Techniques. The pre-treated samples were soaked in the boiling CMZP solution for 30 minutes and remained in the solution while being cooled slowly to room temperature. The samples were withdrawn at a rate of 6.5 cm/min at room temperature. The coated samples were cured at room temperature for 72 hours at a relative humidity of 40-80%, then air-dried at room temperature for an additional 72 hours and dried at 40-60°C for 48 hours, then finally heat treated at 400°C in air for 6 hours.

The rates of increasing and decreasing the temperature were 1°C and 5°C, respectively. The second coating was applied following the same procedure of the first coating. In order to obtain the pure CMZP phase, the samples were fired in large covered crucibles fully lined with CMZP powder at 1200°C for 24 hours. The rates of increasing temperature were 1°C/min and 5°C/min, respectively, before and after 400°C, while the rate of decreasing temperature from 1200°C to room temperature was 5°C/min.

The pre-treated samples were immersed in the unhydrolized Mg-Al₂TiO₅ solution and vibrated for 30 minutes. The dip coating withdrawn rate was 6.5 cm/min. Then the samples were put in a container with saturated humidity for 72 hours. Next, the samples were dried at 65°C for 12 hours. Finally, the samples were fired at 400°C in air for 6 hours. The rates of increasing and decreasing temperature were 1°C/min and 5°C/min, respectively. The second coating was applied following the same procedure of the first coating. The coated samples were fired at 1300°C in air for 10 hours. The rates of increasing temperature were 1°C/min and 5°C/min, respectively, before and after 400°C, while the rate of decreasing temperature from 1300°C to room temperature was 2°C/min.

2). The Test Conditions

The samples labeled with R-prefix, including CMZP and Mg-Al₂TiO₅ coated and uncoated samples, were embedded in the refractory wall of the main combustor near the furnace exit and cemented in place with zircar alumina cement. The samples labeled with

just downstream of the Probe Bank One. Figure 3 shows the isometric drawing of the combustion test system. The samples were exposed for the entire length of the test.

When the furnace exit temperature had achieved 1315°C, firing natural gas since the unit started, problems were encountered with the coal feeder. When the coal feeder was operational and coal firing was initiated, the unit was fired with natural gas and a furnace exit temperature above 1200°C was maintained for approximately 52 hours. Therefore, all samples were exposed to natural gas at these elevated temperature for 52 hours followed by 95-100 hours of coal firing. The radiant zone samples were exposed for the full test period, approximately 52 hours of gas firing followed by 95-100 hours of coal firing. After exposure, slag and ash buildup on the samples was excessive and cemented the samples to the duct. Samples with CI-prefix had to be removed with an air hammer. Most of the samples were broken in this removal process.

During coal firing, the test furnace was fired at 750,000 Btu/hr, achieving a furnace exit gas temperature between 1340 and 1370°C using 15 % excess air. Due to excessive slag formation in the refractory lined ductwork at the furnace exit, the system was shut down periodically for cleaning. After cleaning, the system was brought back up to operating temperature using natural gas prior to switching to coal. The Illinois No. 6 coal was used for testing, which analyses are provided in Table 1.

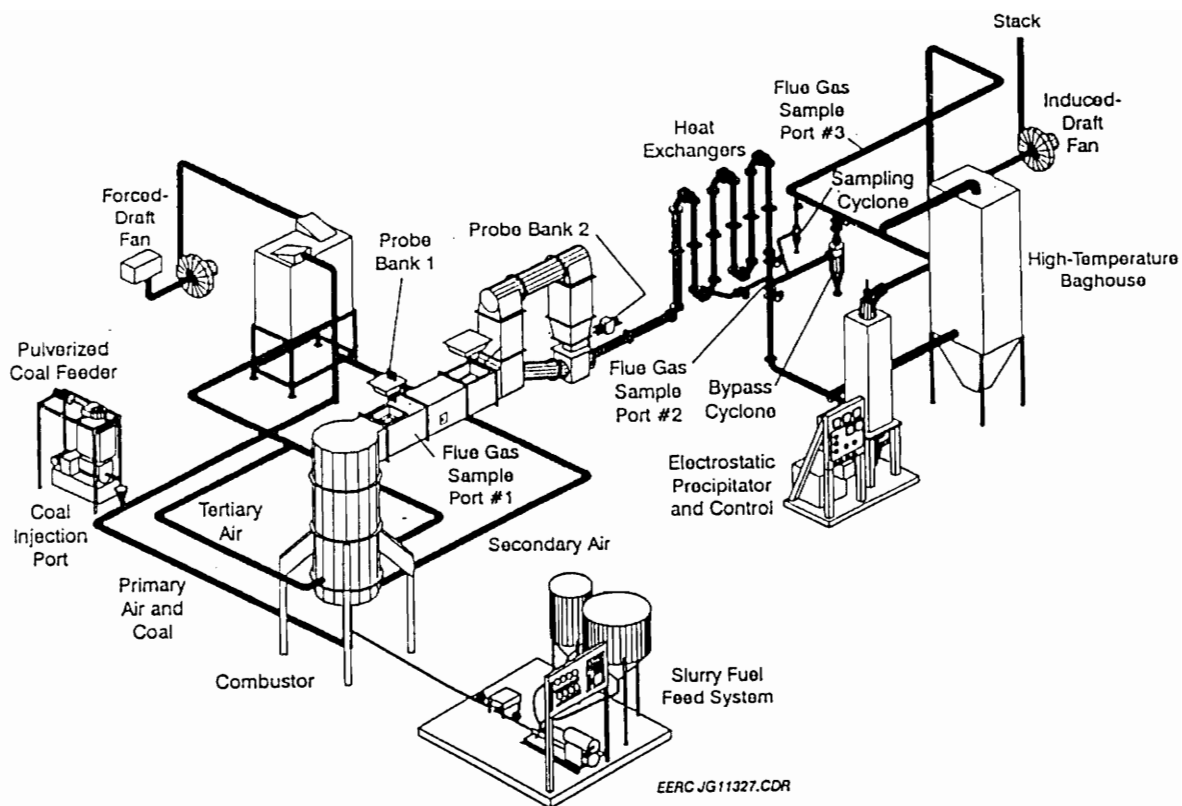


Figure 3. Isometric Drawing of the Combustion Test System

Table 1. The Properties of the Illinois No. 6 Coal

Test Number:	AF-CTS-711	
Date Sampled:	3/14/95	
Sample Number:	95-0254	
Proximate Analysis, %	<u>As-Fired</u>	<u>Moisture-Free</u>
Moisture	6.30	--
Volatile Matter	39.31	41.96
Fixed Carbon	43.95	46.89
Ash	10.45	11.15
Ultimate Analysis, %		
Hydrogen	5.04	4.63
Carbon	65.55	69.97
Nitrogen	1.24	1.33
Sulfur	3.24	3.46
Oxygen	14.49	9.47
Ash	10.45	11.15
Moisture	6.30	--
Heating Value, Btu/lb	11,676	12,464
Sulfur Input, lb SO ₂ /MMBtu	5.55	
Ash Input, lb/MMBtu	8.95	
Sieve Analysis	<u>Sieve Mesh No.</u>	<u>Retained, wt%</u>
	100	4.50
	140	10.88
	200	12.38
	230	7.69
	270	6.38
	325	8.44
	< 325	49.72
% by Weight <200 Mesh		72.23
Ash Analysis, wt%	<u>% by Weight</u>	<u>% SO₃-Free</u>
SiO ₂	48.20	49.65
Al ₂ O ₃	18.51	19.07
Fe ₂ O ₃	18.01	18.56
TiO ₂	0.77	0.80
P ₂ O ₅	0.54	0.55
CaO	4.65	4.79
MgO	1.15	1.18
Na ₂ O	3.55	3.65
K ₂ O	1.70	1.75
SO ₃	2.92	---
Total	85.49	91.08
Ash Fusion Temperatures, °F	<u>Oxidizing</u>	<u>Reducing</u>
Initial Deformation	2307	2047
Softening	2359	2192
Hemispherical	2409	2213
Fluid	2532	2324

3). Measurements of the Samples

The XRD patterns of the samples coated with CMZP and $\text{Mg-Al}_2\text{TiO}_5$ were determined. Before the measurement, all loose slag was removed from the samples.

The microstructure of the surface of the samples coated with CMZP and $\text{Mg-Al}_2\text{TiO}_5$ was examined by SEM. The EDX analysis on the cross-section of the samples coated with CMZP and $\text{Mg-Al}_2\text{TiO}_5$ was done.

3.8 Aging Process

An aging process was utilized to improve the quality of the CMZP and $\text{Mg-Al}_2\text{TiO}_5$ coated samples. The aging process is described below:

The CMZP coated samples were fired in large covered crucibles fully filled with CMZP powder at 1200°C for 100 hours. The cover was sealed with liquid K_2SiO_3 . This technique results in an atmosphere which is nearly oxygen free.

The $\text{Mg-Al}_2\text{TiO}_5$ coated samples were fired in air at 1300°C for 100 hours.

Section 4

Results and discussion

4.1 Characterization of Coatings on SiC

1). CMZP Coatings

In order to obtain dense, homogeneous and crack-free CMZP coatings, the influence of the solution concentration and the lift rate of the samples were investigated. It was found that the quality of the CMZP coatings is strongly dependent on the solution concentration and lift rate. High concentration and fast lift rate resulted in cracking of the coating during subsequent heat treatment. For forming crack-free coatings, the concentration of the CMZP solutions needs to be kept between 0.05 and 0.2 mol/L, while the lift rate stayed between 4.3 and 8.1 cm/min. It was found that the high solution concentration made the coatings thick and inhomogeneous with holes and cracks, while low solution concentration made the coatings too thin, especially in the upper part of the samples due to the influence of gravity.

Figure 4 shows the SEM micrographs of the as-received SiC sample: (a) grains and holes on the sample surface, (b) the interior surface of a hole. Clearly, the good coatings must not only cover the surface of grains but also cover the interior surface of the holes. Figure 5 shows the SEM micrographs of CMZP coatings under the high solution concentration of 0.2 mol/L and lift rate of 6.5 cm/min. Figure 6 shows the SEM micrographs of CMZP coatings under low solution concentration of 0.05 mol/L and lift

rate of 6.5 cm/min. Figure 7 shows the SEM micrographs of CMZP coatings under the medium solution concentration of 0.1 mol/L and lift rate of 6.5/min. Table 2 shows the comparison of different coatings under different solution concentrations and lift rates.

Table 2. Comparison of Different CMZP Coatings under Different Solution Concentrations and Lift Rates

Solution Concentration (mol/L)	Lift Rate (cm/min)	Grain Surface	Interior Surface
0.02	4 - 8	thin	thin
0.05	4 - 8	thin	thin
0.10	4 - 8	good	good
0.15	4 - 8	better	better
0.20	4 - 8	thicker, little cracks	cracks
0.25	4 - 8	thick, cracks	many cracks

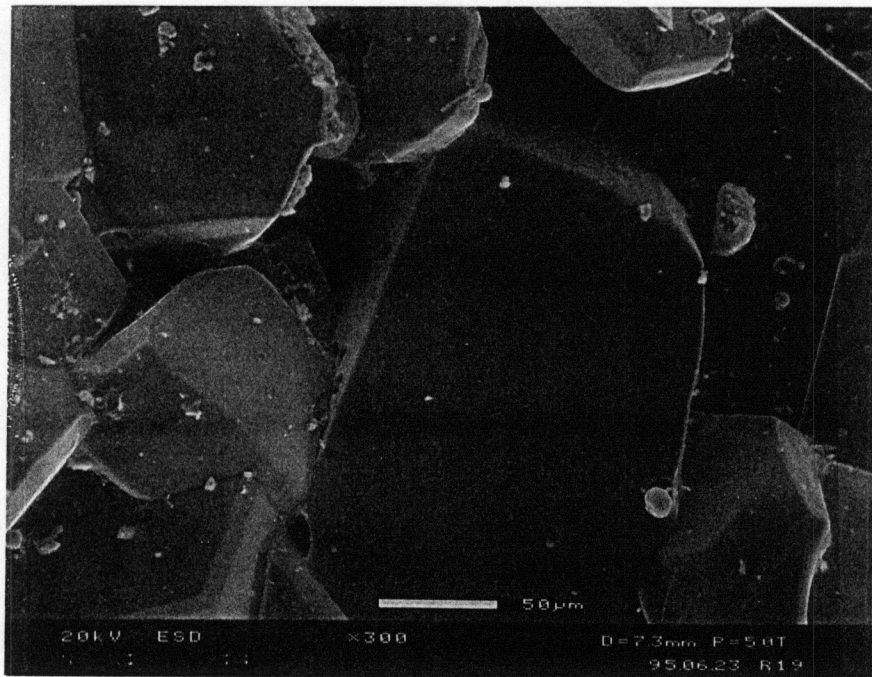
It was found that double coating can improve the quality of the coatings, especially decrease the cracks. Comparison of the results of single and double coatings shows that double coatings are homogeneous and have fewer cracks.

It was found that the different thickness of first coating and second coating also influences the quality of the coatings. Figure 8 shows the SEM micrographs of double CMZP coatings of different first and second coatings: (a) the thickness of first and second coatings is 6 μm and 2 μm , respectively; (b) the thickness of first and second

coatings is 4 μm ; (c) the thickness of first and second coatings is 2 μm and 6 μm , respectively. The results indicate (c) is better. The most likely reason for this is that CMZP adheres more readily to the layer of CMZP than to the surface of SiC. Table 3 shows the comparison of single and double coatings of CMZP.

Table 3. Comparison of Single and Double CMZP Coatings

	Total Thickness (μm)	Thickness of First Coating (μm)	Thickness of Second Coating (μm)	Quality of Coating
Single Coating	8			worse
Double Coating	8	6	2	better
Double Coating	8	4	4	better
Double Coating	8	2	6	good

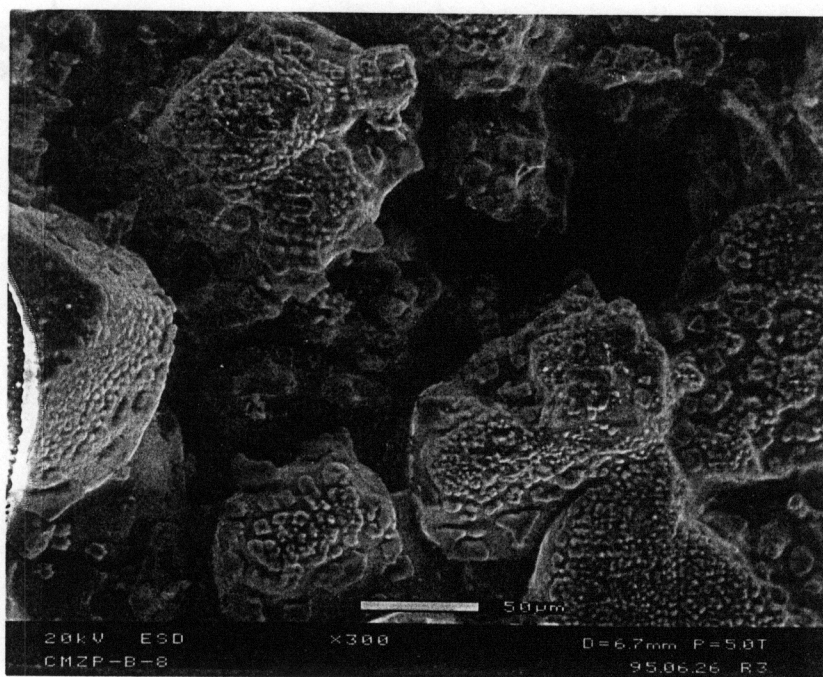


(a)

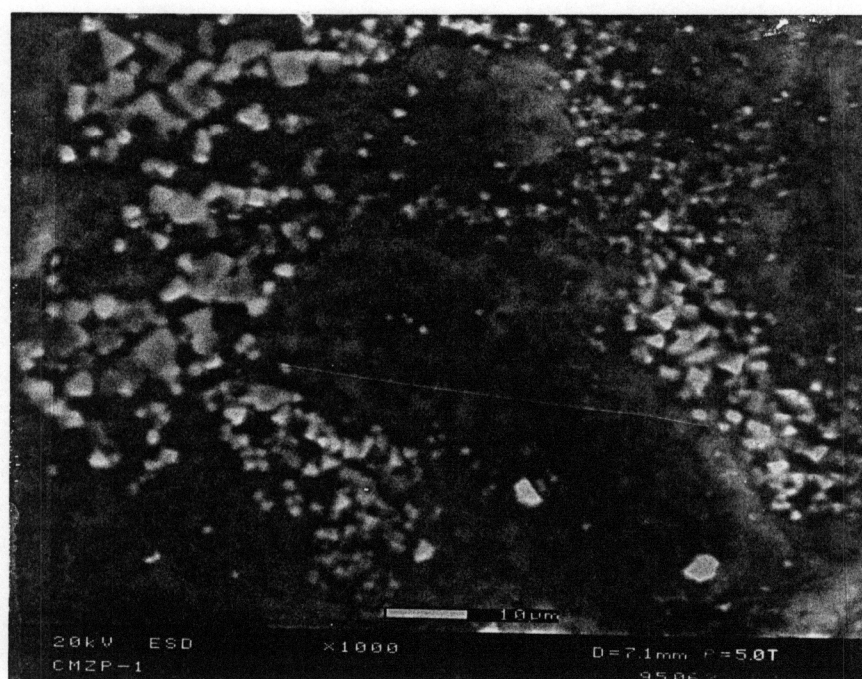


(b)

Figure 4. SEM Micographs of the As-received SiC Samples:
(a) grains and holes on the sample surface
(b) interior surface of a hole

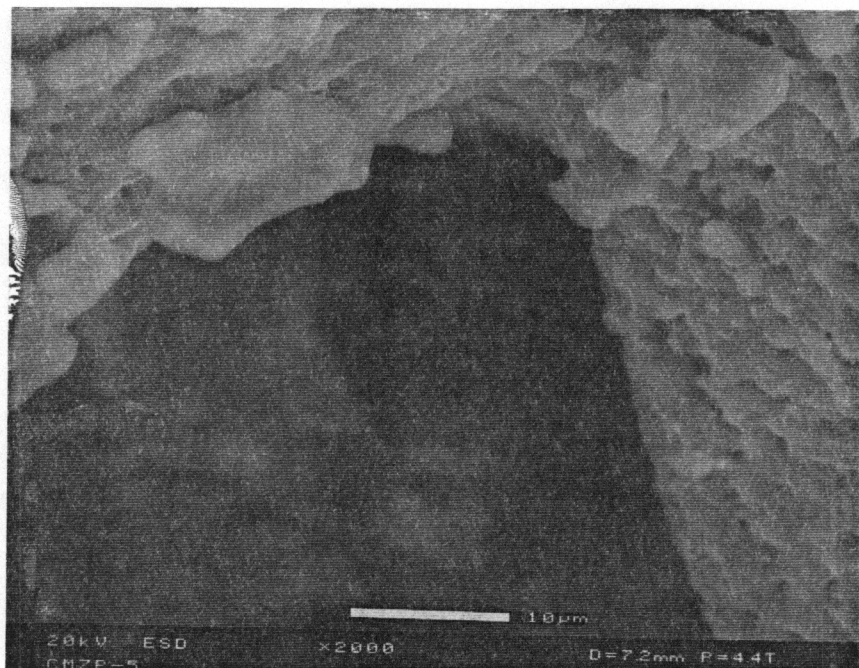


(a)

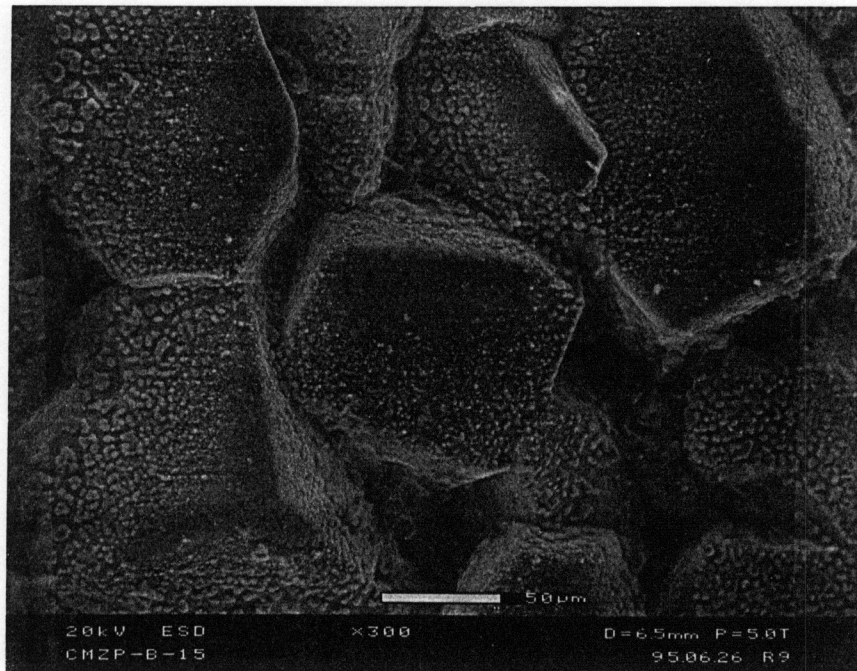


(b)

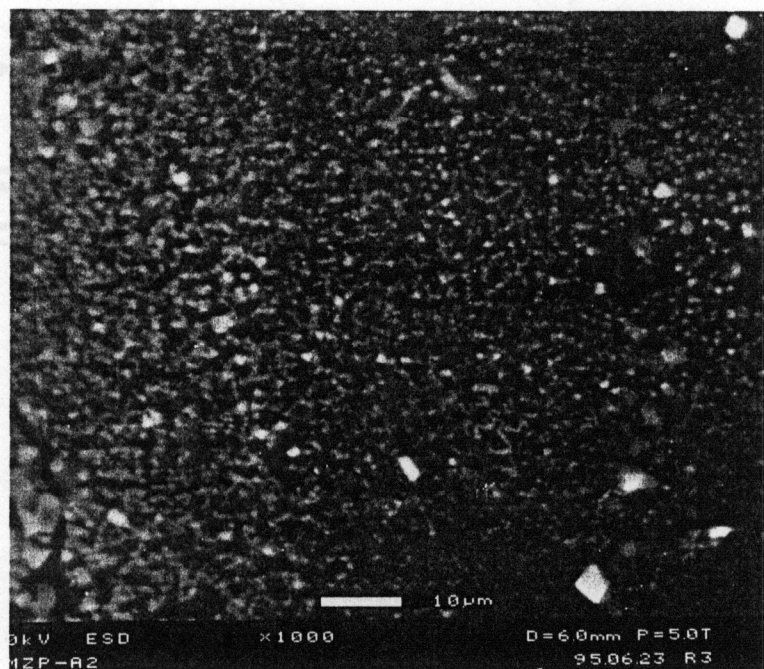
Figure 5. SEM Micrographs of CMZP Coatings under the High Solution Concentration of 0.2 mol/L and Lift Rate of 6.5 cm/min:
 (a) grains on the sample surface, (b) surface of a grain,
 (c) interior surface of a hole



(c)



(a)



(b)

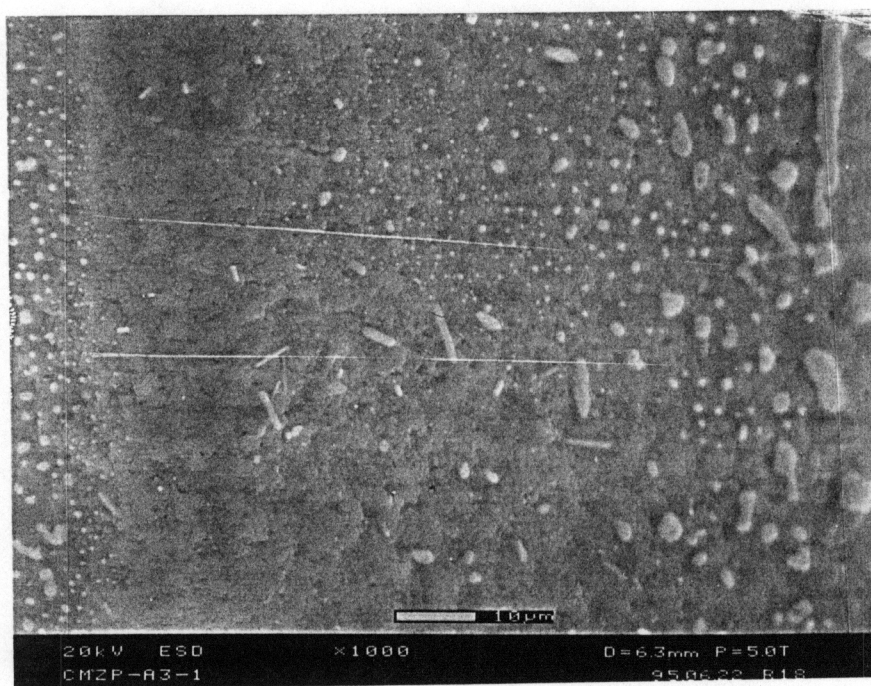
Figure 6. SEM Micrographs of CMZP Coatings under the Low Solution Concentration of 0.05 mol/L and Lit Rate of 6.5 cm/min:
 (a) grains on the sample surface, (b) surface of a grain,
 (c) interior surface of a hole



(c)



(a)

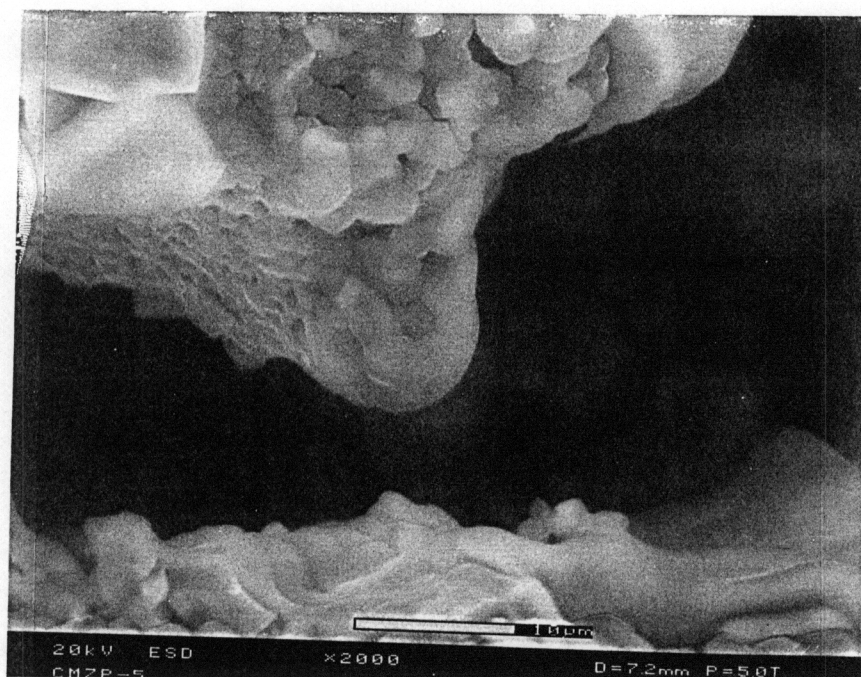


(b)

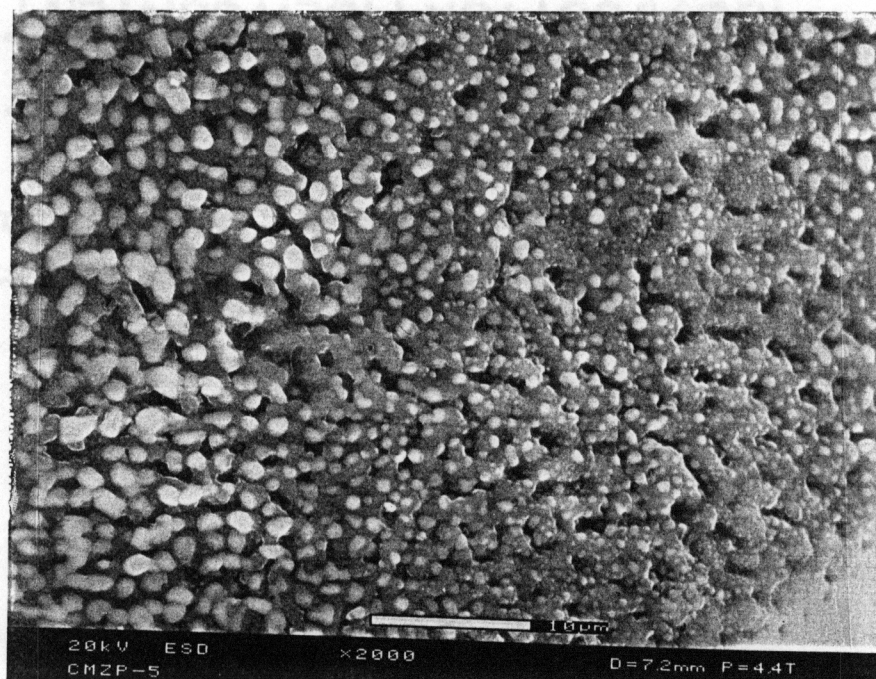
Figure 7. SEM Micrographs of CMZP Coatings under the Medium Solution Concentration of 0.1 mol/L and Lift Rate of 6.5 cm/min:
 (a) grains on the sample surface, (b) surface of a grain,
 (c) interior surface of a hole



(c)



(a)



(b)

Figure 8. SEM Micrographs of Double CMZP Coatings of Different First and Second Coatings:

- (a) thickness of first and second coatings is 6 μm and 2 μm , respectively
- (b) thickness of first and second coatings is 4 μm
- (c) thickness of first and second coatings is 2 μm and 6 μm , respectively



(c)

(2) Mg-Al₂TiO₅ Coatings

It was found that the quality of Mg-Al₂TiO₅ coatings is strongly dependent on the solution concentration and lift rate. Similar to CMZP coatings, high concentration and fast lift rate resulted in cracking of the coatings during subsequent heat treatment. The solution concentration needs to be kept between 0.3 and 2.5 mol/L, while the lift rates are kept between 4 and 8 cm/min. It was found that coatings formed using a high solution concentration were thick and had holes and cracks, while low solution concentration coatings were too thin, especially in the upper end of samples, for the influence of gravity.

Figure 9 shows the SEM micrographs of Mg-Al₂TiO₅ coatings under the high solution concentration of 2.5 mol/L and lift rate of 6.5 cm/min. Figure 10 shows the SEM micrographs of Mg-Al₂TiO₅ coatings under the low solution concentration of 0.3 mol/L and lift rate of 6.5 cm/min. Figure 11 shows the SEM micrographs of Mg-Al₂TiO₅ coatings under the medium solution concentration of 1.2 mol/L and lift rate of 6.5 cm/min. Table 4 shows the comparison of different coatings under different solution concentrations and lift rates.

Table 4. Comparison of Different Mg-Al₂TiO₅ Coatings under Different Solution Concentrations and Lift Rates

Solution Concentration (mol/L)	Lift Rate (cm/min)	Grain Surface	Interior Surface
0.3	6.5	too thin	too thin
0.6	6.5	thin	thin
0.9	6.5	better	better
1.2	6.5	good	good
1.5	6.5	better	better
1.8	6.5	thick	thick
2.1	6.5	too thick	too thick
2.5	6.5	too thick	too thick

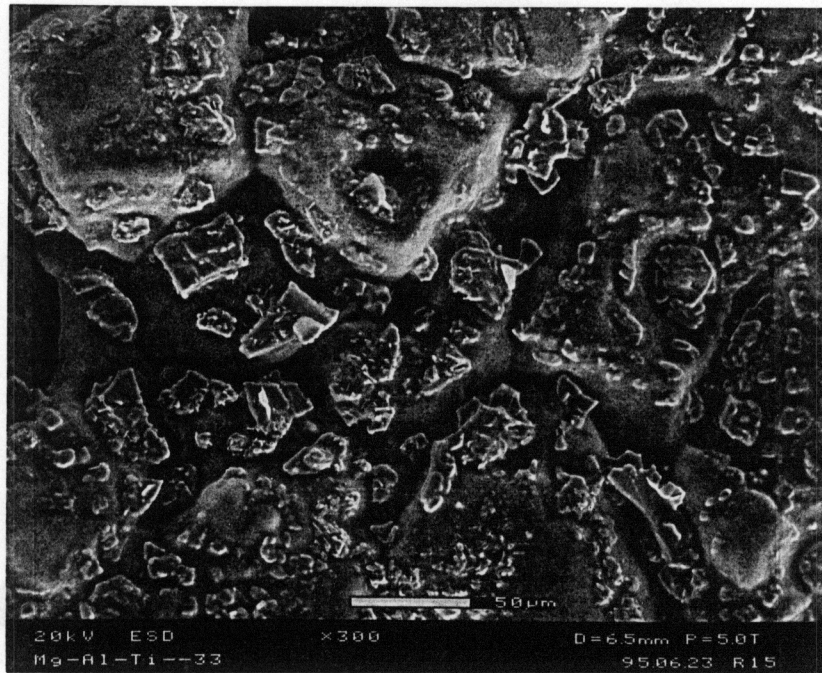
It was found that double coatings can improve the quality of the coatings.

Comparison of the results of single and double coatings shows that double coatings are homogeneous and have fewer cracks. It was found that the quality of double coatings was influenced by different thicknesses of first and second coatings. Figure 12 shows the SEM micrographs of double Mg-Al₂TiO₅ coatings of different first and second coatings:

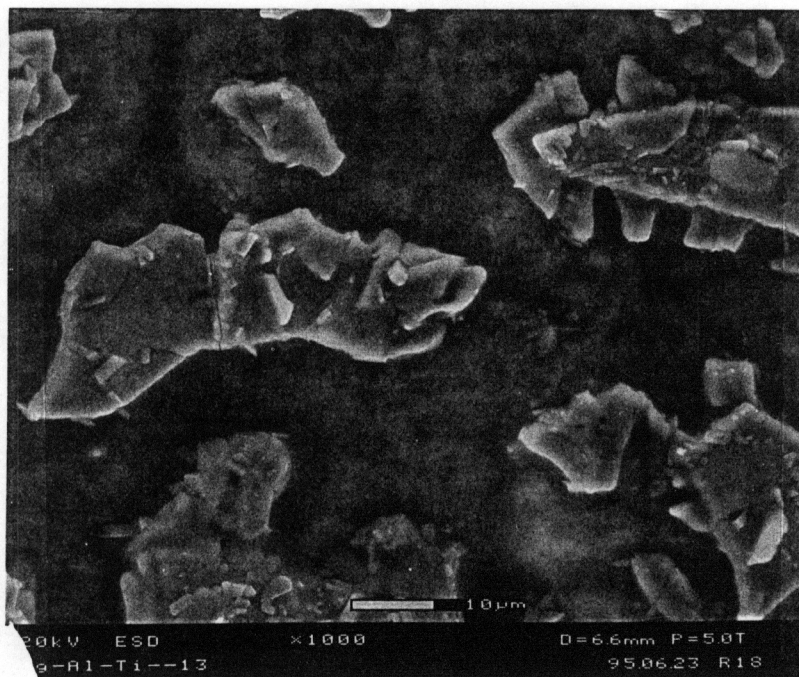
(a) the thickness of first and second coatings is 6 μ m and 2 μ m, respectively; (b) the thickness of first and second coatings is 4 μ m; (c) the thickness of first and second coatings is 2 μ m and 6 μ m, respectively. The results indicated (c) is better. The most likely reason for this is that, like CMZP coatings, Mg-Al₂TiO₅ adheres more readily to the layer of Mg-Al₂TiO₅ than to the surface of SiC. Table 5 shows the comparison of single coating and different double coatings.

Table 5. Comparison of Single and Different Double Mg-Al₂TiO₅ Coatings

	Total Thickness (μm)	Thickness of First Coating (μ m)	Thickness of Second Coating (μm)	Quality of Coating
Single Coating	8			worse
Double Coating	8	6	2	better
Double Coating	8	4	4	better
Double Coating	8	2	6	good

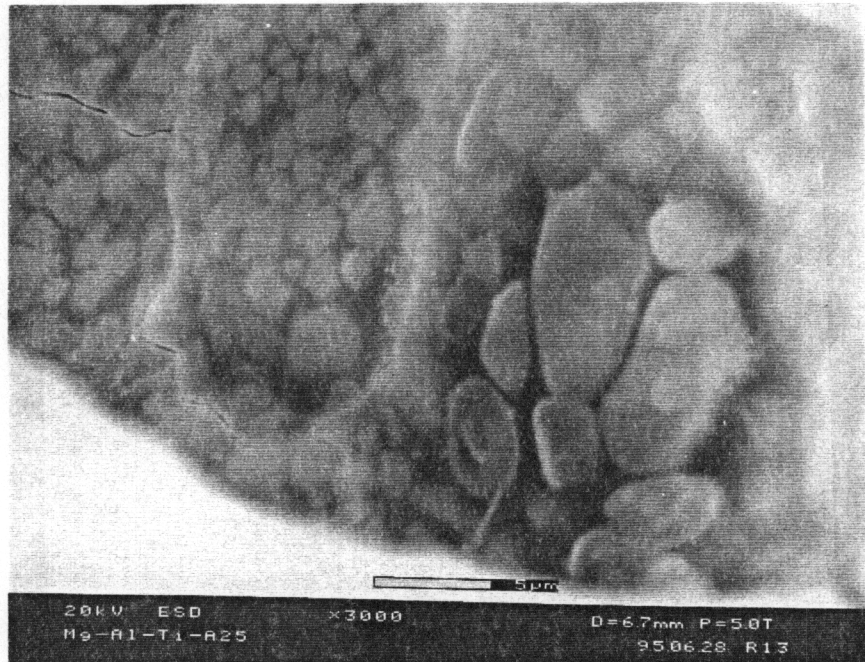


(a)

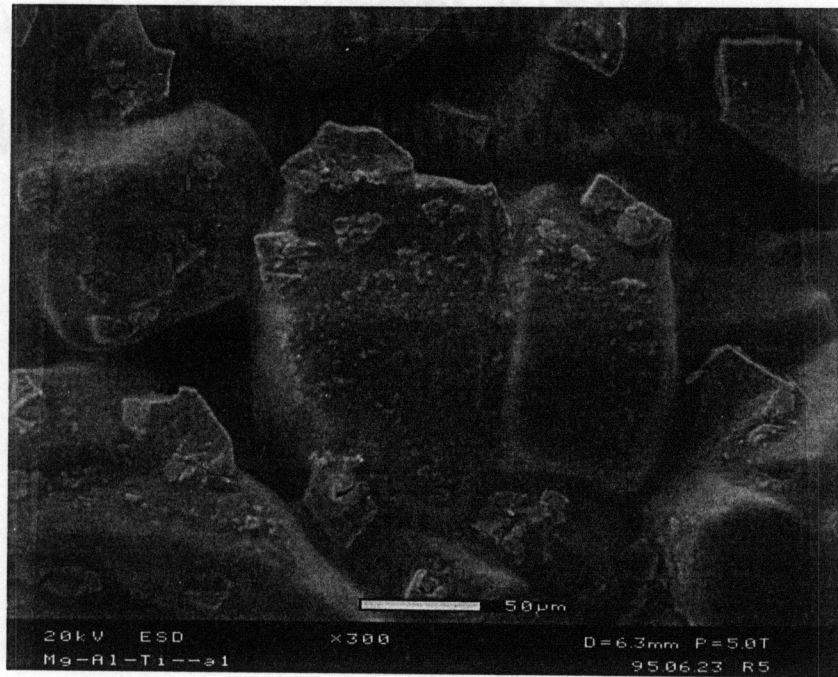


(b)

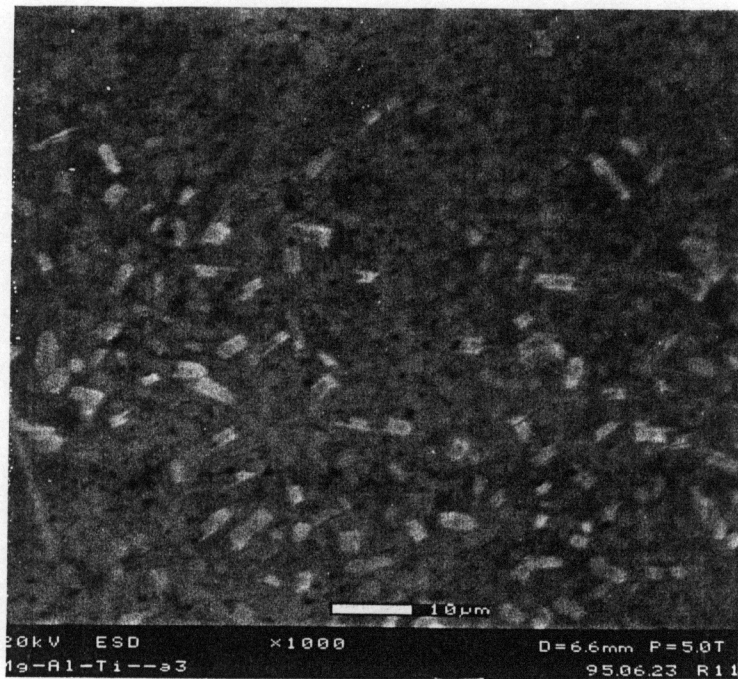
Figure 9. SEM Micrographs of $\text{Mg-Al}_2\text{TiO}_5$ Coatings under the High Solution Concentration of 2.5 mol/L and Lift Rate of 6.5 cm/min:
 (a) grains on the samples surface, (b) surface of a grain,
 (c) interior surface of a hole



(c)



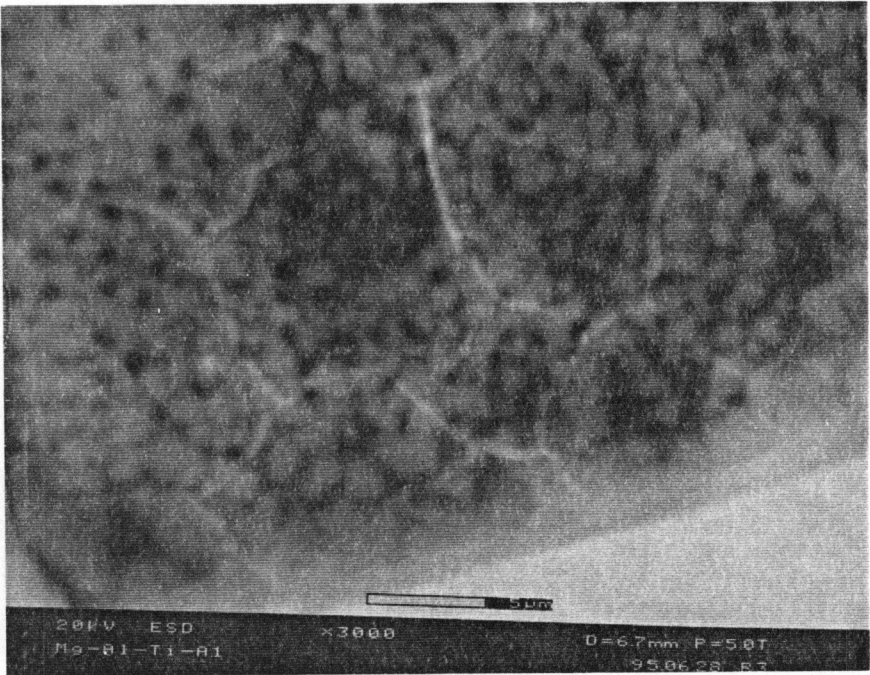
(a)



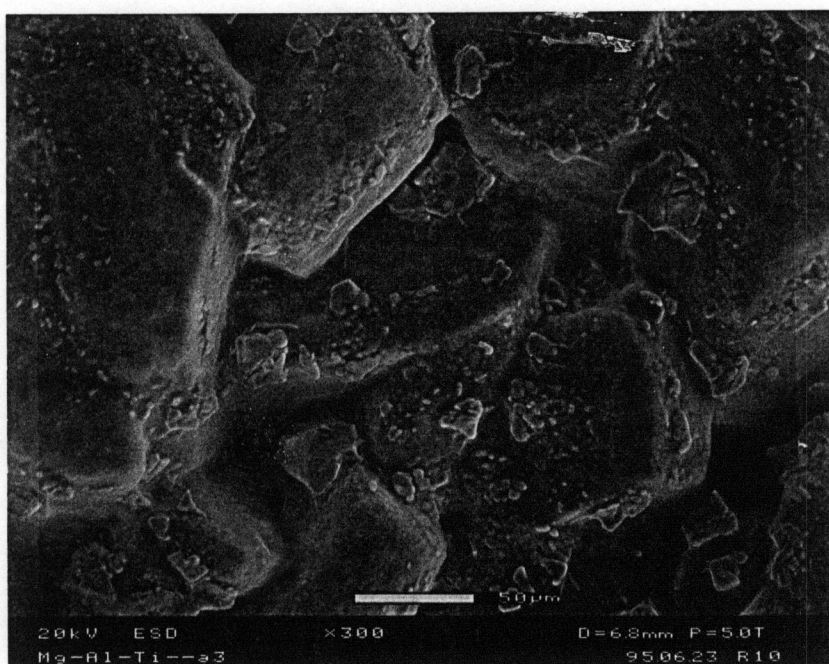
(b)

Figure 10. SEM Micrographs of $\text{Mg-Al}_2\text{TiO}_5$ Coatings under the Low Solution Concentration of 0.3 mol/L and Lift Rate of 6.5 cm/min:

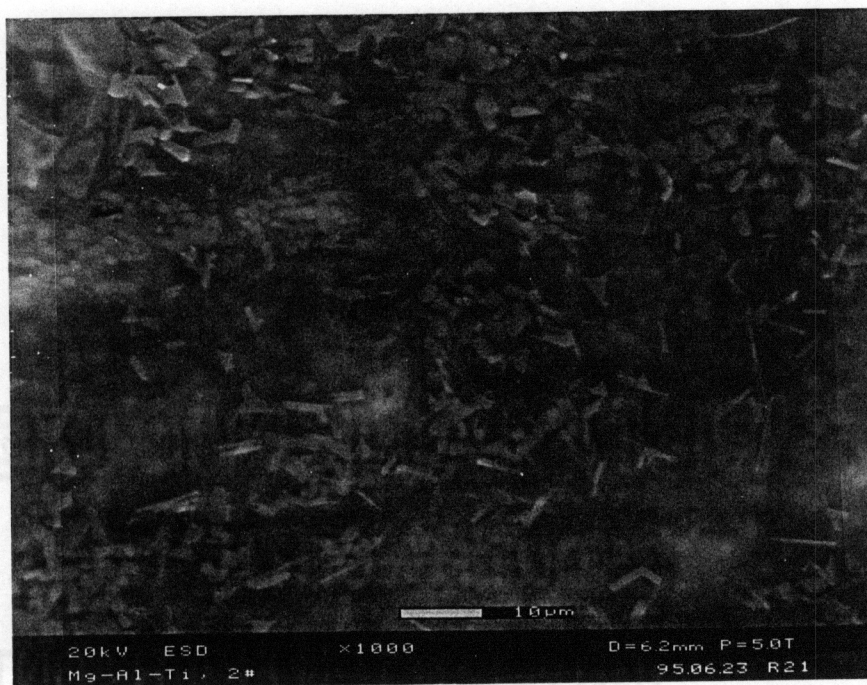
- (a) grains on the samples surface, (b) surface of a grain,
- (c) interior surface of a hole



(c)

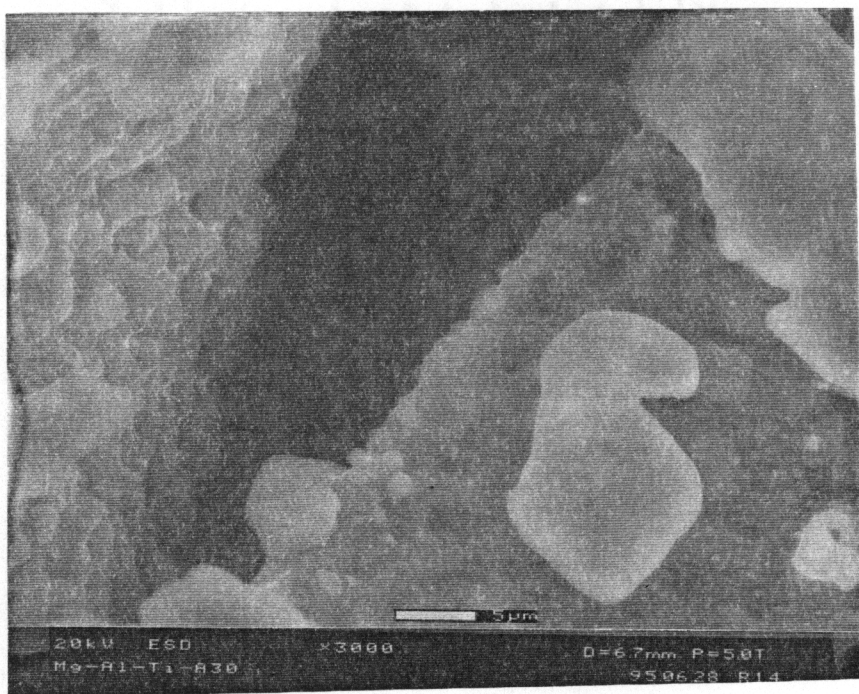


(a)

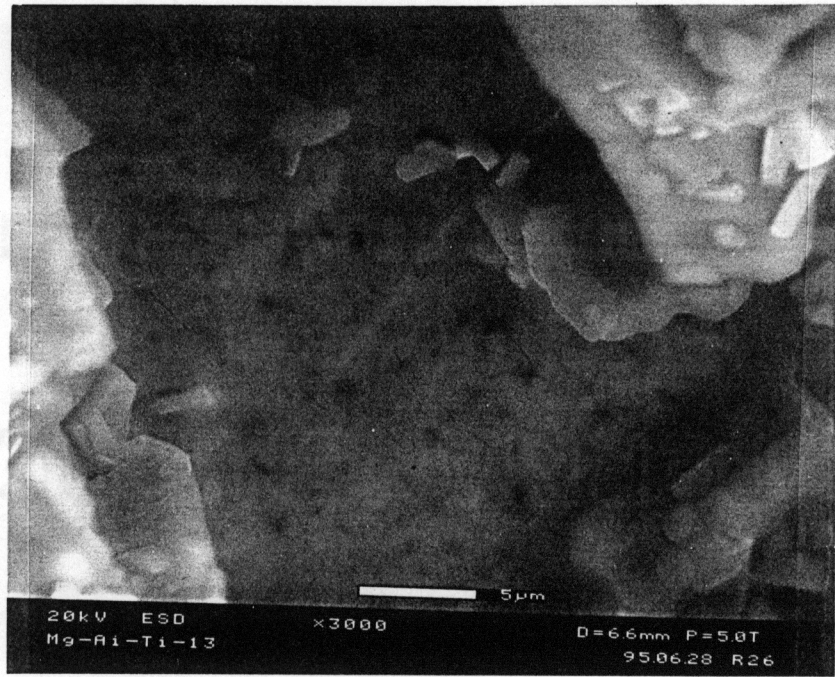


(b)

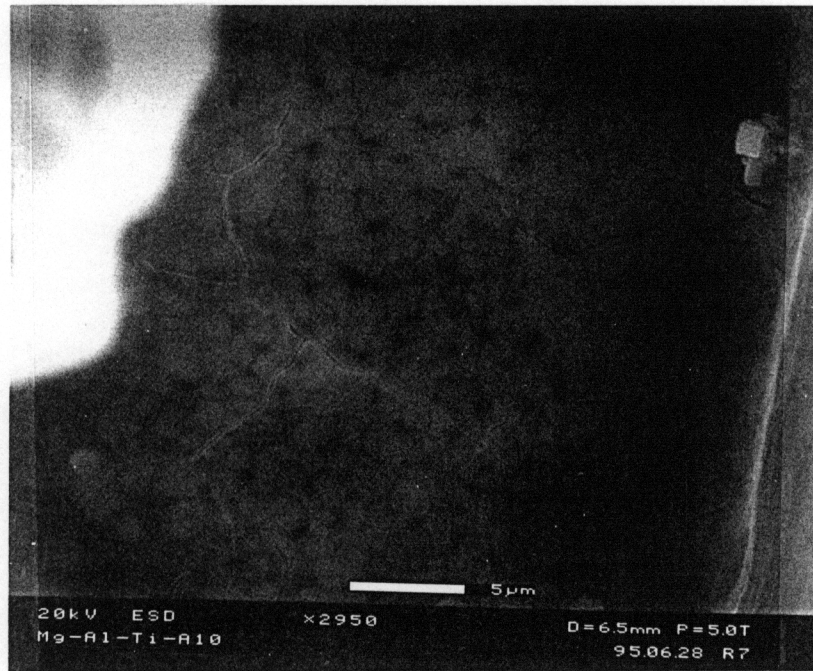
Figure 11. SEM Micrographs of Mg-Al₂TiO₅ Coatings under the Medium Solution Concentration of 1.2 mol/L and Lift Rate of 6.5 cm/min:
 (a) grains on the samples surface, (b) surface of a grain,
 (c) interior surface of a hole



(c)



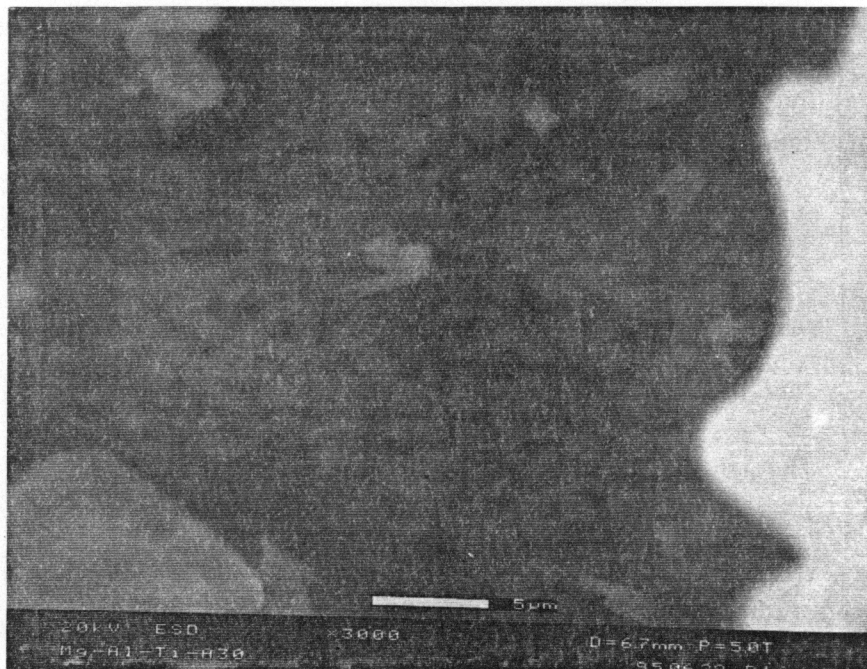
(a)



(b)

Figure 12. SEM Micrographs of Double Mg-Al₂TiO₅ Coatings of Different First and Second Coatings :

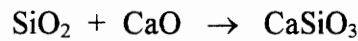
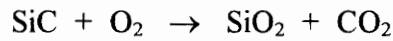
- (a) thickness of first and second coatings is 6 μm and 2 μm, respectively
- (b) thickness of first and second coatings is 4 μm
- (c) thickness of first and second coatings is 2 μm and 6 μm, respectively



(c)

4. 2 Obtaining Pure CMZP Phase

Although over 40 CMZP coated samples have been calcined in air, none of them have yielded pure CMZP phase. The typical X-ray diffraction pattern is shown in Figure 13, indicating a strong peak of CaSiO_3 which originated from the oxidation of SiC and reaction of SiO_2 and CaO creating CaSiO_3 :



The results of these experiments pointed out that it is impossible to obtain pure CMZP phase when samples were fired in air. In order to obtain the pure phase, samples were fired in controlled atmospheres and the results are described bellow:

1). The samples were first fired in air at 400°C for six hours, then fired in a covered crucible fully filled with CMZP powder at 1200°C for 24 hours. Figure 14 is the X-ray diffraction patterns showing the pure CMZP phase.

2). The samples were fired in a mildly reducing atmosphere. The samples were placed in a covered crucible and small amount of carbon powder was put in it, and the lid was sealed with liquid K_2SiO_3 . It was important to utilize just a little carbon powder to keep the atmosphere mildly reducing. The X-ray diffraction pattern in Figure 15 shows the CMZP phase is nearly pure.

3). The samples were fired in CO_2 atmosphere. The samples were placed in a covered crucible which was then filled some CaCO_3 . At high temperature CaCO_3

decomposed into CO₂, keeping the atmosphere CO₂ -rich. The X-ray diffraction pattern in Figure 16 shows that the CMZP phase is nearly pure.

4). The samples were fired in a covered crucible sealed with liquid K₂SiO₃. This results in an atmosphere in which the oxygen is less than in air but richer than in previous cases. The X-ray diffraction pattern in Figure 17 shows only partial CMZP phase formed.

5). The samples were fired in N₂. The samples were fired in the tube furnace with flow of N₂. Carbon powder was found on the internal wall of the tube and surface of the samples, because SiC and N₂ reacted under high temperature creating carbon:



This result pointed out that it is impossible to prevent oxidation when firing coated SiC samples in N₂ atmosphere. Table 6 shows the comparison of different coatings under different firing atmosphere.

Table 6. Comparison of Different CMZP Coatings under Different Firing Atmospheres

Atmosphere	Method	Abundance of O ₂	Purity of CMZP Phase
isolated from air	crucible with lid and fully filled with CMZP powder	no O ₂	high
poor O ₂	crucible with C and lid sealed with K ₂ SiO ₃	poor	good
rich CO ₂	crucible with lid and CaCO ₃	poor	good
partial O ₂	crucible with lid sealed with K ₂ SiO ₃	partial	poor
air	in air	rich	poor

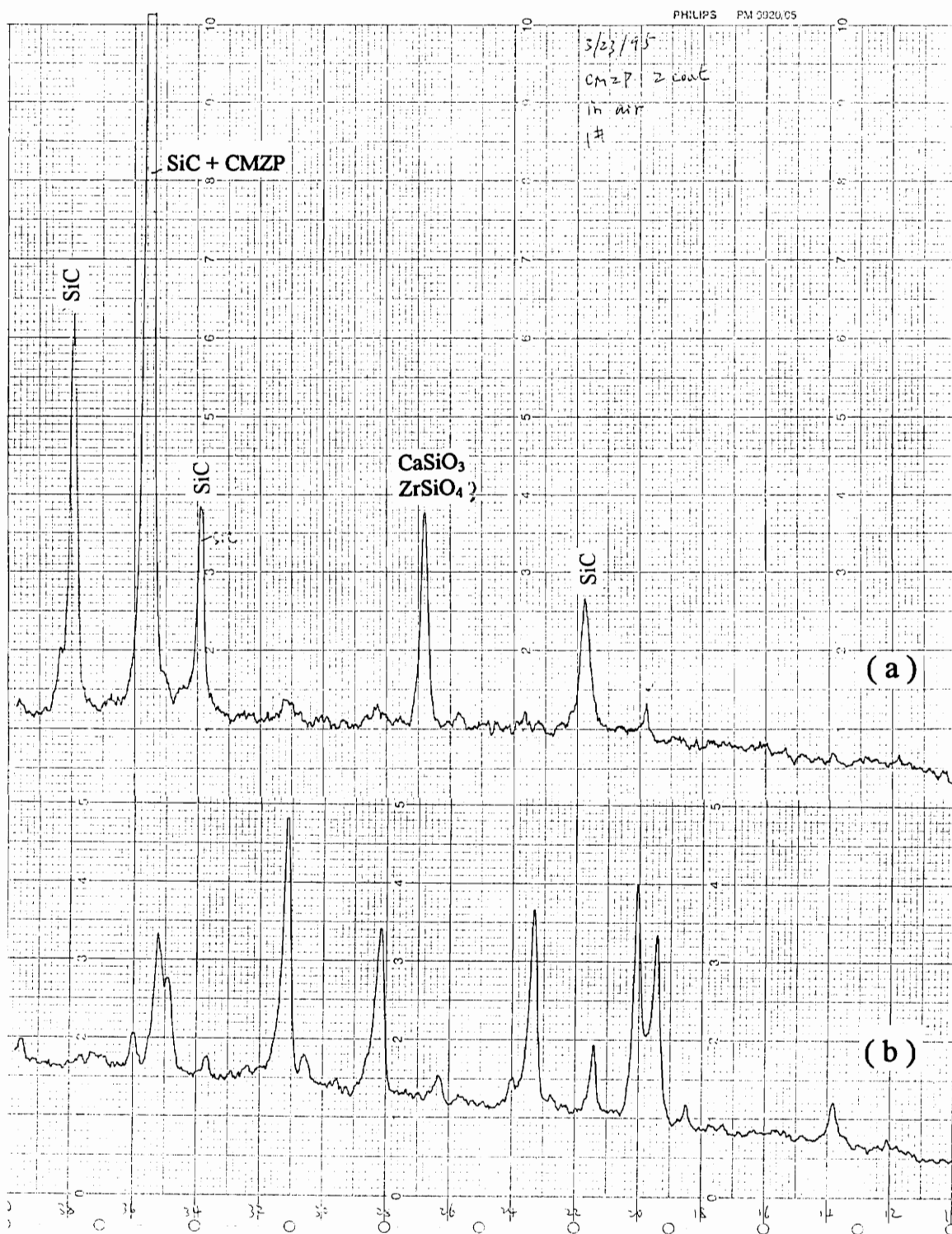


Figure 13. X-Ray Diffraction Patterns of CMZP Coating Fired in Air (a) and CMZP Powder (b)

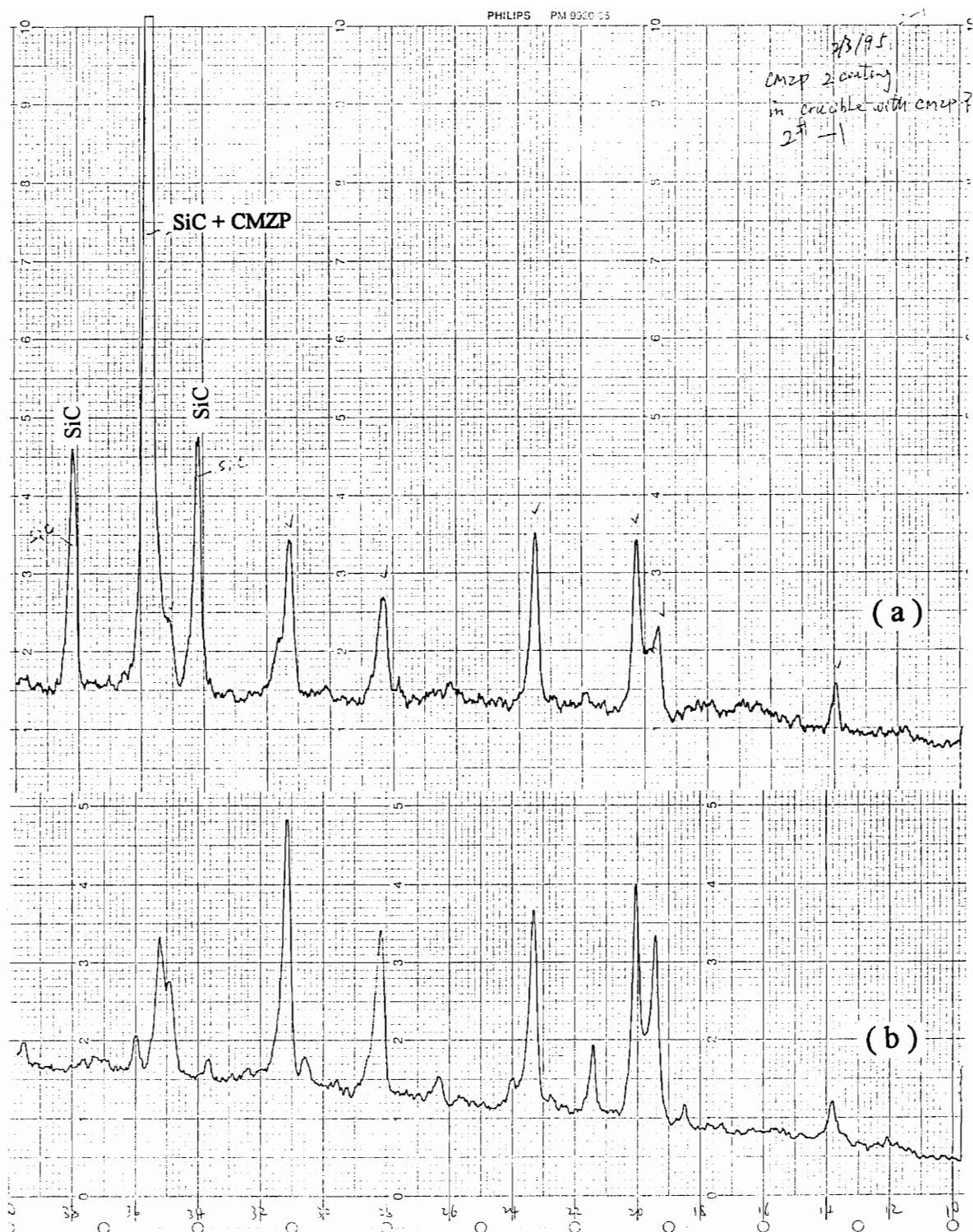


Figure 14. X-Ray Diffraction Patterns of CMZP Coating Fired Isolated from Air (a) and CMZP Powder (b)

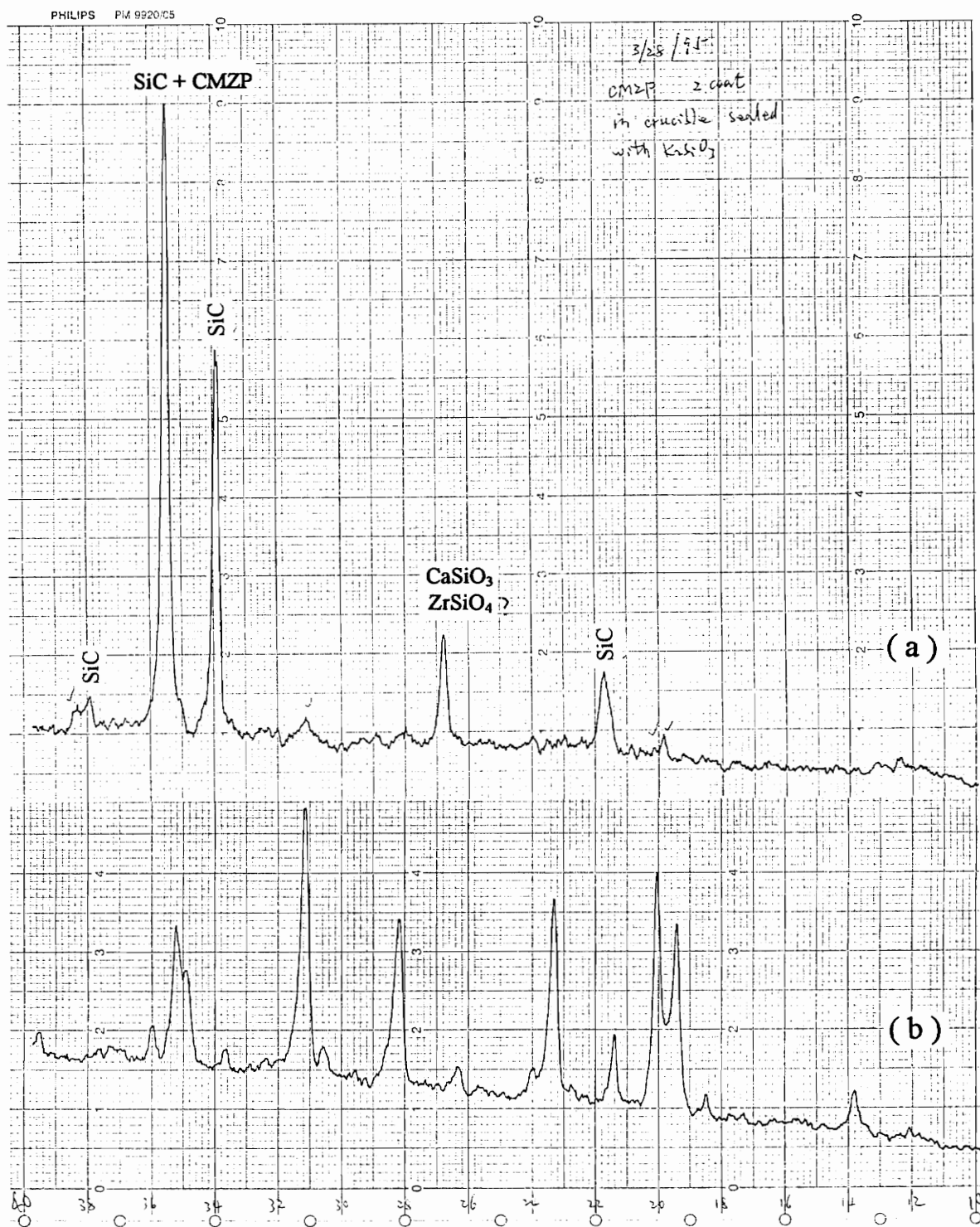


Figure 15. X-Ray Diffraction Patterns of CMZP Coating Fired in the Atmosphere of Poor Oxygen (a) and CMZP Powder (b)

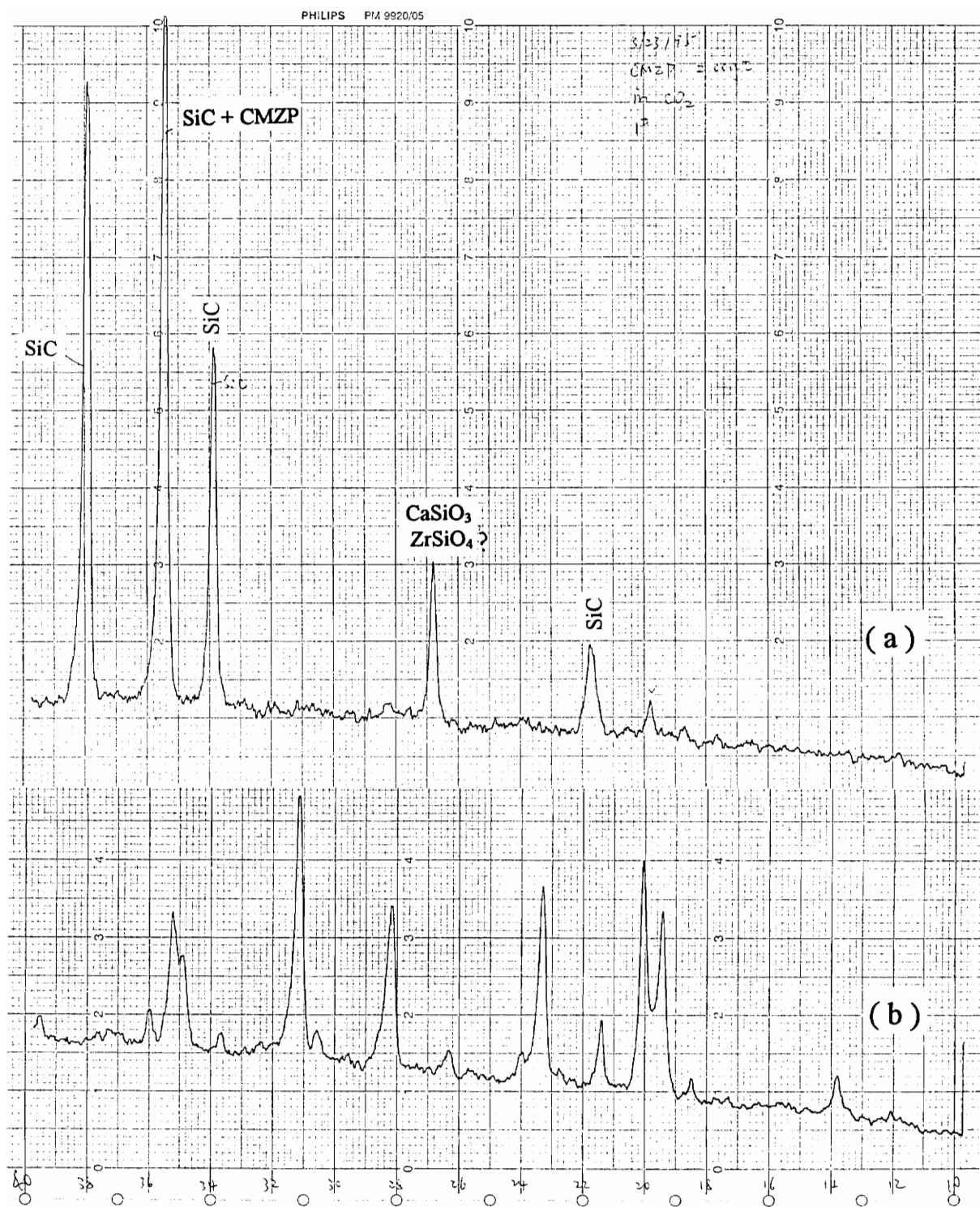


Figure 16. X-Ray Diffraction Patterns of CMZP Coating Fired in the Atmosphere of Rich CO₂ (a) and CMZP Powder (b)

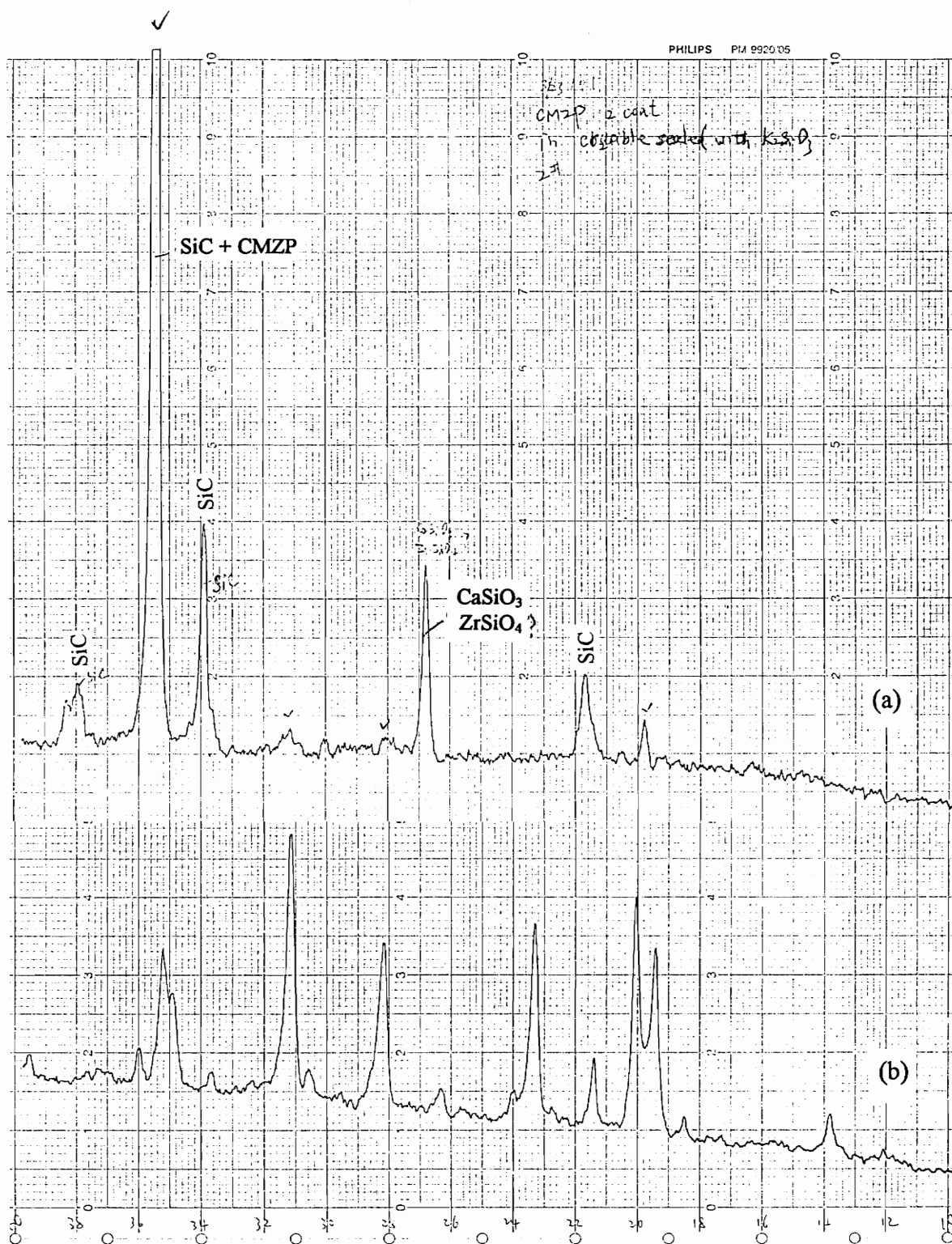


Figure 17. X-Ray Diffraction Patterns of CMZP Coating Fired in the Atmosphere of Partial Oxygen (a) and CMZP Powder (b)

4.3 Improving Mg-Al₂TiO₅ Coating Procedure

A procedure of coating Mg-Al₂TiO₅ to SiC utilizing hydrolyzed solution of Mg-Al₂TiO₅ was described by Kang[9]. However the hydrolyzed solution is very sticky even though the concentration is small. It is , therefore, difficult to obtain homogeneous coating layers. Over 40 samples coated with Mg-Al₂TiO₅ utilizing hydrolyzed Mg-Al₂TiO₅ solution were tested, however, none of them had pure phase. The typical X-ray diffraction pattern is shown in Figure 18.

The process has been changed as follows:

1. Coat the samples utilizing unhydrolyzed Mg-Al₂TiO₅ solution instead of hydrolyzed solution to decrease the viscosity and increase the concentration.
2. Place the samples in a container with saturated humidity for three days for hydrolysis.
3. Dry the samples in air at room temperature for three days.
4. Further dry the samples at 65°C for 12 hours.
5. Fire the samples in air at 400°C for 6 hours.
6. Coat the samples a second time, then hydrolyze and dry the samples similarly to the first coating.

Figure 19 shows the X-ray diffraction patterns of the improved coatings and the formation of nearly pure Mg-Al₂TiO₅ phase.

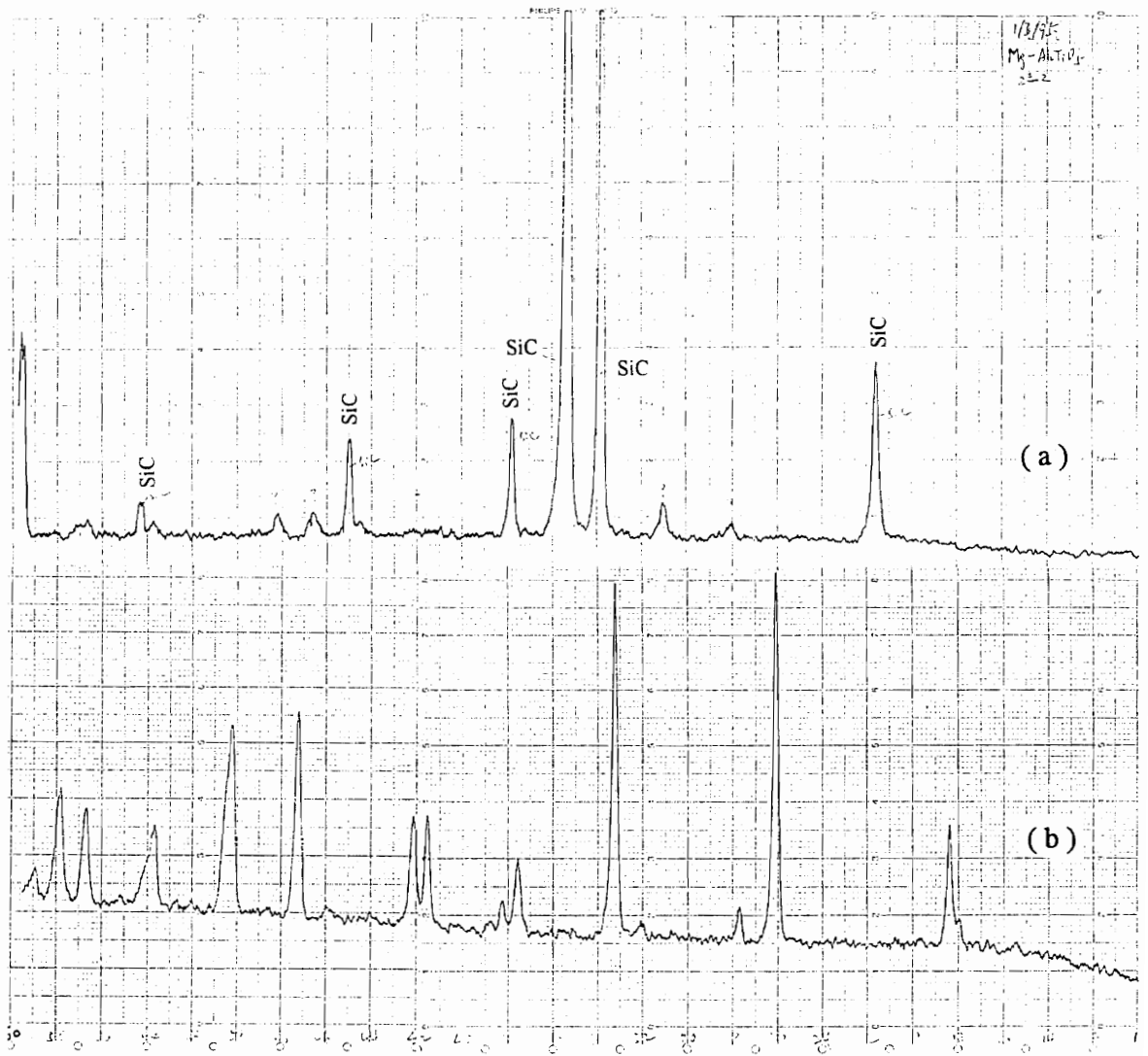


Figure 18. X-Ray Diffraction Patterns of Mg-Al₂TiO₅ Coating Utilizing Hydrolyzed Solution (a) and Mg-Al₂TiO₅ Powder (b)

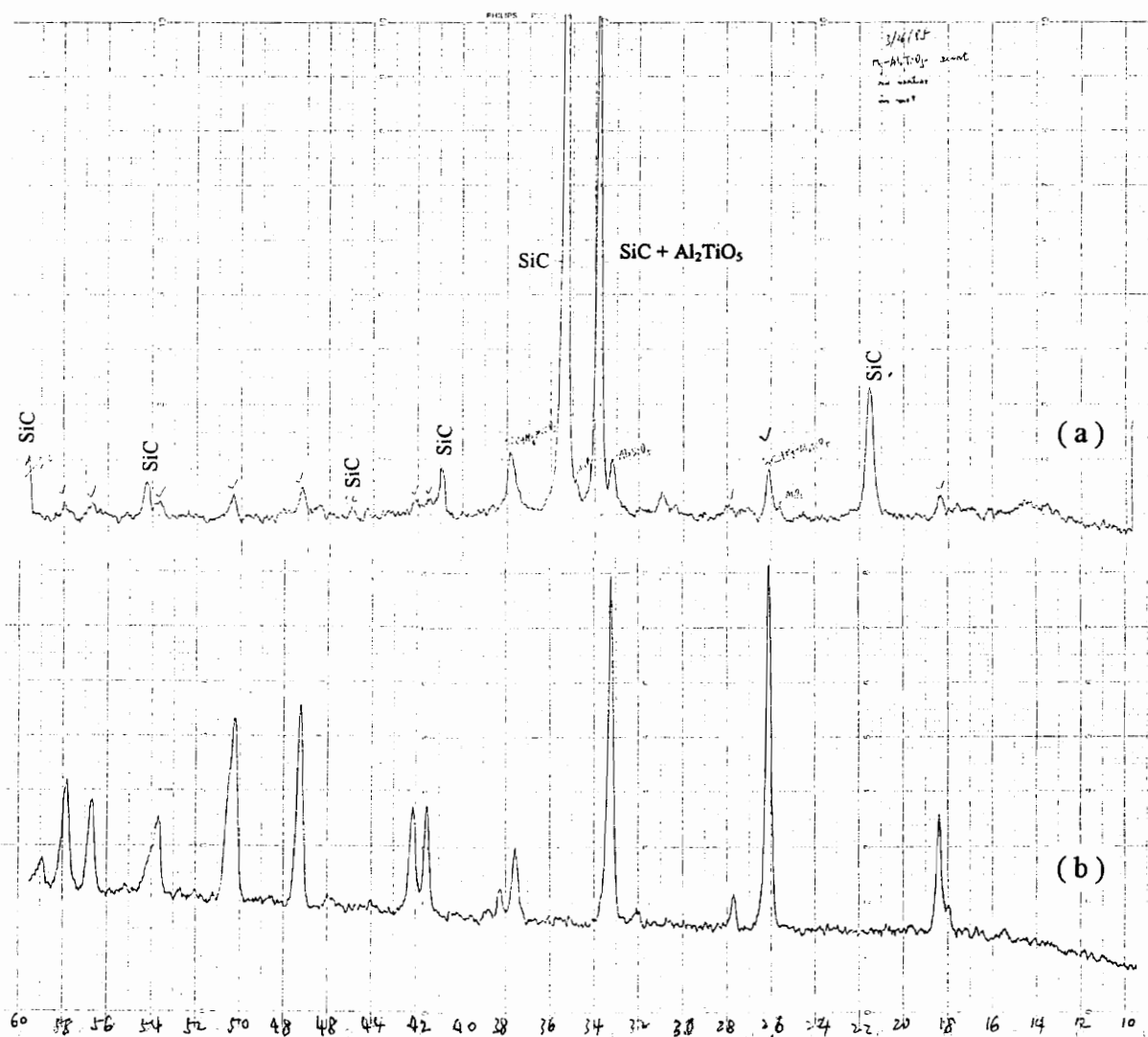


Figure 19. X-Ray Diffraction Patterns of Mg- Al_2TiO_5 Coating Utilizing Unhydrolyzed Solution (a) and Mg- Al_2TiO_5 Powder (b)

4.4 Thermal Shock Resistance

1). CMZP Coatings

Thermal shock resistance of CMZP coatings was examined. The experimental results are shown in Table 7. Surface microstructure of coatings and adhesion between the coatings and substrates were examined by SEM. Figure 20 shows the surface microstructure of the samples after thermal shock of 1000°C exhibited cracks and small spalling. Figure 21 shows after a 750°C thermal shock, cracks appeared but no spalling; and Figure 22 shows after a 500°C thermal shock, no cracks were present.

Table 7. The Thermal Shock Resistance of CMZP Coated SiC Samples

Sample	Heated Temperature and Results			
	300°C	500°C	750°C	1000°C
Group 1 (4 samples)	no cracks			
Group 2 (4 samples)		no cracks		
Group 3 (4 samples)			cracks	
Group 4 (4 samples)				cracks and small spalling

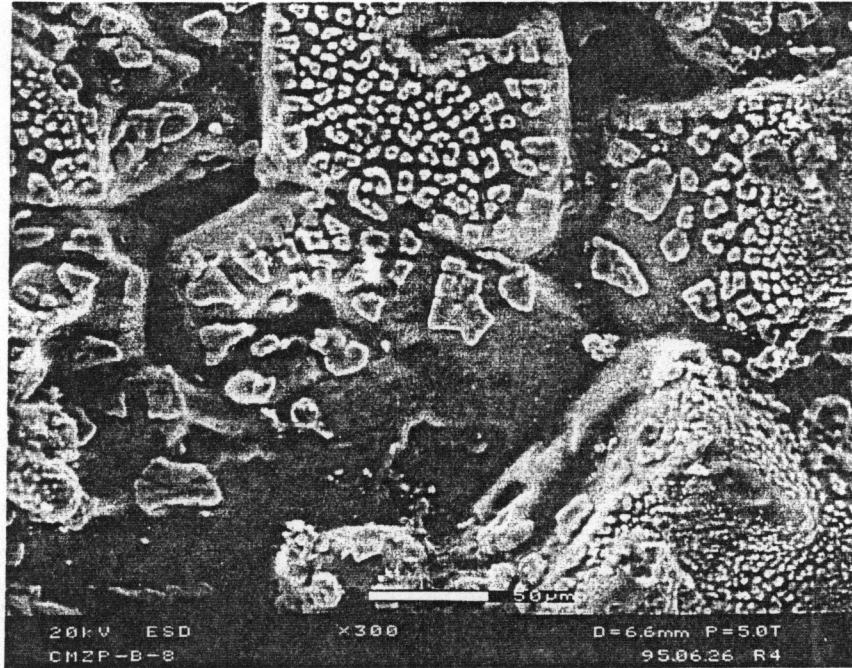


Figure 20. Surface Microstructure of CMZP Coated Samples Exhibited Cracks and Small Spalling after a Thermal Shock of 1000°C

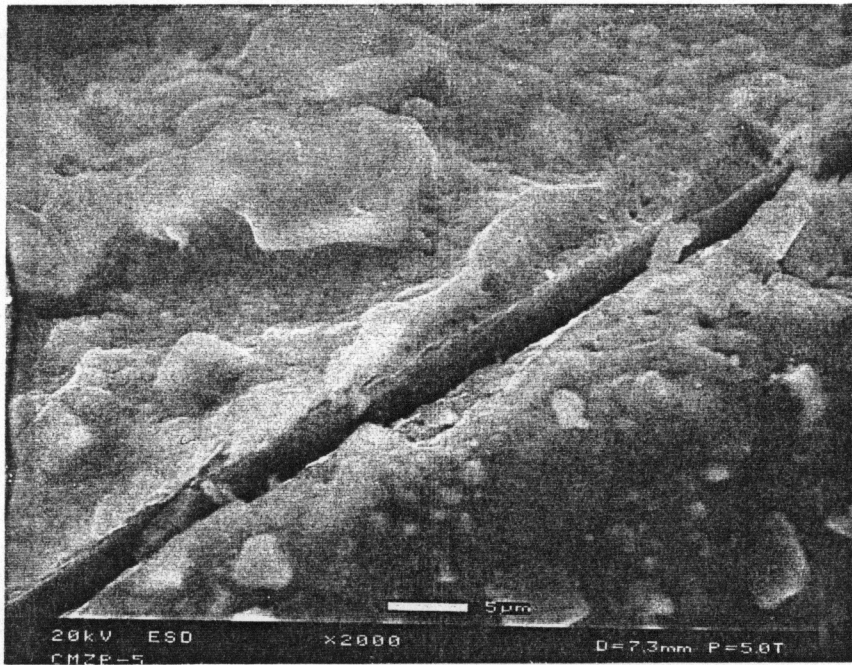


Figure 21. Surface Microstructure of CMZP Coated Samples Exhibited Cracks after a Thermal Shock of 750°C

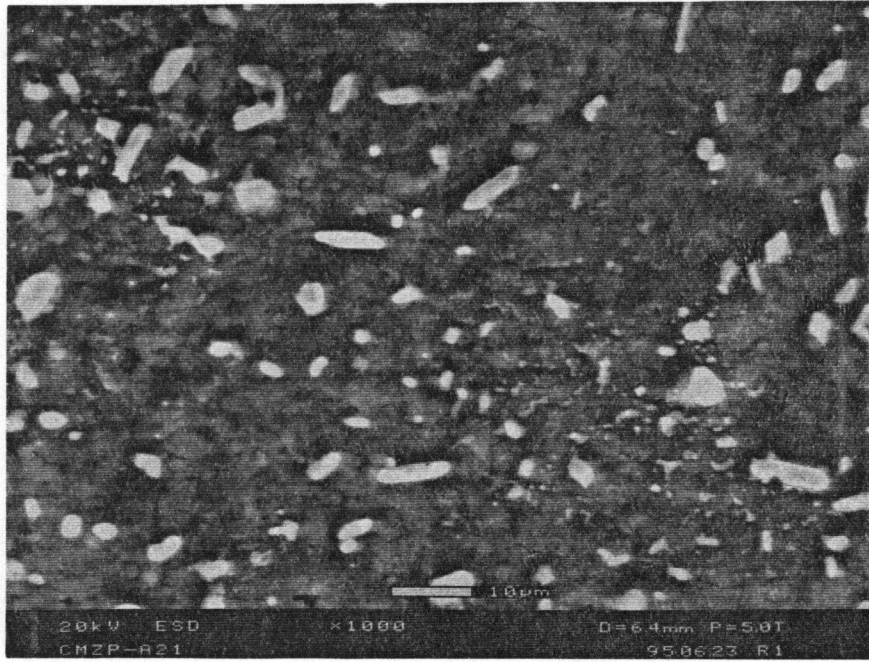


Figure 22. Surface Microstructure of CMZP Coated Samples Exhibited no Cracks after a Thermal Shock of 500°C

(2). Mg-Al₂TiO₅ Coated Samples

The thermal shock resistance of Mg-Al₂TiO₅ coated SiC samples was also examined. The experimental results are shown in Table 8. Surface microstructure of coatings and adhesion between the coatings and substrates were examined by SEM. Figure 23 Shows the surface microstructure of the samples after a thermal shock of 1000°C exhibited cracks and small spalling. Figure 24 shows after 750°C thermal shock, cracks appeared; and Figure 25 shows after a 500°C thermal shock, no cracks present.

Table 8. Thermal Shock Resistance of Mg-Al₂TiO₅ Coated SiC Samples

Sample	Heated Temperature and Results			
	300°C	500°C	750°C	1000°C
Group 1 (4 samples)	no cracks			
Group 2 (4 samples)		no cracks		
Group 3 (4 samples)			cracks	
Group 4 (4 samples)				cracks and small spalling



Figure 23. Surface Microstructure of Mg-Al₂TiO₅ Coated Samples Exhibited Cracks and Small Spalling after a Thermal Shock of 1000°C

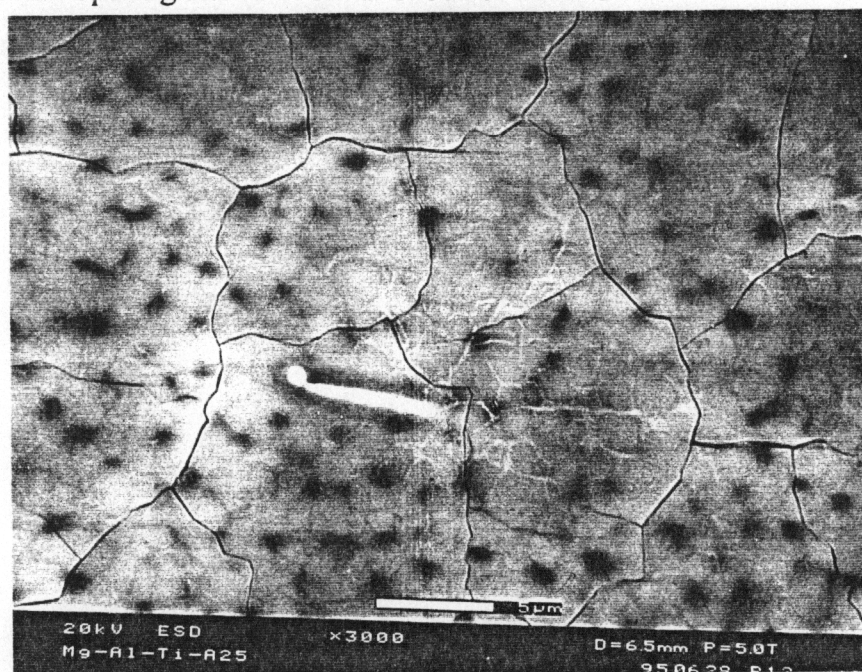


Figure 24. Surface Microstructure of Mg-Al₂TiO₅ Coated Samples Exhibited Cracks after a Thermal Shock of 750°C

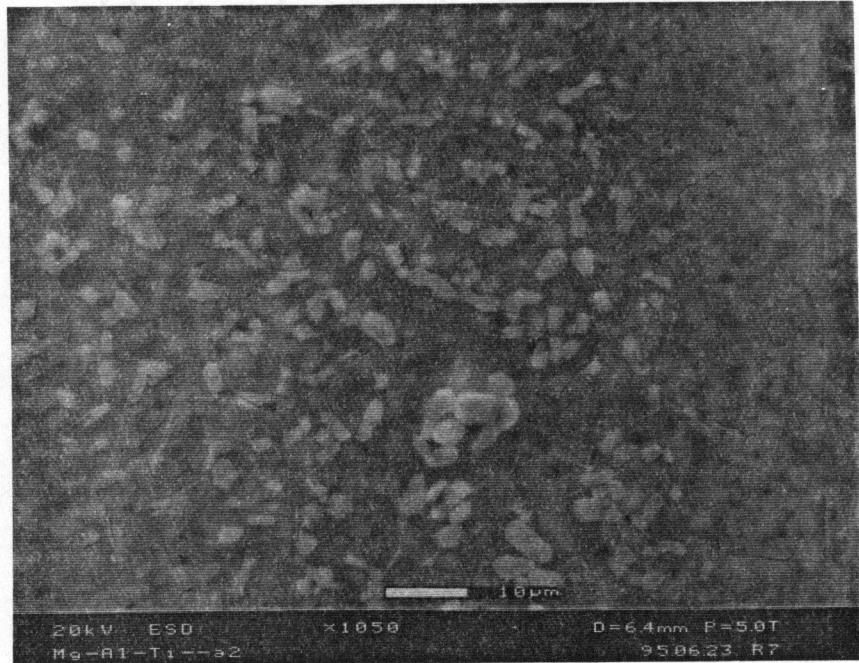


Figure 25. Surface Microstructure of Mg-Al₂TiO₅ Coated Samples Exhibited no Cracks after a Thermal Shock of 500°C

4.5 Alkali Corrosion Resistance

1). CMZP Coatings

Table 9 shows the weight loss and Table 10 shows the room temperature flexural strength of both as-received and corroded SiC samples determined by 4-point bending using an ATS Test System. To decrease the effect of random errors, the average strengths of every group were reported. Many other groups of CMZP coated and as-received samples were also examined and the statistical results were similar to the results as described above.

Table 9. The Weight Loss of CMZP Coated and Uncoated Samples after Sodium Corrosion (%)

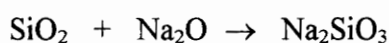
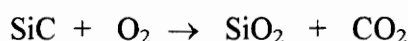
	1100°C		1000°C		900°C	
	Coated	Uncoated	Coated	Uncoated	Coated	Uncoated
Obtained Value	2.8	3.7	2.1	3.6	2.3	3.7
	2.4	3.6	2.0	3.5	2.7	3.4
	2.1	3.3	2.7	3.2	1.9	3.3
	2.2	2.6	2.6	2.5	2.1	2.4
Average Value	2.4	3.3	2.4	3.2	2.3	3.2

Table 10. Flexural Strength of CMZP Coated and Uncoated SiC Samples before and after Sodium Corrosion (Mpa)

	Before Corrosion		1100°C		1000°C		900°	
	Coated	Uncoated	Coated	Uncoated	Coated	Uncoated	Coated	Uncoated
Obtained Value	468	424	417	432	432	414	449	426
	455	468	469	407	411	432	438	397
	432	465	438	402	448	412	436	411
	444	447	425	410	436	398	443	408
Average Value	450	450	437	413	432	414	442	411

The sodium corrosion resistance of CMZP coated SiC samples was improved over that of uncoated samples as indicated in Figure 26 and 27. Compared to CMZP coated samples, uncoated samples exhibited a greater weight loss and reduction in strength. The SEM micrograph of uncoated SiC after corrosion, Figure 28, shows the formation of holes on surface and considerable penetration of alkali.

SiC is thermodynamically unstable in air and relies on a thin film of SiO₂ for oxidation protection. The SiO₂ film on SiC, although very thin, is normally protective in an oxidizing atmosphere at high temperature. The presence of sodium with SiC dissolves the SiO₂ protective film and enhances oxidation. It is believed that the following reactions occur:



The protective SiO₂ film is dissolved to form Na₂SiO₃. Accelerated scale growth occurs because the silicate is liquid at 1000°C. The CMZP reacts with SiO₂ film on the surface of the SiC substrates and sodium to produce a more refractory layer, which assists in maintaining a continuous reaction layer and minimizes corrosion. The SEM micrograph, Figure 29, shows that a dense protective layer on the surface of CMZP coated SiC samples was formed after sodium corrosion. Figure 30 shows the distribution of Ca, Mg, Zr, P and Si on the sample surface, obtained by EDX, which proves that the protective layer came from CMZP.

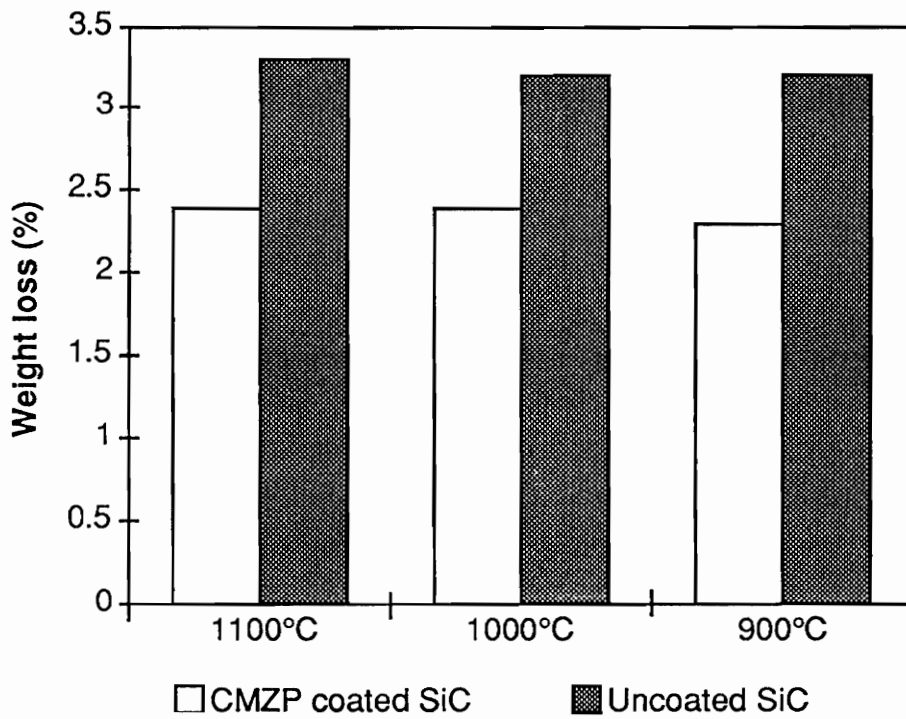


Figure 26. Weight Loss of CMZP Coated and Uncoated SiC Samples after Sodium Corrosion

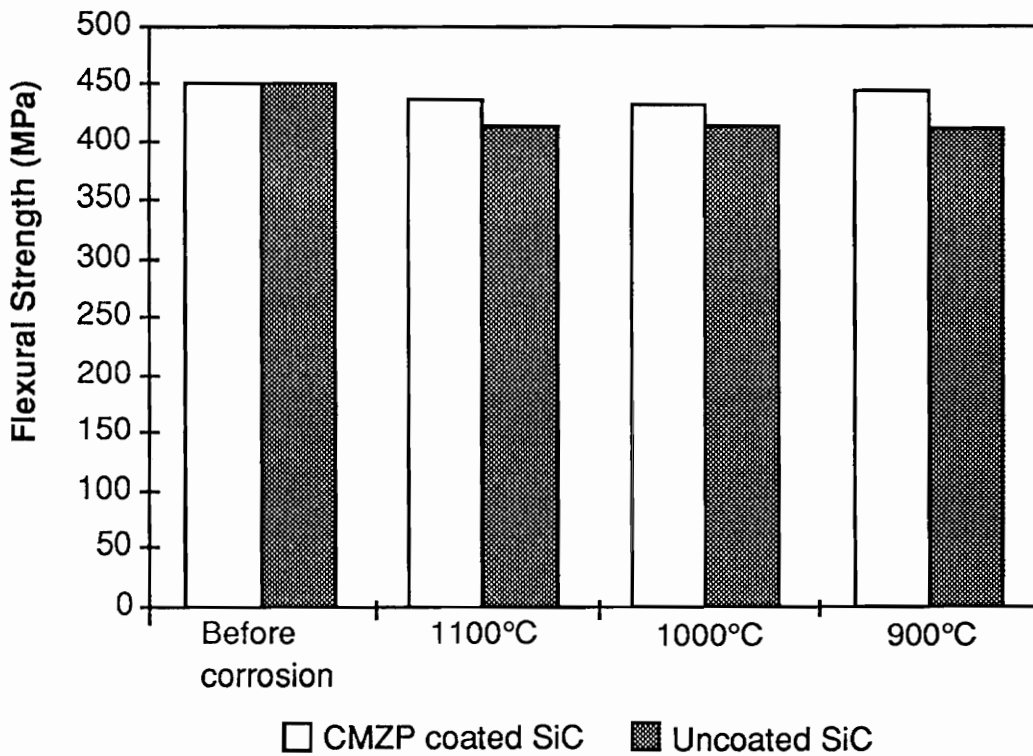


Figure 27. Flexural Strength of CMZP Coated and Uncoated SiC Samples before and after Sodium Corrosion

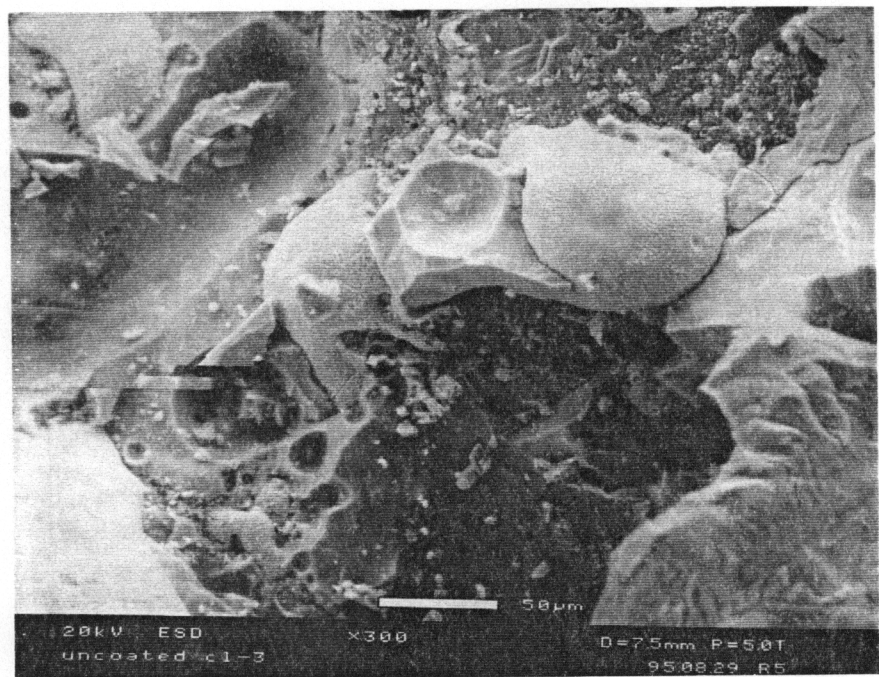


Figure 28. Corrosion of Uncoated SiC Samples by Sodium Carbonate

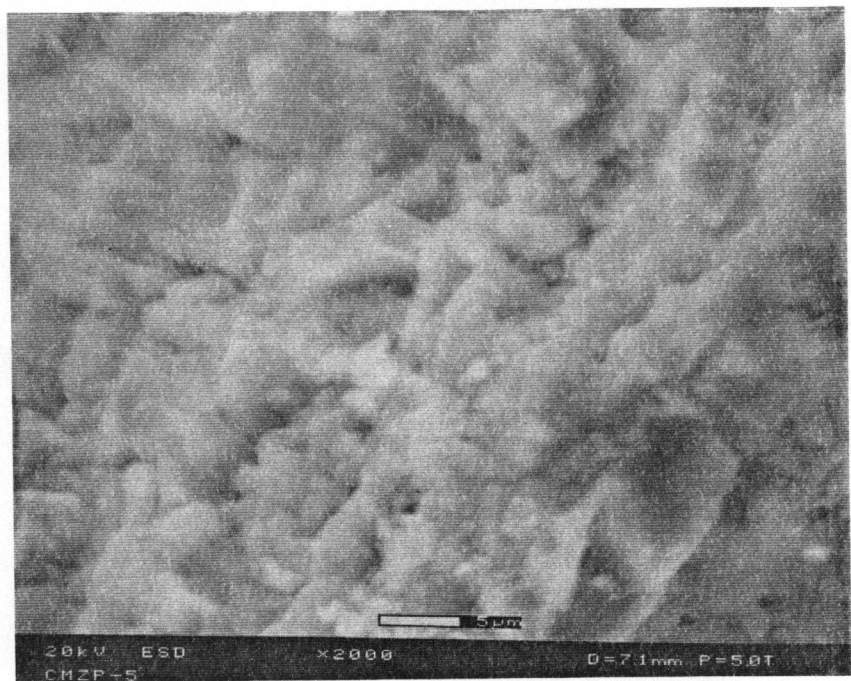


Figure 29. Dense Protective Layer on Surface of CMZP Coated SiC Samples Formed after Sodium Corrosion

Spectrum: CMZP
Comments:

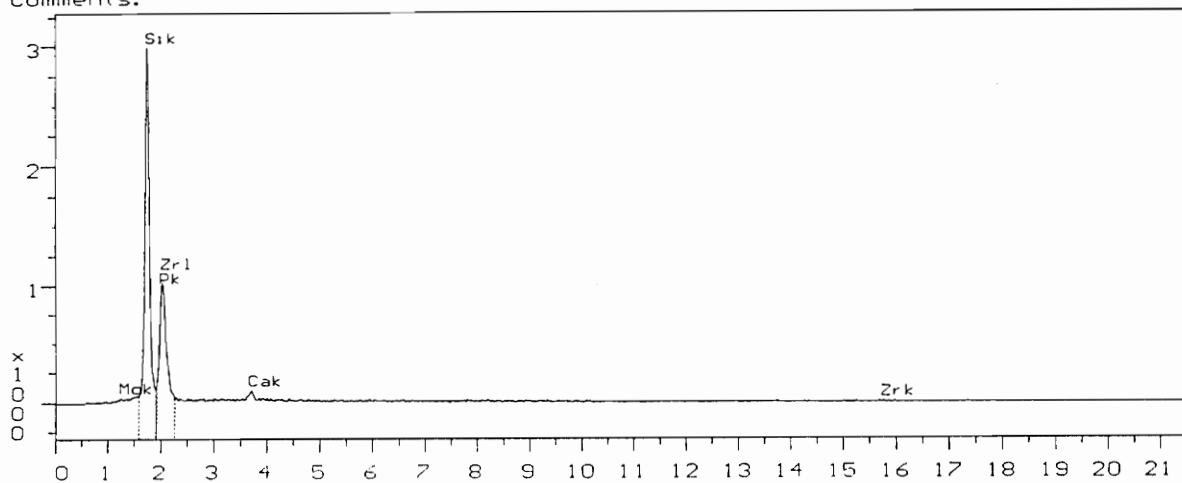


Figure 30. Distribution of Ca, Mg, Zr, P and Si on Sample Surfaces, Obtained by EDX, Proves that the Protective Layer Came from CMZP Coating

2). $\text{Mg-Al}_2\text{TiO}_5$ Coatings

The sodium corrosion resistance of $\text{Mg-Al}_2\text{TiO}_5$ coated SiC samples was improved over that of uncoated samples as indicated in Table 11 and 12, and Figure 31 and 32.

Compared to $\text{Mg-Al}_2\text{TiO}_5$ coated SiC samples, uncoated samples exhibited a greater weight loss. Many other groups of $\text{Mg-Al}_2\text{TiO}_5$ coated and as-received samples were also examined and the statistical results were similar to the results as described above.

Table 11. The Weight Loss of $\text{Mg-Al}_2\text{TiO}_5$ Coated and Uncoated Samples after Sodium Corrosion (%)

	1100°C		1000°C		900°C	
	Coated	Uncoated	Coated	Uncoated	Coated	Uncoated
Obtained Value	3.1	2.9	2.4	4.1	3.2	3.2
	2.8	3.0	2.2	3.8	2.1	3.7
	2.4	3.5	2.6	3.6	2.5	4.0
	2.3	3.8	3.3	3.0	2.3	4.3
Average Value	2.7	3.3	2.6	3.6	2.5	3.8

Table 12. Flexural Strength of $\text{Mg-Al}_2\text{TiO}_5$ Coated and Uncoated SiC Samples before and after Sodium Corrosion (Mpa)

	Before Corrosion		1100°C		1000°C		900°	
	Coated	Uncoated	Coated	Uncoated	Coated	Uncoated	Coated	Uncoated
Obtaind Value	464	469	424	401	441	434	447	419
	432	423	462	404	419	409	436	437
	453	446	441	413	456	404	432	416
	447	463	414	431	442	413	443	403
Average Value	449	450	435	412	439	415	440	419

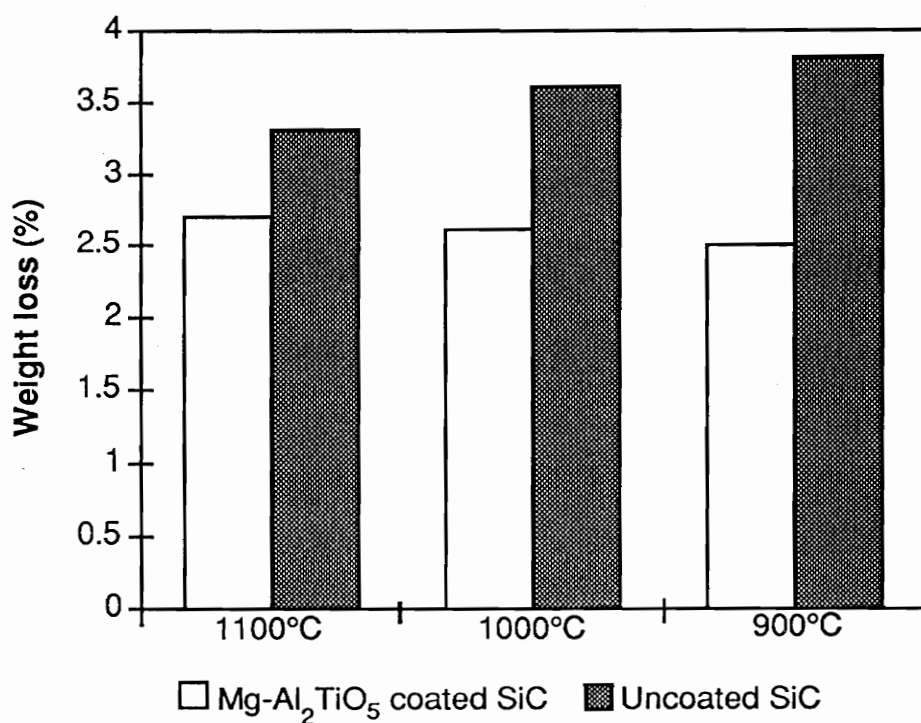


Figure 31. Weight Loss of Mg-Al₂TiO₅ Coated and Uncoated SiC Samples after Sodium Corrosion

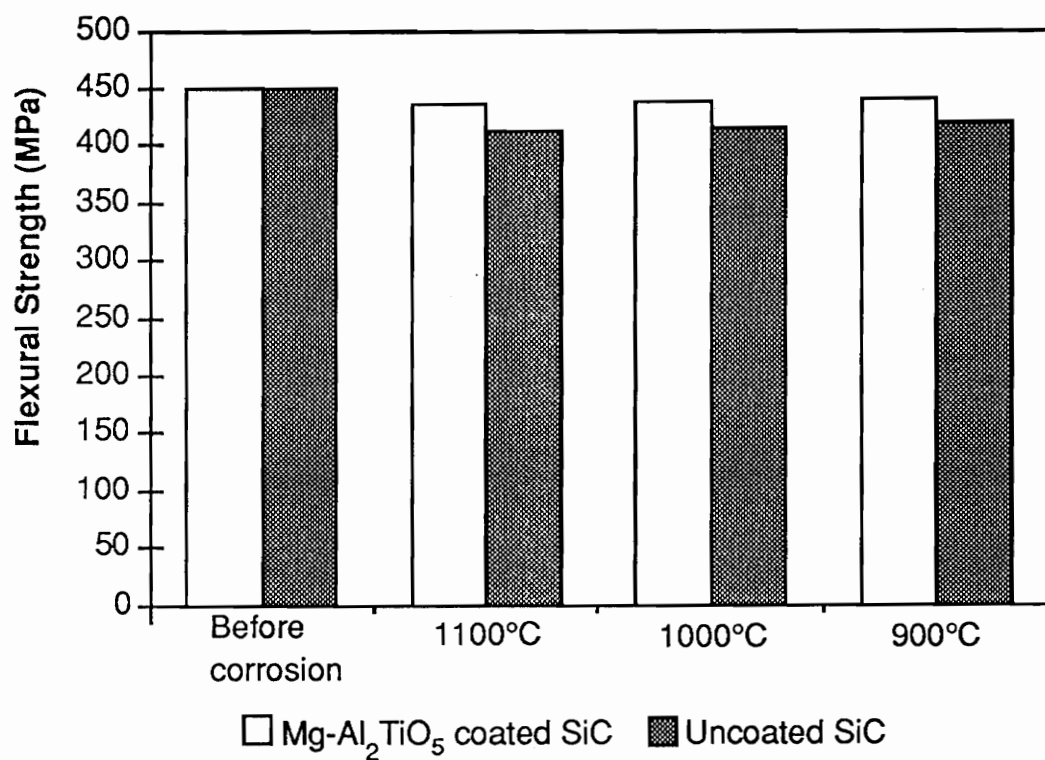


Figure 32. Flexural Strength of Mg-Al₂TiO₅ Coated and Uncoated SiC Samples before and after Sodium Corrosion

The mechanism of improving corrosion resistance of Mg-Al₂TiO₅ coated SiC samples is similar to that of CMZP coated samples described above. SEM micrograph, Figure 33, shows that a dense protective layer on the surface of Mg-Al₂TiO₅ coated SiC samples was formed after sodium corrosion. Figure 34 shows the distribution of Mg, Al, Ti and Si on the sample surface, obtained by EDX, proves that the protective layer came from Mg-Al₂TiO₅ coating.

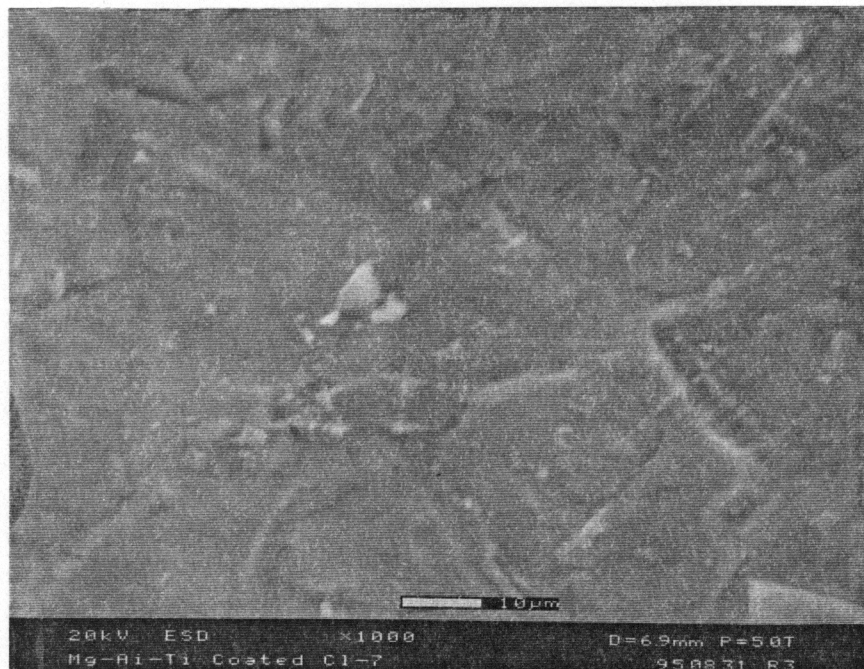
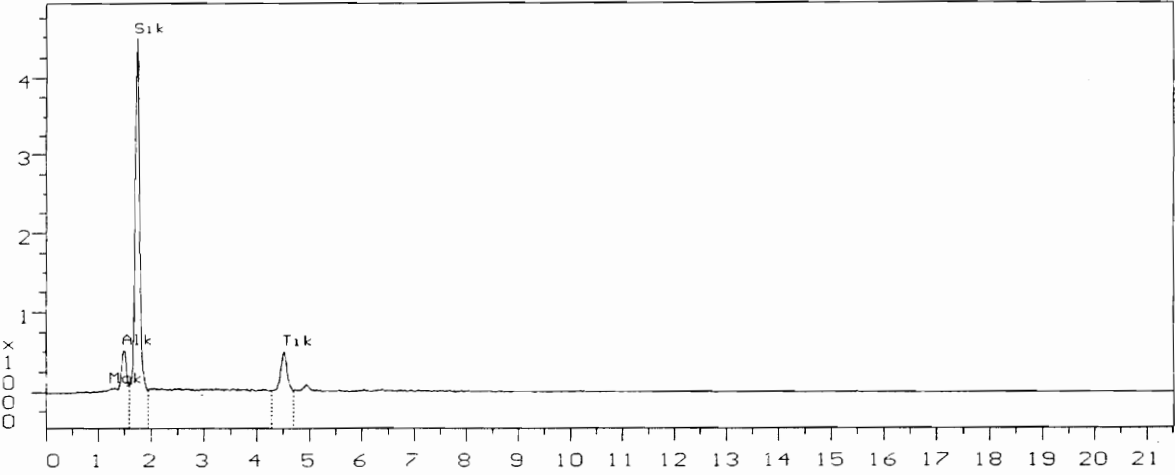


Figure 33. Dense Protective Layer on Surface of $\text{Mg-Al}_2\text{TiO}_5$ Coated SiC Samples Formed after Sodium Corrosion

Spectrum: MGAL2TIO
Comments:



**Figure 34. Distribution of Al, Ti and Si on Samples Surface, Obtained by EDX,
Proves that the Protective Layer Came from Mg-Al₂TiO₅ Coating**

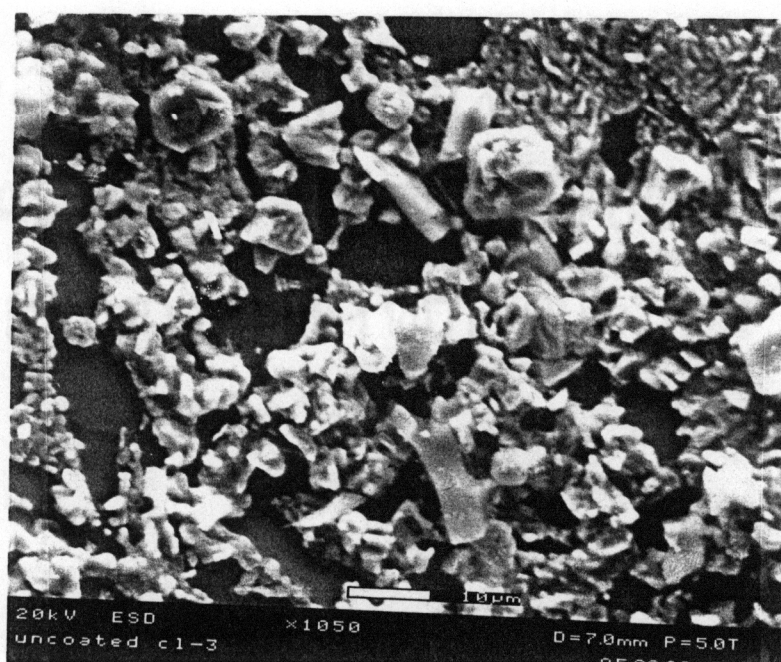
4.6 100-Hour Slagging Combustion Test

1). CMZP Coated Samples

Figure 35 shows the SEM micrographs of the uncorroded and corroded areas of the CMZP coated samples. Figure 36 shows the XRD results of the uncorroded areas of the CMZP coated samples. The CMZP phase can be distinguished although there were some other phases which were from the slag. Figure 37 shows the EDX results of the uncorroded areas of the CMZP coated samples indicating the existence of elements Ca, Mg, Zr and P. This proves the existence of the CMZP coating after the test in the coal combustion atmospheres at high temperature. It can be seen that the uncorroded SiC was coated while the corroded SiC did not have the coating on it. It is clear that the CMZP coatings improve the corrosion resistance under coal combustion atmosphere at high temperature. It was noticed that the SiC substrate was corroded if there were defects in the CMZP coating; that is, the corroded areas originated from crack or poor adhesion of the CMZP coating. So homogeneous and crack-free coating as well as enhanced adhesion of the coating are important for quality coatings. There were also some corroded areas on the sample surface which are difficult to distinguish the CMZP phase because of interference from the slag. Figure 38 shows the result of EDX analysis, indicating that the peaks of Ca, Mg, Zr and P were weak.



(a)



(b)

Figure 35. SEM Micrographs of Uncorroded Areas (a) and Corroded Areas (b) of the CMZP Coated Samples

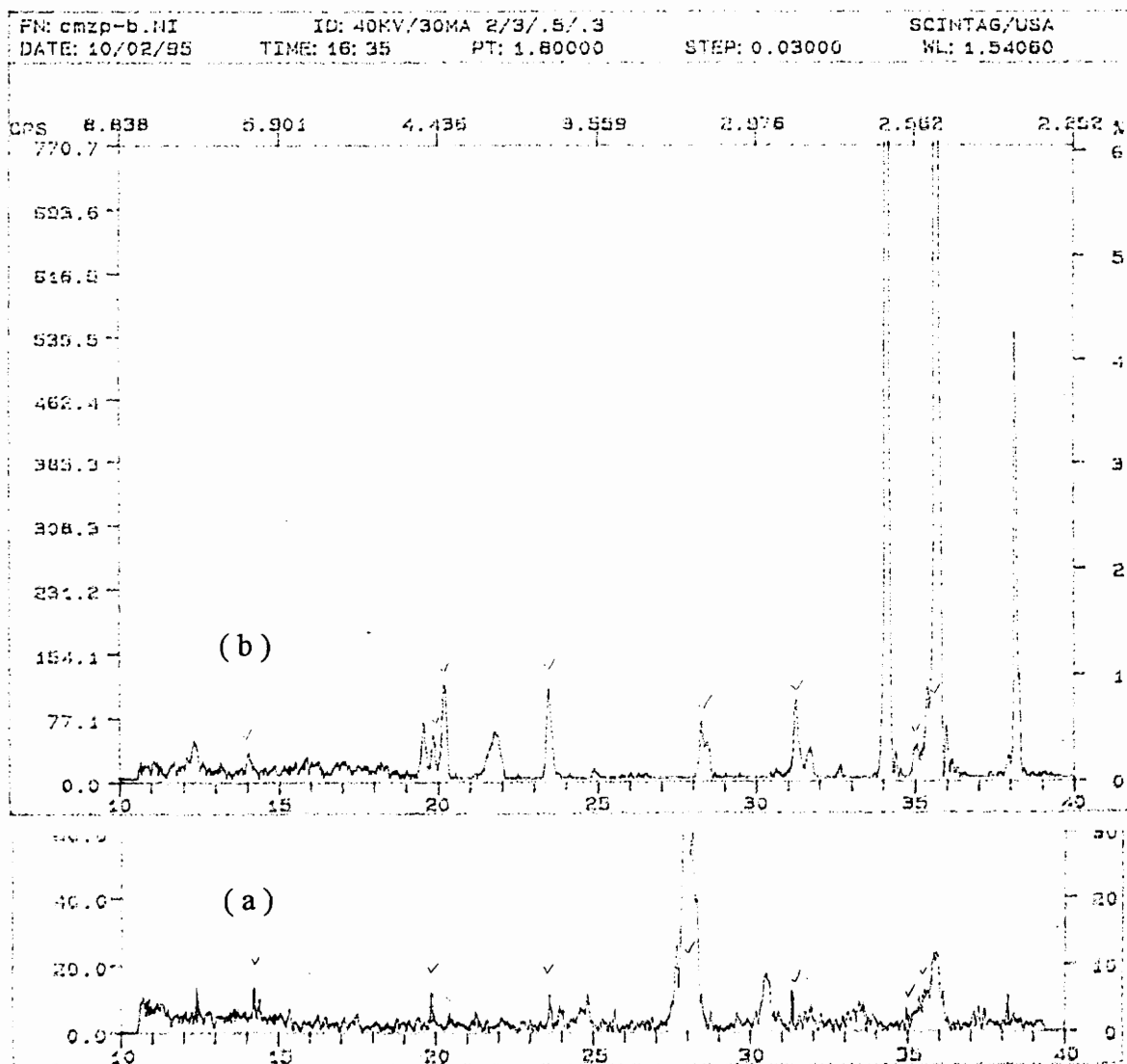


Figure 36. X-Ray Diffraction of the Uncorroded Areas of the CMZP Coating (a)and the Sample before the Corrosion Test (b)

Spectrum: CM02
Comments:

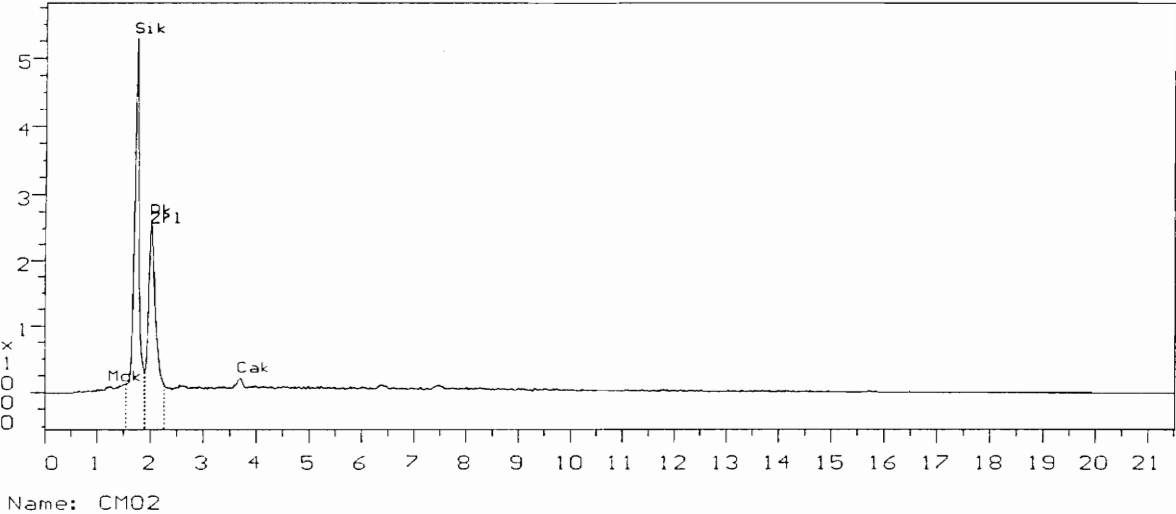


Figure 37. EDX Spectrum on a Cross-Section of the Uncorroded Areas of the CMZP Coating

Spectrum: CMZP3
Comments:

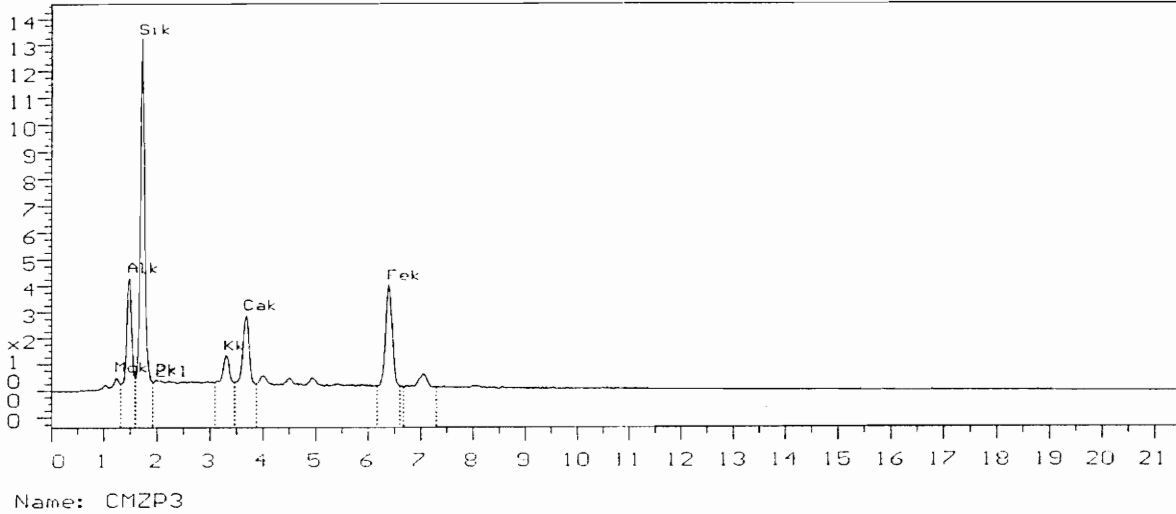
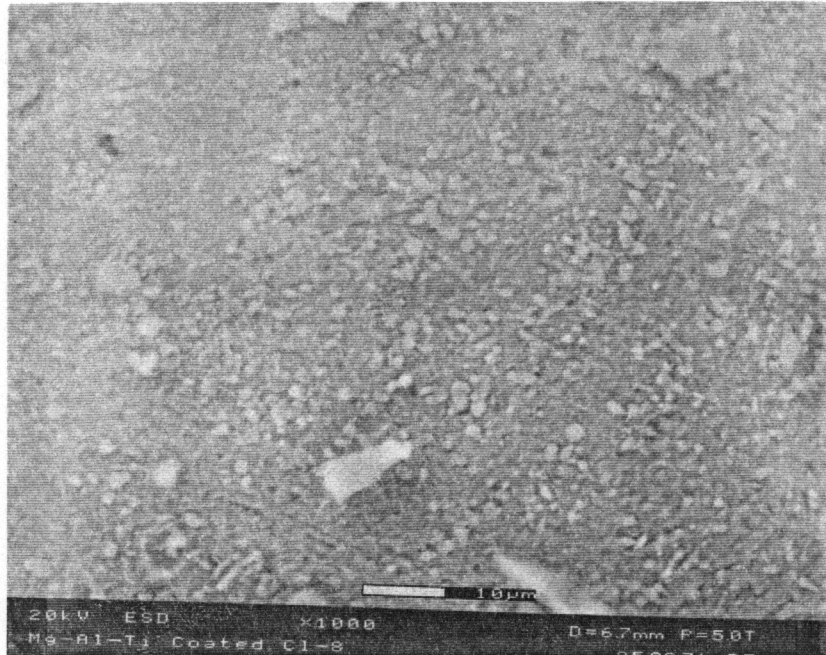


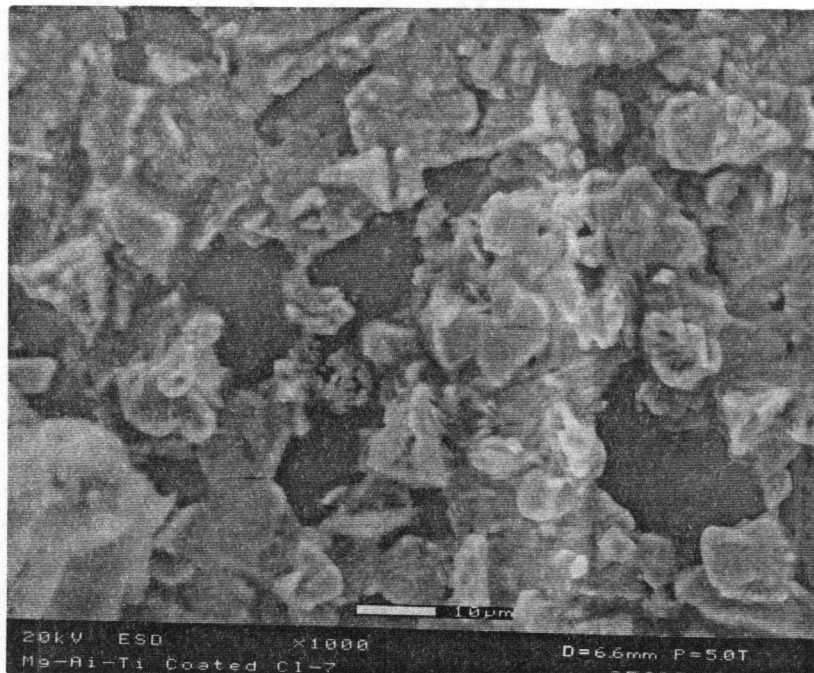
Figure 38. EDX Spectrum on a Cross-Section of the Corroded Areas of the CMZP Coating

2). Mg-Al₂TiO₅ Coated Samples

The SEM results, in Figure 39, show the uncorroded areas and corroded areas of the Mg-Al₂TiO₅ coated samples. The XRD result, in Figure 40, shows the uncorroded areas of the Mg-Al₂TiO₅ coated samples, indicating the existence of Mg-Al₂TiO₅ phase although there were some other phase from the slag. The EDX result, in Figure 41, shows the existence of elements Al, Ti and Mg, indicating the existence of Mg-Al₂TiO₅ coating after the test of coal combustion atmosphere at high temperature. It can be seen that, similar to CMZP coatings, the uncorroded SiC substrate had the Mg-Al₂TiO₅ coating on it while the corroded SiC substrate did not have the coating on it. Also the SiC substrate was corroded if there were defects in the Mg-Al₂TiO₅ coating; that is, the corroded areas originated from crack or poor adhesion of the coating. Homogeneous and crack-free coatings as well as enhanced adhesion of the coatings are clearly important for high quality coatings. At the corroded areas of the samples the Mg-Al₂TiO₅ phase can not be distinguished from the covering slag. The EDX result, in Figure 42, shows the existence of the elements Al, Ti and Mg; however, the peaks were weak.



(a)



(b)

Figure 39. SEM Micrographs of Uncorroded Areas (a) and Corroded Areas (b) of the $\text{Mg-Al}_2\text{TiO}_5$ Coated Samples

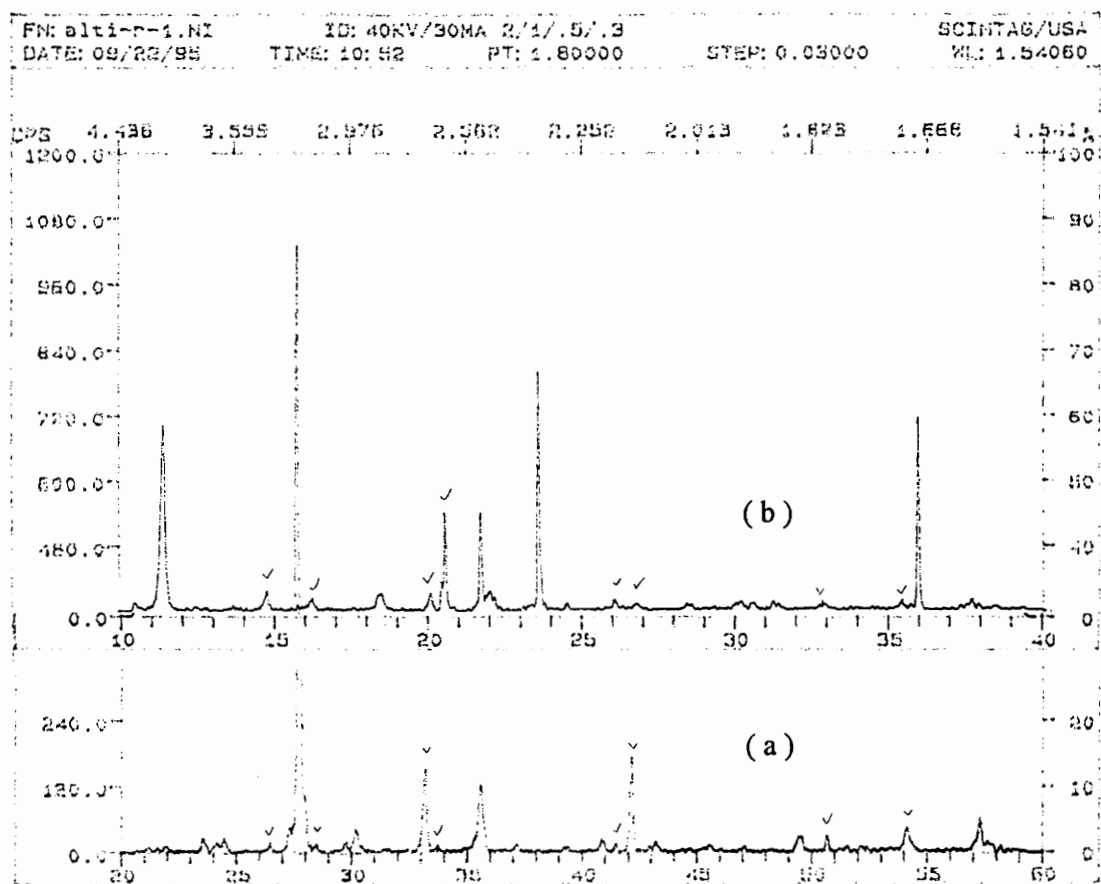


Figure 40. X-Ray Diffraction of the Uncorroded Areas of the $\text{Mg-Al}_2\text{TiO}_5$ Coating (a) and the Sample before the Corrosion Test (b)

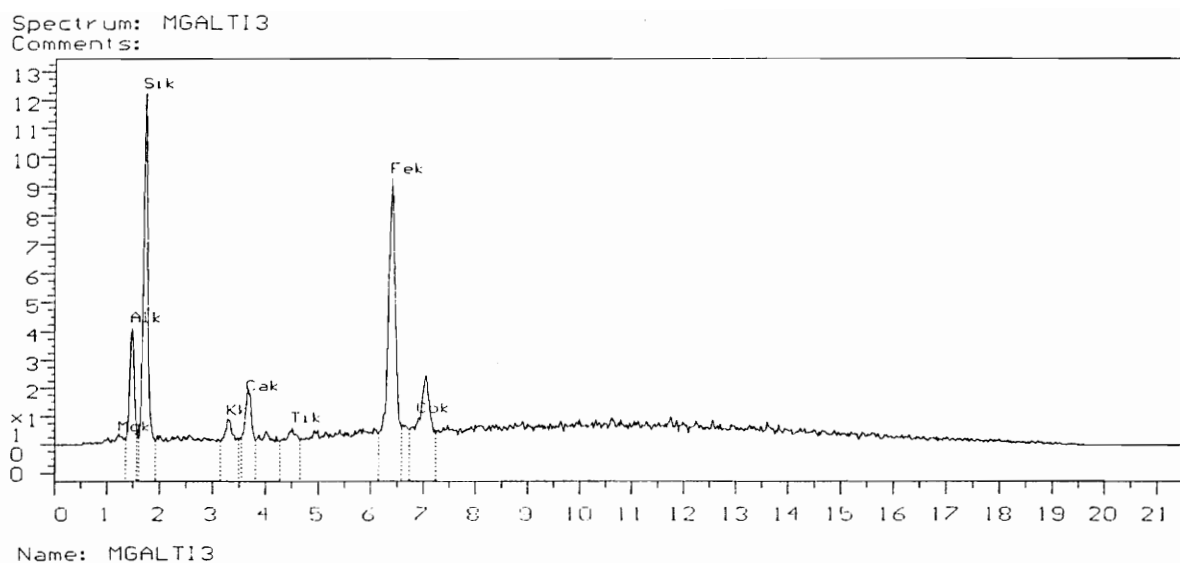


Figure 41. EDX Spectrum on a Cross-Section of the Uncorroded Areas of the $\text{Mg-Al}_2\text{TiO}_5$ Coating

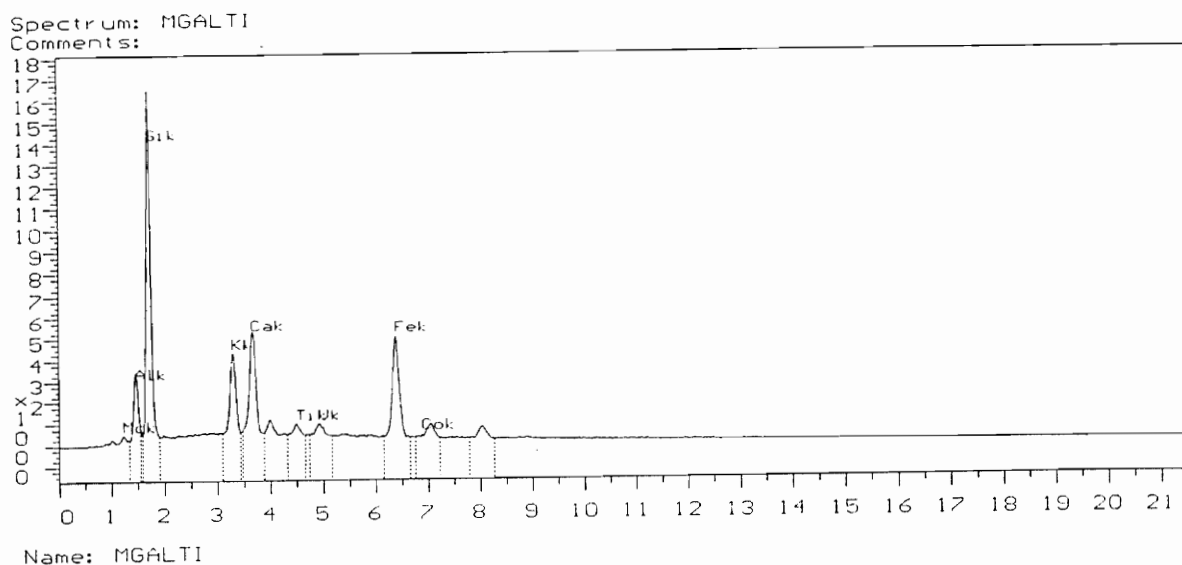


Figure 42. EDX Spectrum on a Cross-Section of the Corroded Areas of the $\text{Mg-Al}_2\text{TiO}_5$ Coating

4.7 Aging Process

1). Thermal Shock Resistance Test

(a). CMZP Coated SiC Samples

The thermal shock resistance of aged and unaged CMZP coated SiC samples was determined. The samples were heated to 300, 500, 750 and 1000°C, respectively, and then quenched in water at room temperature (25°C). The results are shown in Table 13. The surface microstructure of coatings and adhesion between the coatings and substrates were examined by SEM. The surface microstructure of the aged and unaged samples after a thermal shock of 1000°C and 750°C (Figures 43, 44, 45 and 46) shows that aging process improved the quality of CMZP coatings.

Table 13. The thermal shock resistance of aged and unaged CMZP coated SiC samples

Sample	Heated Temperature and Results			
	300°C	500°C	750°C	1000°C
Aged (4 samples)	No cracks	No cracks	Small cracks	Cracks
Unaged (4 samples)	No cracks	Small cracks	Cracks	Cracks and small spalling

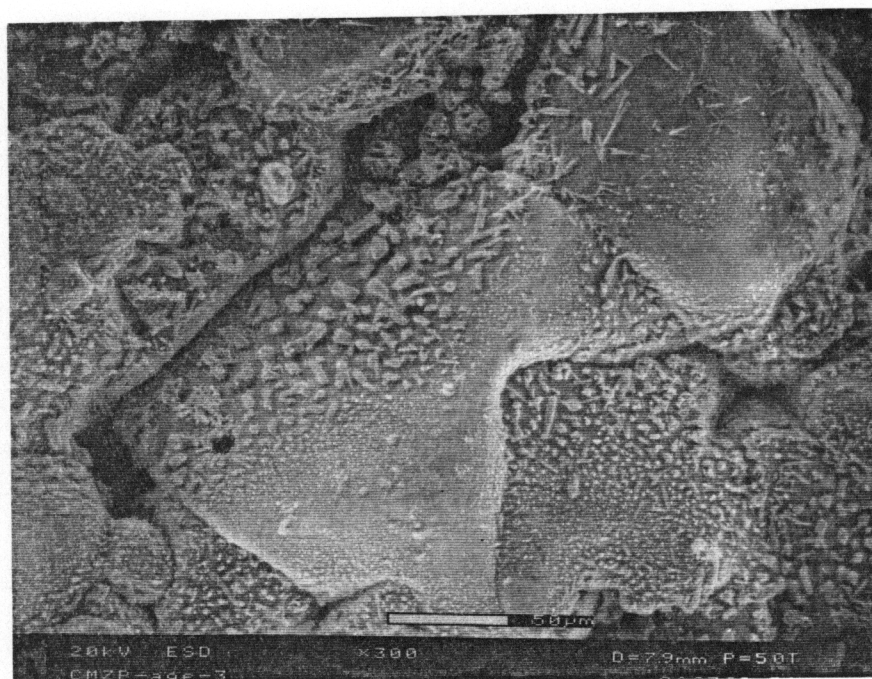


Figure 43. Surface Microstructure of Aged CMZP Coated Samples after a Thermal Shock of 1000°C



Figure 44. Surface Microstructure of Unaged CMZP Coated Samples after a Thermal Shock of 1000°C

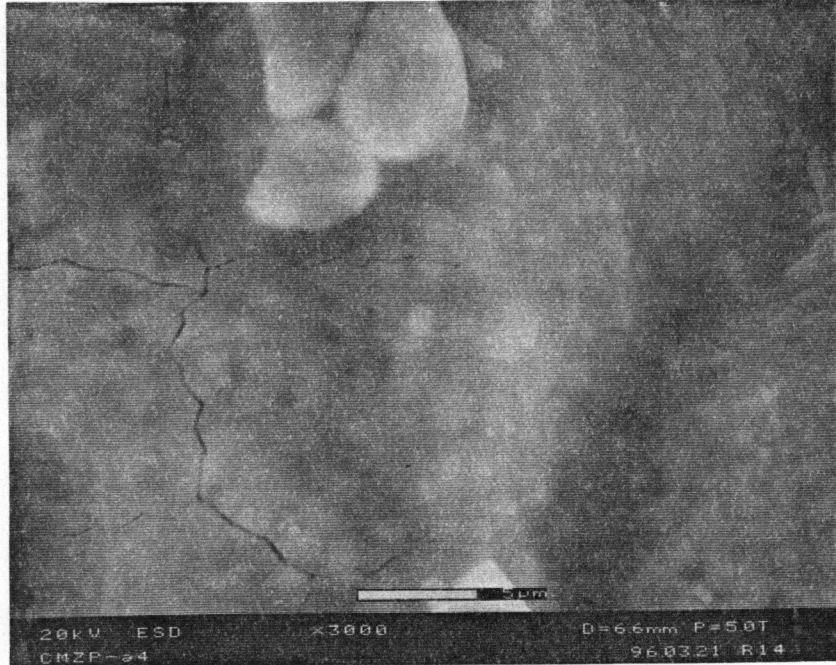


Figure 45. Surface Microstructure of Aged CMZP Coated Samples after a Thermal Shock of 750°C

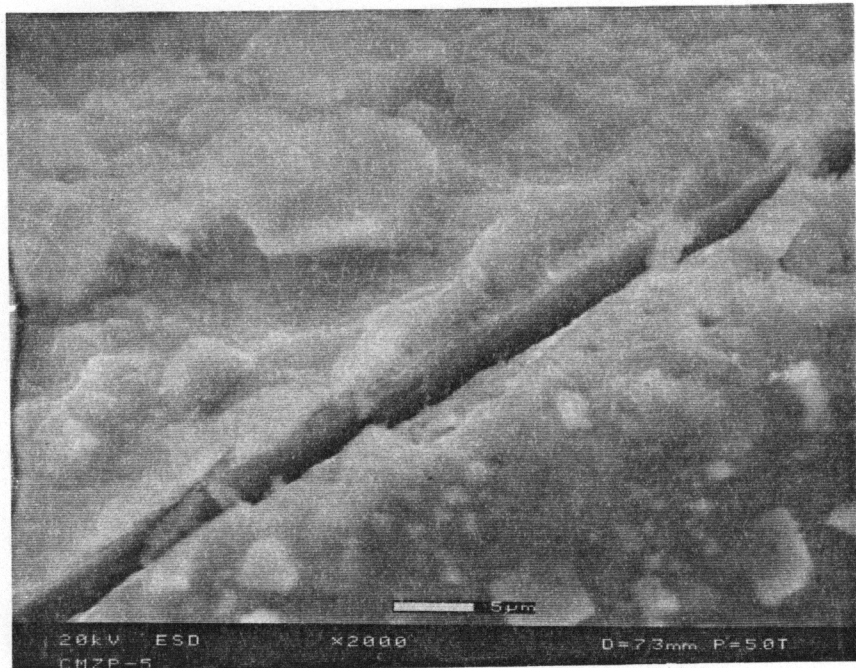


Figure 46. Surface Microstructure of Unaged CMZP Coated Samples after a Thermal Shock of 750°C

(b). Mg-Al₂TiO₅ Coated SiC Samples

The thermal shock resistance of aged and unaged Mg-Al₂TiO₅ coated SiC samples was tested. The samples were heated to 300, 500, 750 and 1000°C, respectively, and then quenched in water at room temperature (25°C). The results are shown in Table 14. The surface microstructure of coatings and adhesion between the coatings and substrates were examined by SEM. The surface microstructure of the aged and unaged samples after a thermal shock of 1000°C and 750°C (Figures 47, 48, 49 and 50) shows that ageing process improved the quality of Mg-Al₂TiO₅ coatings.

Table 14. The thermal shock resistance of aged and unaged Mg-Al₂TiO₅ coated SiC samples

Sample	Heated Temperature and Results			
	300°C	500°C	750°C	1000°C
Aged (4 samples)	No cracks	No cracks	Small cracks	Cracks
Unaged (4 samples)	No cracks	Small cracks	Cracks	Cracks and small spalling



Figure 47. Surface Microstructure of Aged Mg-Al₂TiO₅ Coated Samples after a Thermal Shock of 1000°C



Figure 48. Surface Microstructure of Unaged Mg-Al₂TiO₅ Coated Samples after a Thermal Shock of 1000°C

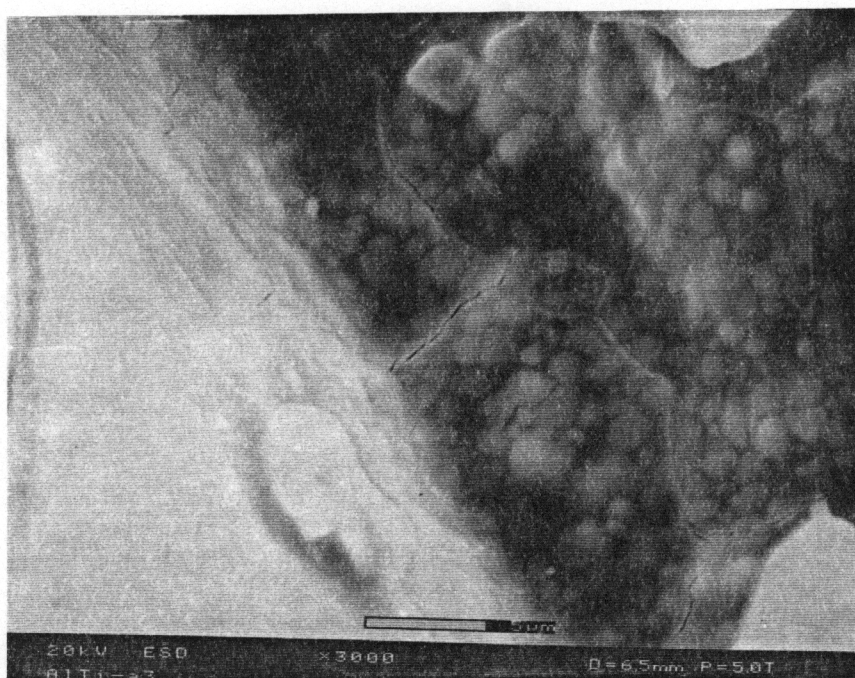


Figure 49. Surface Microstructure of Aged Mg-Al₂TiO₅ Coated Samples after a Thermal Shock of 750°C

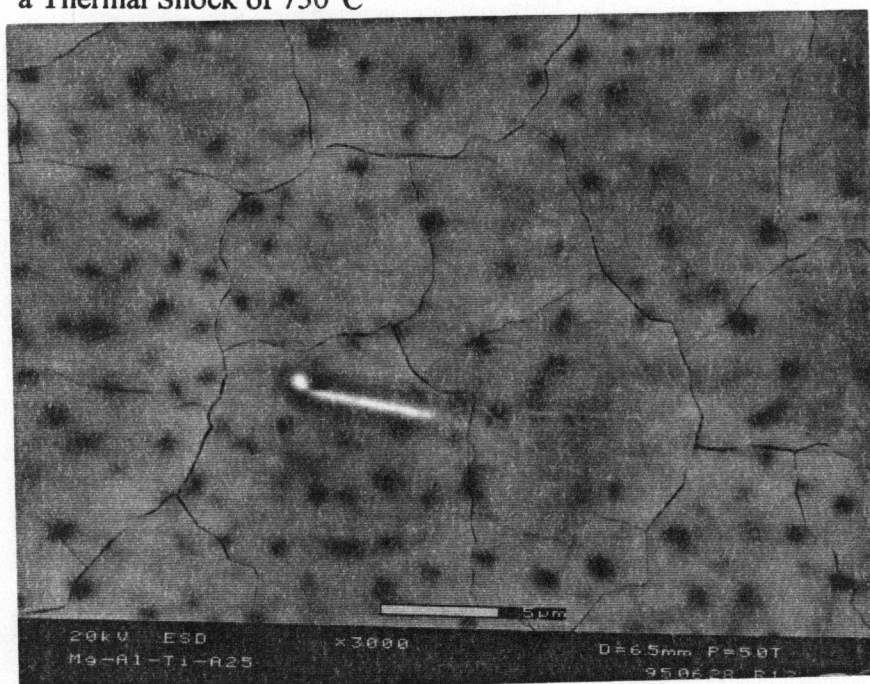


Figure 50. Surface Microstructure of Unaged Mg-Al₂TiO₅ Coated Samples after a Thermal Shock of 750°C

2). Alkali Corrosion Resistance Test

(a). CMZP Coated SiC Samples

The alkali corrosion resistance of both aged and unaged CMZP coated SiC samples was examined by determining the weight loss and flexural strength degradation of samples exposed to sodium-containing atmosphere. The room temperature flexural strength of both aged and unaged SiC samples was determined by 4-point bending using an ATS Test System. To decrease the random errors the average strengths of every group were selected. The distribution of Ca, Mg, Zr, P and Si on sample surfaces both before and after corrosion were examined by EDX.

The sodium corrosion resistance of aged CMZP coated SiC samples is improved over that of unaged samples as indicated in Table 15 and 16 and Figures 51 and 52. Compared to aged CMZP coated SiC samples, unaged samples exhibited a greater weight loss and reduction in strength.

Table 15. The weight loss of aged and unaged CMZP coated SiC samples after sodium corrosion (%)

	1100°C		1000°C		900°C	
	Aged	Unaged	Aged	Unaged	Aged	Unaged
Obtained Value	2.5	2.8	2.2	2.1	2.2	2.3
	2.3	2.4	2.2	2.0	2.1	2.7
	2.1	2.1	2.4	2.7	2.1	1.9
	2.1	2.2	2.3	2.6	1.7	2.1
Average Value	2.3	2.4	2.3	2.4	2.0	2.3

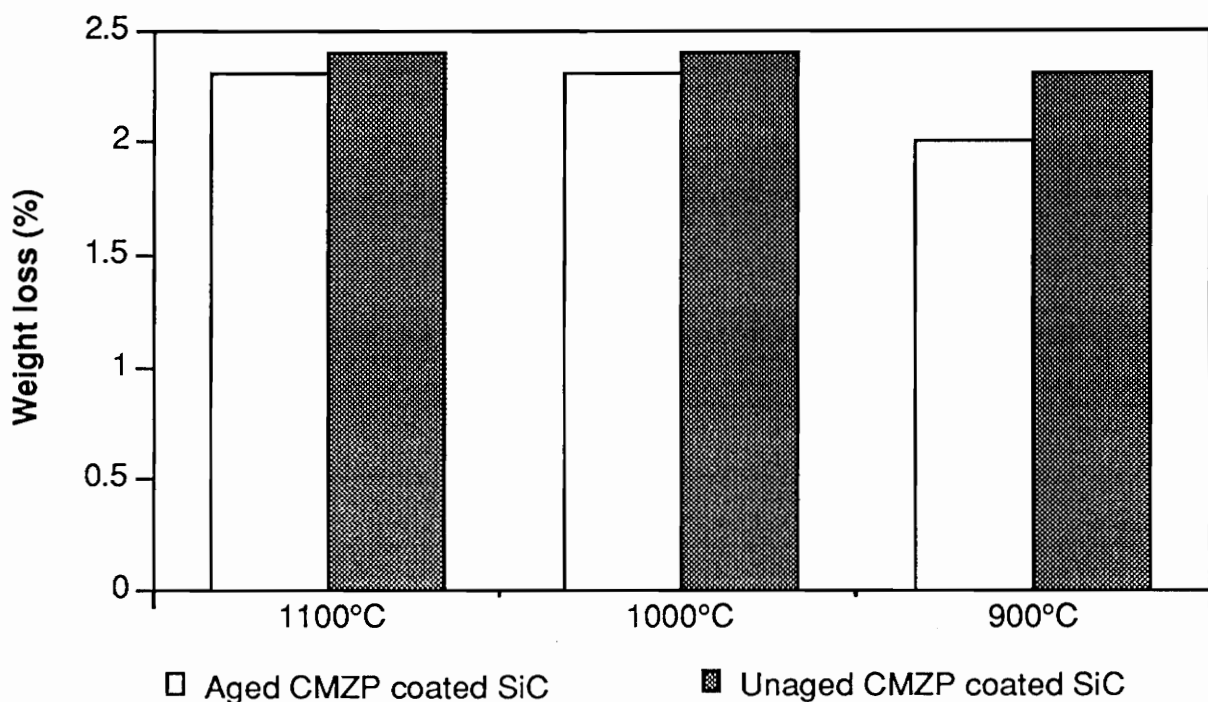


Figure 51. Weight Loss of Aged and Unaged CMZP Coated SiC Samples after Sodium Corrosion

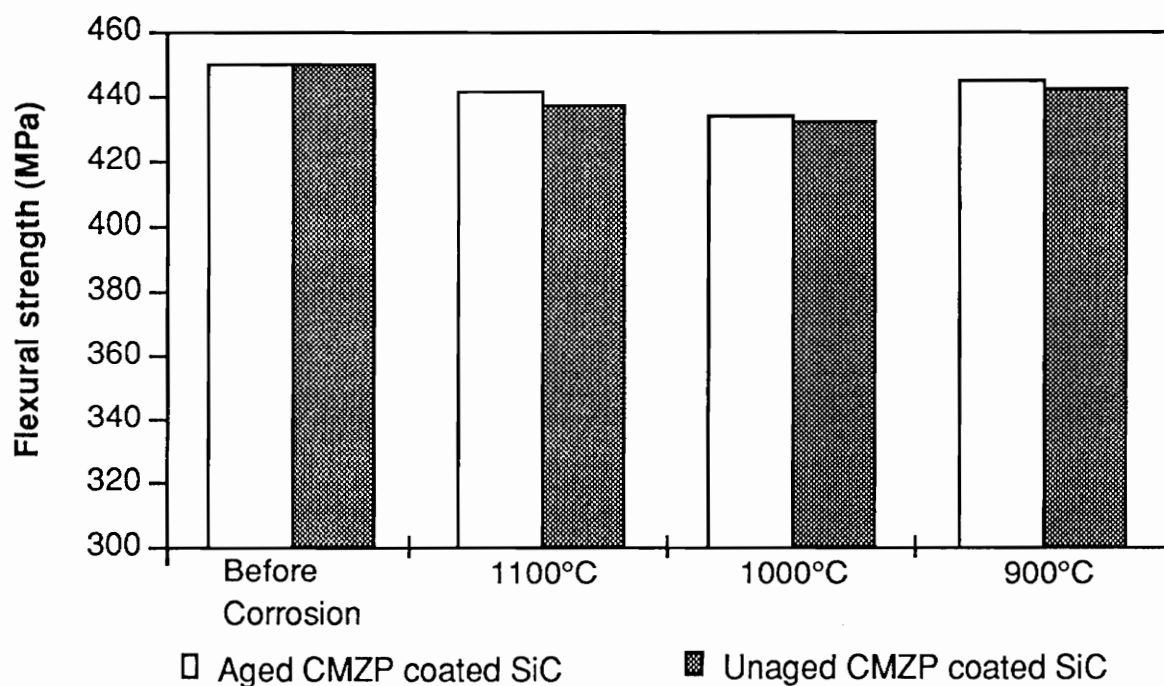


Figure 52. Flexural Strength of Aged and Unaged CMZP Coated SiC Samples before and after Sodium Corrosion

Table 16. The flexural strength of aged and unaged CMZP coated SiC samples before and after sodium corrosion (Mpa)

	Before corrosion		1100°C		1000°C		900°C	
	Aged	Unaged	Aged	Unaged	Aged	Unaged	Aged	Unaged
Obtained value	442	468	429	417	448	432	449	449
	453	455	467	469	424	411	436	338
	455	432	457	438	427	448	453	436
	450	444	411	425	436	436	442	443
Average value	450	450	441	437	434	432	445	442

Many other groups of the aged and unaged samples were also examined and the statistical results were similar to the results as described above.

Figure 53 and 54 and Table 17 show the distribution of Ca, Mg, Zr, P and Si on the aged and unaged sample surfaces after the sodium corrosion at 1000°C obtained by EDX. This proves that the aging process improves the quality of CMZP coatings.

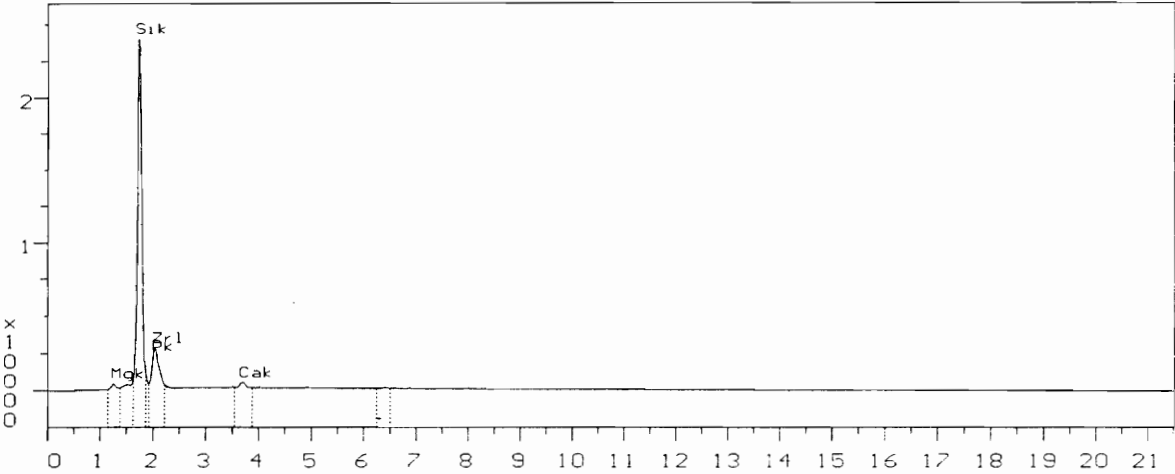
Table 17. Distribution of Ca, Mg, Zr, P and Si on the sample surfaces after the sodium corrosion at 1000°C (%)

Aged				Unaged			
Ca	Mg	Zr, P *	Si	Ca	Mg	Zr, P *	Si
3.97	2.09	14.83	77.36	2.13	0	11.23	85.43

* The peaks of Zr and P overlap

The mechanism of aging effect is the aging process fines the crystal structure of CMZP coatings.

Spectrum: CMZP-A-2
Comments:

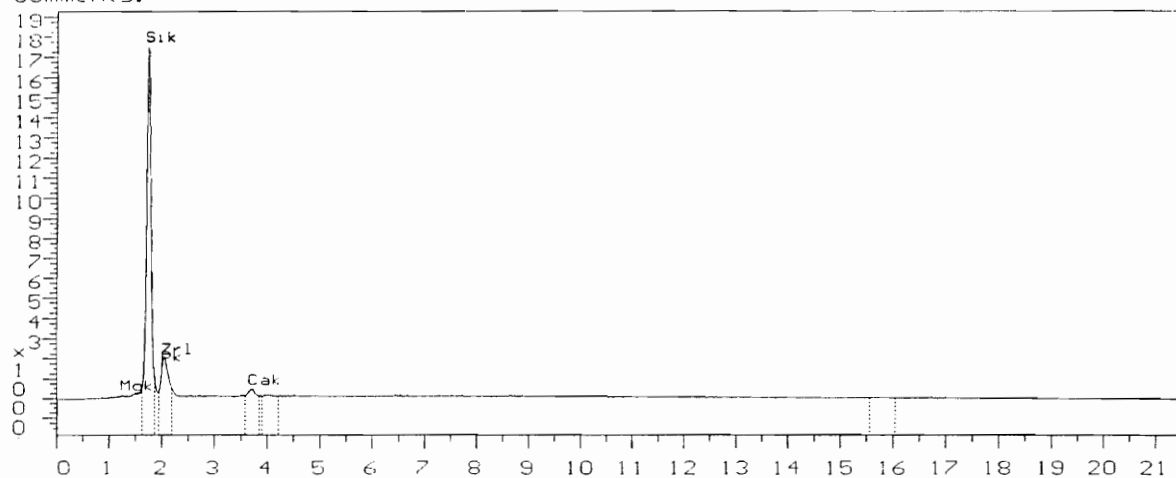


Name: CMZP-A-2
Comments:

Centroid (KeV)	Gross Area	Normalized	Comments
1.260	3112.47	2.09	Mgk
1.743	115377.9	77.36	SiK
2.037	22125.63	14.83	ZrL
3.717	5922.33	3.97	CaK
6.447	2611.99	1.75	

Figure 53. Distribution of Ca, Mg, Zr, P and Si on Aged CMZP Coated Sample Surfaces, Obtained by EDX

Spectrum: CMZP-A-3
Comments:



Name: CMZP-A-3
Comments:

Centroid (KeV)	Net Area	Normalized	Comments
1.743	75669.01	85.43	Si
2.058	9944.37	11.23	Zr
3.717	1885.15	2.13	Ca
4.032	500.36	0.56	
15.834	577.84	0.65	

Figure 54. Distribution of Ca, Mg, Zr, P and Si on Unaged CMZP Coated Sample Surfaces, Obtained by EDX

(b). Mg-Al₂TiO₅ Coated SiC Samples

The alkali corrosion resistance of both aged and unaged Mg-Al₂TiO₅ coated SiC samples was examined by determining the weight loss and flexural strength degradation of samples exposed to sodium containing atmospheres.

The sodium corrosion resistance of aged Mg-Al₂TiO₅ coated SiC samples is improved over that of unaged samples as indicated in Table 18, 19 and Figure 55 and 56.

Table 18. The weight loss of aged and unaged Mg-Al₂TiO₅ coated SiC samples after sodium corrosion (%)

	1100°C		1000°C		900°C	
	Aged	Unaged	Aged	Unaged	Aged	Unaged
Obtained value	2.1	3.1	2.7	2.4	2.5	3.2
	2.1	2.8	2.4	2.2	2.0	2.1
	2.6	2.4	2.5	2.6	2.2	2.5
	2.4	2.3	2.3	3.3	2.4	2.3
Average value	2.3	2.7	2.5	2.6	2.3	2.5

Table 19. The flexural strength of agee and unafed Mg-Al₂TiO₅ coated SiC samples before and after sodium corrosion (Mpa)

	Before corrosion		1100°C		1000°C		900°C	
	Aged	Unaged	Aged	Unaged	Aged	Unaged	Aged	Unaged
Obtained value	432	464	423	424	438	441	435	447
	458	432	450	462	431	419	451	436
	455	453	451	441	453	455	441	432
	452	447	426	414	452	442	449	443
Average value	449	449	438	435	444	439	444	440

Compared aged Mg-Al₂TiO₅ coated samples, unaged samples exhibited a great weight loss and reduction in strength. Many other groups of aged and unaged samples were also examined and the statistical results were similar to the results as described above.

Figure 57 and 58 and Table 20 show the distribution of Mg, Al, Ti and Si on the aged and unaged sample surfaces after the sodium corrosion at 1000°C obtained by EDX, which proves that the aging process improves the quality of Mg-Al₂TiO₅ coatings.

Table 20. Distribution of Mg, Al, Ti and Si on the sample surfaces after the sodium corrosion at 1000°C (%)

Aged				Unaged			
Mg	Al	Ti	Si	Mg	Al	Ti	Si
0.23	5.00	9.36	81.89	0.12	2.69	3.29	92.27

The mechanism of aging effect is the aging process fines the crystal structure of Mg-Al₂TiO₅ coatings.

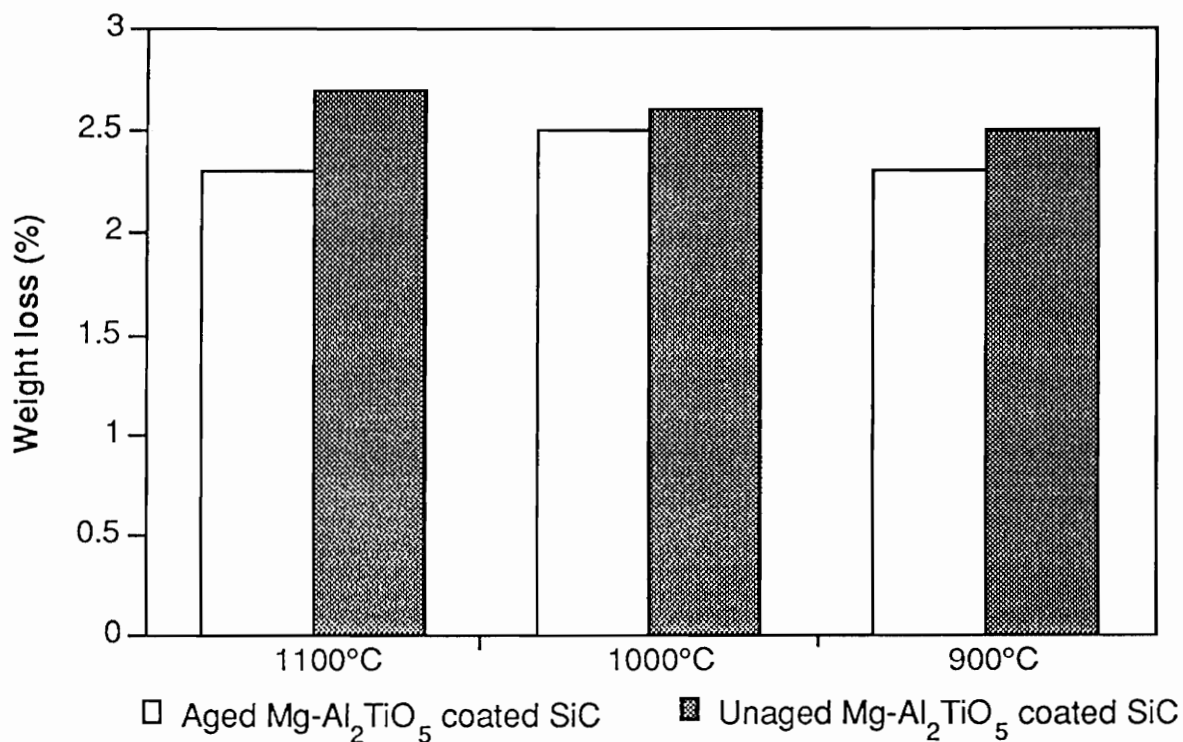


Figure 55. Weight Loss of Aged and Unaged Mg-Al₂TiO₅ Coated SiC Samples after Sodium Corrosion

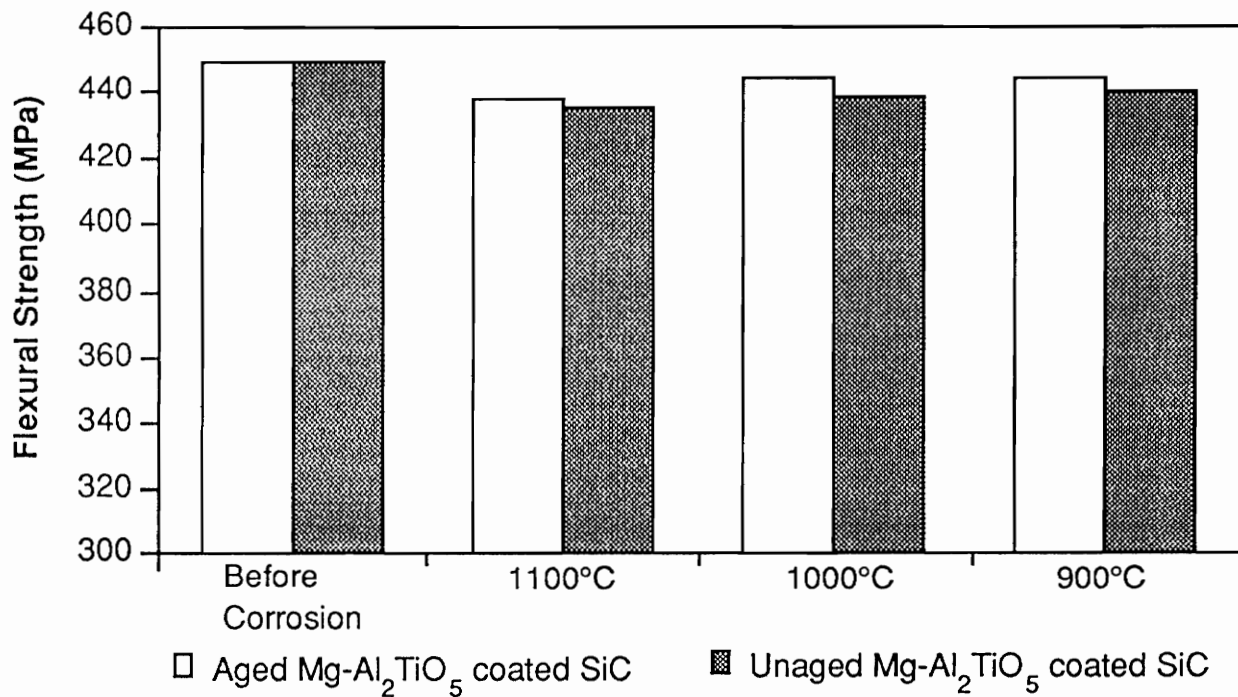
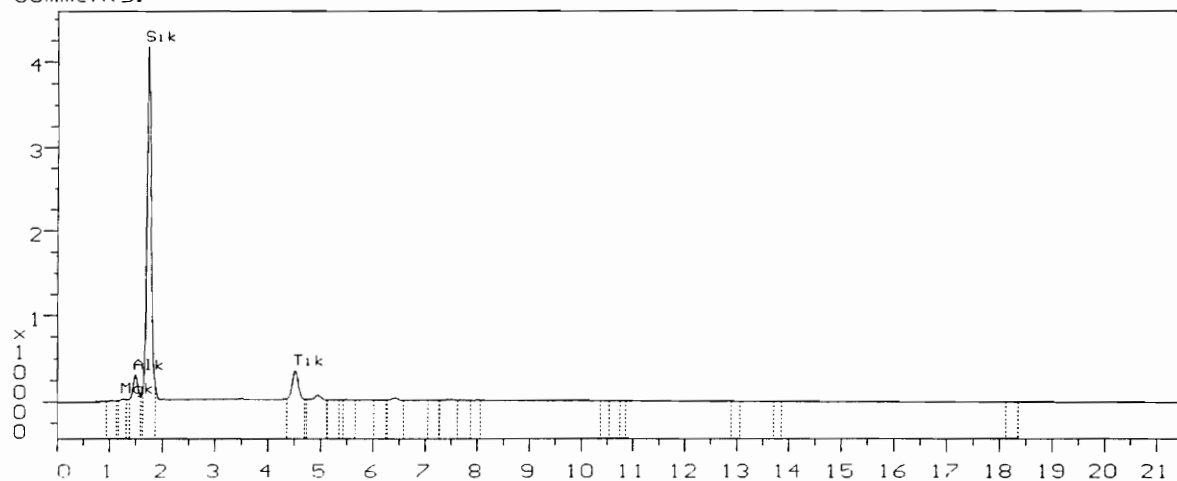


Figure. 56. Flexural Strength of Aged and Unaged Mg-Al₂TiO₅ Coated SiC Samples before and after Sodium Corrosion

Spectrum: MGTIAL7E
Comments:

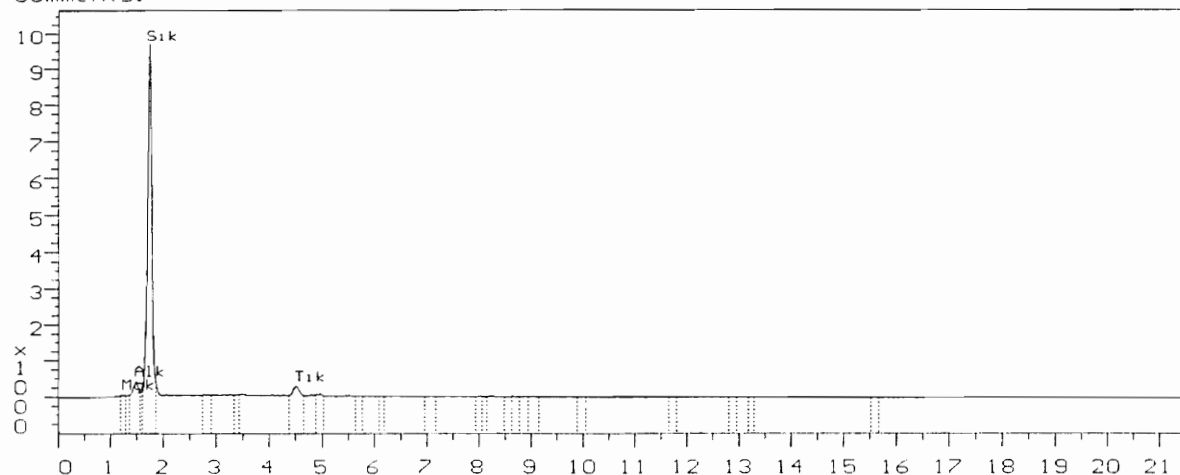


Name: MGTIAL7E
Comments:

Centroid (KeV)	Net Area	Normalized	Comments
1.050	362.63	0.16	
1.260	507.88	0.23	Mgk
1.491	11016.50	5.00	Alk
1.743	180379.6	81.89	SiK
4.536	20608.54	9.36	TiK
4.956	3440.68	1.56	
5.229	63.05	0.03	
5.586	456.20	0.21	
6.090	66.22	0.03	

Figure 57. Distribution of Mg, Al, Ti and Si on Aged Mg-Al₂TiO₃ Coated Sample Surfaces, Obtained by EDX

Spectrum: MGTIAL5C
Comments:



Name: MGTIAL5C
Comments:

Centroid (KeV)	Net Area	Normalized	Comments
1.281	54.05	0.12	Mgk
1.491	1207.12	2.69	Alk
1.743	41385.61	92.27	SiK
2.772	101.15	0.23	
3.423	28.75	0.06	
4.515	1474.45	3.29	Tik
4.977	122.91	0.27	
5.670	41.89	0.09	

Figure 58. Distribution of Mg, Al, Ti and Si on Unaged Mg-Al₂TiO₃ Coated Sample Surfaces, Obtained by EDX

Section 5

Conclusion

1. CMZP and Mg-Al₂TiO₅ coatings on dense SiC substrates using sol-gel techniques were developed.
2. The thickness and quality of both CMZP and Mg-Al₂TiO₅ coatings were found to depend on the solution concentration and lift rate.
3. Double coatings were applied to obtain homogeneous and crack-free coatings. The quality of double coatings was influenced by different thickness of the first and second coatings.
4. The CMZP coated samples were fired in controlled atmospheres to obtain the pure CMZP phase.
5. Unhydrolyzed Mg-Al₂TiO₅ solution was utilized instead of hydrolyzed solution to improve the quality of Mg-Al₂TiO₅ coatings.
6. Aging process was found to improve the quality of CMZP and Mg-Al₂TiO₅ coatings.
7. CMZP and Mg-Al₂TiO₅ coatings exhibit good thermal shock resistance.
8. CMZP and Mg-Al₂TiO₅ coatings improve alkali corrosion resistance of SiC.

REFERENCES

- [1] D. A. Hirschfeld, S. M. VanAke, T. K. Li, Y. P. Yang and J. J. Brown, *Proceedings of the Annual Automotive Technology Development Contractor's Coordination Meeting*, p. 239, 1990.
- [2] D. Hirschfeld, Y. Yang, T. K. Li and J. J. Brown, *Proceedings of Annual Automotive Technology Development Contractor's Coordination Meeting*, p. 145-157, 1991.
- [3] D. Hirschfeld, D. Liu and J. J. Brown, 4th International Symposium on Ceramic Materials and Components for Engines, Goteborg, Sweden, 1991.
- [4] J. J. Brown and N. R. Brown, "Durability Testing of Ceramic Particulate Filters under PFBC Conditions", EPRI TR-103286, Project 3161-06, Final Report, Nov. 1993.
- [5] J. J. Brown, D. A. Hirschfeld, D. M. Liu, Y. Yang, T. K. Li, R. E. Svanson, S. VanAken and J. M. Kim, "Ceramic Materials with Low thermal Conductivity and Low Coefficients of Thermal Expansion", U. S. Patent 5,102,836, April 7, 1992.
- [6] T. Sun, N. R. Brown and J. J. Brown, "Investigations of Long-Term Thermal/Chemical Degradation of Ceramic Filter Materials", Final Report, Center for Advanced Ceramic Materials, Virginia Tech, 1991.
- [7] T. K. Li, D. A. Hirschfeld and J. J. Brown, "Thin Film Coatings of $(\text{Ca}_{0.6}\text{Mg}_{0.4})\text{Zr}_4(\text{PO}_4)_6$ on Si_3N_4 and SiC ", *J. Mater. Res.*, 9, 8, 2014, 1994.
- [8] J. J. Brown, N. R. Brown and T. Sun, "Sol-Gel Beta-Aluminum Titanate Thin Film Coating", Patent Application Filed July 1993.
- [9] M. Kang, "Alkali/Steam Corrosion Resistance of Commercial SiC Products Coated with Sol-Gel Deposited Mg-Doped Al_2TiO_5 and CMZP", Master's Thesis, Dept. Materials Science and Engineering, Virginia Tech, 1994.
- [10] Y. Inomata, *Silicon Carbide Ceramics-1*, p. 9, Edited by S. Somoya and Y. Inomata, Elsevier Science Publishers, New York, 1991.
- [11] A. Bennett, "Requirements for Engineering Ceramics in Gas Turbine Engines", *Mater. Sci. Technol.*, 2, 895-99, 1986.

- [12] D. W. Richerson, Modern Ceramic Engineering, p. 116-34, Marcel Dekker, NY, New York, 1982.
- [13] H. Kim, and A. J. Moorehead, "High-Temperature Gaseous Corrosion of Silicon Nitride in H₂-H₂O and Ar-O₂ Environments", *J. Am. Ceram. Soc.*, 73, 10, 3007-14, 1990.
- [14] E. Gulbransen, K. Andrew and F. Brassart, "the Oxidation of SiC at 1150 to 1400°C and at 9×10^{-3} to 5×10^{-1} Torr Oxygen Pressure", *J. Electrochem. Soc.*, 113, 12, 1311-14, 1966.
- [15] W. Vaughn and H. Maahs, "Active to Passive Transition in the Oxidation of Silicon Carbide and Silicon Nitride in Air", *J. Am. Ceram. Soc.*, 73, 6, 1540-43, 1990.
- [16] S. M. McNallan and D. Park, "Active Oxidation of SiC-Based Ceramics in Ar-2% Cl₂-O₂ Gas Mixtures at 100°C", *J. Am. Ceram. Soc.*, 75, 7, 1942-48, 1992.
- [17] J. Hinze and H. Graham, "The Active Oxidation of Si and SiC in the Viscous Gas-Flow Regime", *J. Electrochem. Soc.*, 123, 7, 1066-73, 1976.
- [18] L. Ogbuji, "Development of Oxide Scale Microstructure on Single-Crystal SiC", *J. Mater. Sci.*, 16, 2753-59, 1981.
- [19] M. Maeda, K. Nakamura and M. Yamada, "Oxidation Resistance Evaluation of Silicon Carbide Ceramics with Various Additives", *J. Am. Ceram. Soc.*, 72, 3, 512-12, 1989.
- [20] T. Narushima, T. Goto and T. Hirai, "High Temperature Passive Oxidation of Chemically Vapor Deposited Silicon Carbide", *J. Am. Ceram. Soc.*, 72, 8, 1386-90, 1989.
- [21] D. Mieskowski, T. Mitchell and A. Heuer, "Bubble Formation in Oxide Scale on SiC", *J. Am. Ceram. Soc.*, 67, 1, C17-18, 1984.
- [22] J. Costello and R. Tressler, "Isotope Labeling Studies of the Oxidation of Silicon at 1000°C and 1300°C", *J. Electrochem. Soc.*, 131, 8, 1944-47, 1984.
- [23] S. Singhal and F. Lange, "Effect of Alumina Content on the Oxidation of Hot-Pressed Silicon Carbide", *J. Am. Ceram. Soc.*, 58, 9-10, 433-35, 1975.

- [24] Z. Zheng, R. Tressler and K. Spear, "Oxidation of Single-Crystal Silicon Carbide", *J. Electrochem. Soc.*, 137, 3, 854-58, 1990.
- [25] A. Heuer, L. Ogbuji and T. Mitchell, "The Microstructure of Oxide Scales on Oxidized Si and SiC Single Crystals", *J. Am. Ceram. Soc.*, 63, 5-6, 354-55, 1980.
- [26] N. Jacobson, K. Lee and D. Fox, "Reactions of Silicon Carbide and Silicon(IV) Oxide at Elevated Temperatures", *J. Am. Ceram. Soc.*, 75, 6, 1603-11, 1992.
- [27] D. Butt, R. Tressler and K. Spear, "Corrosion of SiC Materials in N₂-H₂-CO Gaseous Environments: II, Durability and Mechanical Properties", *J. Am. Ceram. Soc.*, 75, 12, 3268-77, 1992.
- [28] A. Bennett, "Requirements for Engineering Ceramics in Gas Turbine Engines", *Mater. Sci. Tech.*, 2895-99, 1986.
- [29] L. Hinze and H. Graham, "The Active Oxidation of Si and Silicon Carbide in the Viscous Gas-Flow Regime", *J. Electrochem. Soc.*, 123, 7, 1066-1073, 1976.
- [30] K. Luthra, "A Mixed Interface Reaction/Diffusion Control Model for Oxidation of Si₃N₄", *J. Electrochem. Soc.*, 138, 10, 3001-3007, 1991.
- [31] H. Du, R. Tressler, K. Spear, and C. Pantano "Oxidation Studies of Crystalline CVD Silicon Nitride", *J. Electrochem. Soc.*, 136, 5, 1527-36, 1989.
- [32] T. Narushima, T. Goto, Y. Iguchi and T. Hirai, "High Temperature Oxidation of CVD Silicon Carbide in Wet Oxygen at 1823 to 1923K", *J. Am. Ceram. Soc.*, 73, 12, 3580-84, 1990.
- [33] R. Harris and R. Call, "Oxidation of 6H Alpha-Silicon Carbide", in *Silicon Carbide 1973*, p.329-36, Edited by R. C. Marshall et al, University of South Carolina Press, Columbia, SC, 1974.
- [34] C. Fung and J. Kopanski, "Thermal Oxidation of 3C Silicon Carbide Single-Crystal Layers on Silicon", *Appl. Phys. Lett.*, 45, 7, 757-59, 1984.
- [35] H. Cappelen, K. Johansen and K. Motzfeldt, "Oxidation of Silicon Carbide in Oxygen and Water Vapor at 1500°C", *Acta Chem. Scand. Ser.*, 35, 247-54, 1981.

- [36] P. Jorgensen, M. Wadsworth and I. Cutler, "Effects of Water Vapor on Oxidation of Silicon Carbide", *J. Am. Ceram. Soc.*, 44, 6, 258-62, 1961.
- [37] W. Lu, Steckl, T. Chow and W. Katz, "Thermal Oxidation of Sputtered Silicon Carbide Thin Films", *J. Electrochem. Soc.*, 131, 8, 1907-14, 1984.
- [38] M. Maeda, K. Nakamura and T. Ohkubo, "Oxidation of Silicon Carbide in a Wet Atmosphere", *J. Mater. Sci.*, 23, 3933-38, 1988.
- [39] F. H. Horn, "Screw Dislocation, Etch Figures, and Holes", *Philos. Mag.*, 43, 1210-13, 1952.
- [40] S. Amelinckx, G. Strumane and W. W. Webb, "Dislocation in Silicon Carbide", *J. Appl. Phys.*, 31, 1359-70, 1960.
- [41] E. Buchner and O. Rubisch, Silicon Carbide-1973, p. 428, Edited by R. C. Mashal and J. W. Faust, University of South Carolina Press, Columbia, SC, 1974.
- [42] D. McKee and D. Chatterji, "Corrosion of Silicon Carbide in Gases and Alkaline Melts", *J. Am. Ceram. Soc.*, 59, 9-10, 441-44, 1976.
- [43] N. Jacobson, C. Stearn and J. Smialek, "Burner Rig Corrosion of SiC at 1000°C", *Adv. Ceram. Mater.*, 1, 2, 154-61, 1986.
- [44] H. E. Kim and A. J. Moorhead, "Effect of Hydrogen-Water Atmospheres on Corrosion and Flexural Strength of Sintered α -Silicon Carbide", *J. Am. Ceram. Soc.*, 73, 3, 694, 1990.
- [45] L. O. Hagman and P. Kierkegaard, "The crystal Structure of $\text{NaMe}_2^{\text{IV}}(\text{PO}_4)_3$ ($\text{Me}^{\text{IV}}=\text{Ge, Ti, Zr}$)", *Acta Chemica Scandinavica*, 22, 1822-32, 1968.
- [46] H. Y. Hong, "Crystal Structures and Crystal Chemistry in the System $\text{Na}_{1+x}\text{Zr}_2\text{Si}_x\text{P}_{3-x}\text{O}_{12}$ ", *Mat. Res. Bull.*, 11, 173-182, 1976.
- [47] J. B. Goodenough, H. Y. Hong and J. A. Kafalas, "Fast Na^+ -Ion Transport in Skeleton Structures", *Mat. Res. Bull.*, 11, 203-220, 1976.
- [48] D. T. Qui, J. J. Capponi, J. C. Joubert, R. D. Shannon and C. K. Johnson, "Structure Analysis of $\text{Na}_4\text{Zr}_2\text{Si}_3\text{O}_{12}$ at 300 and 600°C", in Fast Ion Transport in Solids, p.439-442, Edited by Vashishta, Mundy and Shenoy, North Holland, Inc., New York, 1979.

- [49] J. P. Boilot, J. P. Salanie G. Desplanches and D. Le Potier, "Phase Transportation in $\text{Na}_{1+x}\text{Zr}_2\text{Si}_x\text{P}_{3-x}\text{O}_{12}$ Compounds", *Mat. Res. Bull.*, 14, 1469-1477, 1979.
- [50] R. S. Gorden, G. R. Miller, B. J. McEntire, E. D. Beck and J. R. Rasmussen, "Fabrication and Characterization of Nasicon Electrolytes", *Solid State Ionics*, 3-4, 243-248, 1981.
- [51] J. J. Brow, D. A. Hirschfeld, D. M. Lui, Y. Yang, T. K. Li, R. E. Svanson, S. VanAken, J. M. Kim, "Ceramic Materials with Low Thermal Conductivity and Low Coefficients of Thermal Expansion", U. S. Patent 5,102,836, April 7, 1992.
- [52] S. J. Charlton and M. J. Watts, "An Investigation of Thermal Insulation of IDI Diesel Engines Swirl Chambers", *Proc. Instn. Mech. Eng.*, 205, 263-69, 1991.
- [53] T. Mani and A. Damodaran, "Aluminum Titanate Powder Synthesis via Thermal Decomposition of Transparent Gel", *J. Am. Ceram. Soc.*, 74, 8, 1807-10, 1991.
- [54] H. Morishima and N. Ootsuka, "Development of AluminumTitanate-Mullite Composite Having High Thermal Shock Resistance", *J. Am. Ceram. Soc.*, 69, 10, C266-277, 1986.
- [55] F. Parker, "Aluminum Titanate-Zirconium Titanate-Zirconia Composites: A New Family of Low-Thermal-Expansion Ceramics", *J. Am. Ceram. Soc.*, 73, 4, 929-32, 1990.
- [56] C. J. Brinker and G. W. Schere Edited, *Sol-Gel Science: The Physics and Chemistry of Sol-Gel Processing*, p. 48-53, Academic Press, Inc. San Diego, CA, 1990.
- [57] L. C. Klein, Edited, *Sol-Gel Technology for Thin Film, Fibers, Preforms, Electronics and Specialty Shapes*, p. 407, Noyes, Park Ridge, N. J., 1988.

VITA

Shaokai Yang was born in Haicheng, Liaoning, China on January 4, 1946. He graduated from Beijing University in 1974. From 1980 to 1985 he had worked in Changchun Institute of Physics, Changchun, China. From 1985 to 1991 He had worked in Huaxia Development Corporation of Applied Technology, Changchun, China. Since 1991 he began to work in the Department of Materials Science and Engineering at Virginia Polytechnic Institute and State University. He completed the requirements for a Master of Science in Materials Science and Engineering in May 1996.

A handwritten signature in black ink that reads "Shaokai Yang". The signature is written in a cursive, flowing style with a large, stylized 'S' and 'Y'.